AD-A153 210 INJECTION LASER STRUCTURE DESIGN(U) SOUTHERN METHODIST 1/1
UNIV DALLAS TX J K BUTLER 30 JAN 85 ARO-16436.7-EL
DAAG29-80-K-0004

UNCLASSIFIED F/G 20/5 NL

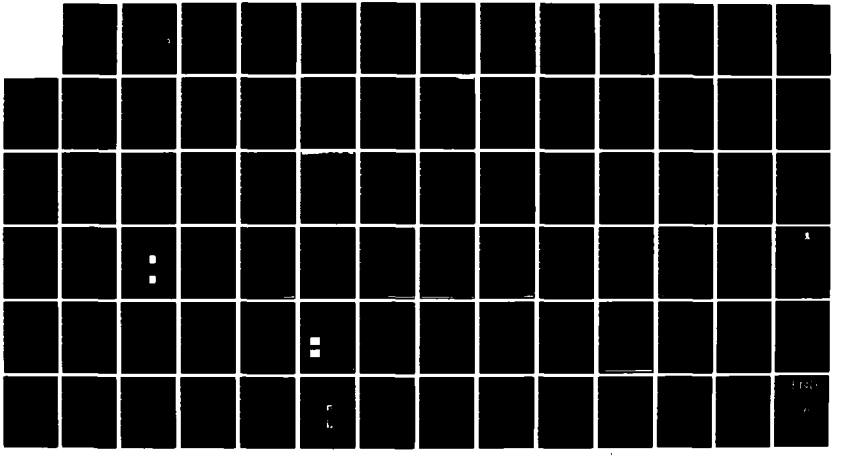

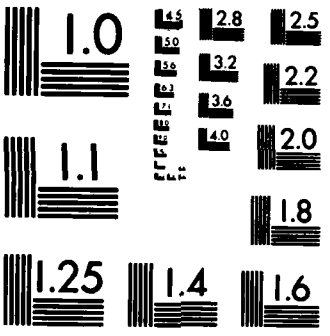

MICROCOPY RESOLUTION TEST CHART
NATIONAL BUREAU OF STANDARDS-1963-A

AD-A153 210

UNCLASSIFIED

SECURITY CLASSIFICATION OF THIS PAGE (When Data Entered)

REPORT DOCUMENTATION PAGE

READ INSTRUCTIONS BEFORE COMPLETING FORM

1. REPORT NUMBER	2. GOVT ACCESSION NO.	3. RECIPIENT'S CATALOG NUMBER
ARO 16436.7-EL	N/A	N/A

4. TITLE (and Subtitle)

INJECTION LASER STRUCTURE DESIGN

5. TYPE OF REPORT & PERIOD COVERED
FINAL
May 1, 1980 - Aug. 31, 1984

6. PERFORMING ORG. REPORT NUMBER

7. AUTHOR(s)

JEROME K. BUTLER

8. CONTRACT OR GRANT NUMBER(s)

DAAG 29-80-K-0004

9. PERFORMING ORGANIZATION NAME AND ADDRESS

Southern Methodist University
Dallas, Texas

10. PROGRAM ELEMENT, PROJECT, TASK AREA & WORK UNIT NUMBERS

11. CONTROLLING OFFICE NAME AND ADDRESS

U. S. Army Research Office
Post Office Box 12211
Research Triangle Park, NC 27709

12. REPORT DATE
January 30,1985

13. NUMBER OF PAGES
16 plus appendices

14. MONITORING AGENCY NAME & ADDRESS(if different from Controlling Office)

15. SECURITY CLASS. (of this report)
Unclassified

15a. DECLASSIFICATION/DOWNGRADING SCHEDULE

16. DISTRIBUTION STATEMENT (of this Report)

Approved for public release; distribution unlimited.

DTIC ELECTE MAY 03 1985 S D E

17. DISTRIBUTION STATEMENT (of the abstract entered in Block 20, if different from Report)

NA

18. SUPPLEMENTARY NOTES

The view, opinions, and/or findings contained in this report are those of the author(s) and should not be construed as an official Department of the Army position, policy, or decision, unless so designated by other documentation.

19. KEY WORDS (Continue on reverse side if necessary and identify by block number)

Semiconductor Laser,
Injection Laser,
Mode Characteristics,
Waveguide mode design,

20. ABSTRACT (Continue on reverse side if necessary and identify by block number)

Injection lasers have potential for replacing many of the high-power conventional gas lasers. The research performed in this project was aimed at the design of high-power semiconductor lasers for communications, printing, and others. Diode lasers have been analyzed for obtaining high output power at single frequencies and for optical pattern stability. We have analyzed the following laser types: 1) Gain guided, 2) Index guided, and 3) W-Guides.

DD FORM 1 JAN 73 1473 EDITION OF 1 NOV 65 IS OBSOLETE

UNCLASSIFIED

SECURITY CLASSIFICATION OF THIS PAGE (When Data Entered)

OTIC FILE COPY

ARO 16436.7-EL

INJECTION LASER STRUCTURE DESIGN

FINAL REPORT

by

JEROME K. BUTLER

JANUARY 30, 1985

U. S. ARMY RESEARCH OFFICE

GRANT DAAG29-80-K-004

SOUTHERN METHODIST UNIVERSITY

FOREWORD

This final report was prepared by Southern Methodist University, Dallas, Texas, under U. S. Army Research Office Grant DAAG 29-80-K-004. The work performed in the grant covered a period beginning May 1, 1980 to August 31, 1985. The work was carried out in the Electrical Engineering Department of the School of Engineering and Applied Science of Southern Methodist University, and was directed by the Principal Investigator, Dr. Jerome K. Butler. The contract monitor at the U. S. Army Research Office was Dr. James Mink.

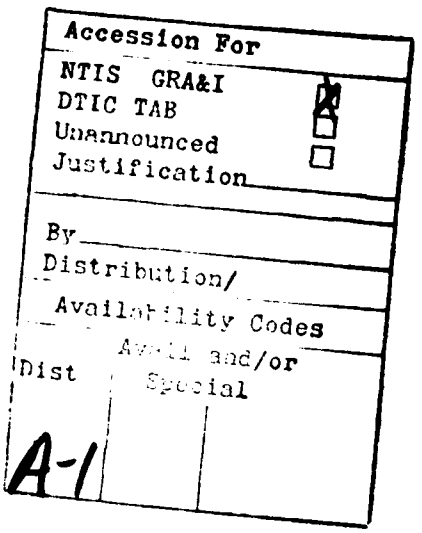

TABLE OF CONTENTS

1. STATEMENT OF PROBLEM

This research project covered a period of approximately four years. The program was aimed at an understanding of the design and fabrication of semiconductor injection lasers for both communication and high power applications. Lasers fabricated for communication systems are typically of the low power type which emit power in 10 to 30 milliwatt range while high power devices (single element types) have emission powers of over 50 milliwatts. Communication devices, fabricated for long wavelength (approximately 15,000 Angstroms) operation where optical fibers have both low attenuation and dispersion, use compounds of indium, gallium, arsenic, and phosphorus. On the other hand, contemporary high-power devices (with emission wavelengths around 8,000 Angstroms) are fabricated with aluminum, gallium and arsenic. Although the research of this project was concerned with aluminum and gallium arsenide compounds, the theory developed is applicable to all semiconductor lasers.

The electromagnetic resonant modes in a semiconductor laser are obtained from solving Maxwell's equations. The ultimate mode operation is inextricably tied to the geometry of the laser as well as to its interaction or coupling with the external world. The particular mode that operates is determined by its interaction with the active region of the laser. Most system applications require devices that emit power in a single and coherent beam of radiation. However, a majority of lasers radiate in either multiple beams or a single unstable beam (drive sensitive). On the other hand, gas lasers can be fabricated to emit power in a single stable beam of radiation because the modes in a gas laser are

formed by the cavity mirrors; the modal selection process is thus independent of drive. In an injection laser the drive dependent gain region plays a major role in the formation of the waveguide geometry. Consequently, we must carefully design structures that can operate only in a single mode.

Because of design restrictions, many contemporary lasers are constrained to low powers. To increase the output power, several exotic structures have been proposed in the literature. But, these newly conceived devices have pushed the fabrication technology to its limits which adversely affects manufacturing yields.

Design sophistication of single laser elements is one method of achieving high overall emission powers. Another approach is to couple several lasers together to form a linear array. Since the devices are fabricated on a single wafer, locking of the elements to obtain a single coherent source can be accomplished *via* internal field coupling. This coupling is possible because the waveguides are open types. Nevertheless, proper design of the single element to achieve the "right" coupling is necessary.

Thus, the problem of analyzing the individual laser element, the central theme of this research project, is the single most important aspect required for the ultimate realization of the semiconductor injection laser.

SUMMARY

INTRODUCTION

Semiconductor lasers are finding applications in many areas, such as optical recording, high-speed printing, fiber optic systems, communication through free space, optical pumping of various lasers which operate at different wavelength and others. Development of high-power lasers has made it possible to fabricate single element lasers that radiate over 100 milliwatts in continuous operation and much higher powers in pulsed operation. Also, recent work in phased-laser-arrays has shown that it is possible to fabricate individual devices with relatively high packing densities. Thus, the overall power emission from the single coherent source is very high.

Semiconductor lasers will begin to replace many of the very high-power optical sources in the next 5 to 10 years. There are two main reasons that will propel the growth in the high power applications. (1) Semiconductor devices are superior to "vacuum tube" components in terms of reliability. (2) For a given volume, the power emission from a semiconductor laser compared to that obtained from a gas laser is extremely large. High powers are possible because of the packing density of excited electrons or inversion levels is semiconductors.

The operation of injection lasers can be categorized into several areas. These include (1) power emission capacity, (2) operational wavelength, (3) wavelength or mode stability, and (4) spatial radiation stability. Typically, many of the above are interconnected. For example, high-power lasers tend to develop many operational instabilities. These

instabilities occur because of the strong nonlinear relationships between optical waveguide formation in the material and the optical mode intensity.

Much of the work accomplished from this grant concerned the development and understanding of single-component high-power injection lasers. Our models of electromagnetic phenomena in nonplanar lasers have helped researchers in the laser field to push toward optimum designs. At this point in time, many possible structures can produce high powers. These include the channel-substrate-planar (CSP), the constricted-double-heterojunction large-optical-cavity (CDH-LOC), and others. In terms of modeling the various devices, the CDH-LOC laser is the most difficult. We discuss some of its properties below. Extension of these models to other nonplanar lasers such as the CSP is easily accomplished.

MODELS OF NONPLANAR SEMICONDUCTOR LASERS

The CDH-LOC laser provides[1,2] high single-mode power because of the nonplanarity of the various epitaxially grown layers. Because this device is nonplanar, it is very difficult to model many of its subtle characteristics. However, our model of the CDH-LOC optical modes is confirmed by excellent fits of theoretically generated far-field patterns to experimental ones. A major finding discovered by our model was the combined effect of lateral variations in transverse (optical) confinement factor,[3] Γ, and gain-induced index depressions on lateral mode control.

Figure 1 depicts schematically the basic geometry of CDH-LOC devices: a "convex-lens-shaped" active layer atop a "concave-lens-shaped" guide layer. The bulk refractive indices are such that $n_1 > n_2 > n_3 > n_4$. We have shown[4] that such structures translate into passive W-shaped lateral waveguides. Unlike the waveguiding structures usually analyzed,[2] the W-

guide has no known solutions of the wave equation. Thus it was necessary to employ numerical methods to solve Maxwell's equations for arbitrary dielectric profiles, and thus to solve for the lateral mode content of the W-guides as described below.

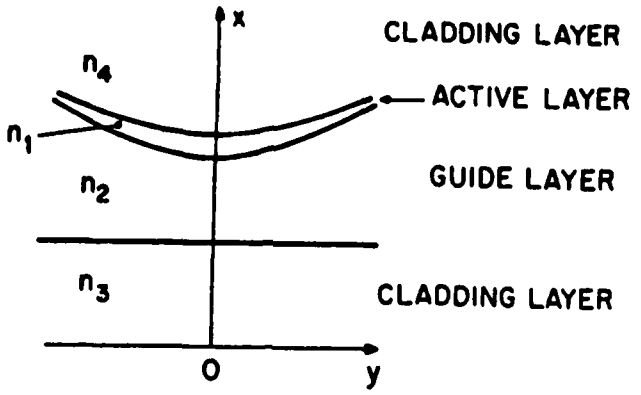

Fig. 1 Cross section of a constricted-double-heterojunction laser with a large-optical-cavity. Light is confined to the regions 1 and 2 and to the lateral region near y = 0.

Solutions to Maxwell's equations were restricted to fields polarized along the junction with $E(x,y) = f(x,y)\ h(y)\ exp(j\omega t - \gamma z)$ where $f(x,y)$ and $h(y)$ describes the transverse and lateral fields respectively. The lateral modes are obtained from a solution of

$$d^2h/dy^2 = [\gamma^2 - \gamma_0^2 + k_0^2\ \Gamma(y)\ \delta\kappa_1(y)]h = 0 \qquad (1)$$

where $k_0 = 2\pi/\lambda_0$, with λ_0 the free-space wavelength and $\delta\kappa_1(y)$ is the current dependent change in the complex dielectric constant of the active layer. The passive structures have $\delta\kappa_1 = 0$. γ_0 is the one-dimensional propagation constant that determines the effective index of the passive structure, n_{eo} ($n_{eo} = j\gamma_0/k_0$); and γ is the two-dimensional propagation

constant to be determined. The values of $\delta\kappa_1$ are found from the current distribution flowing into the active layer. An estimate of the current spreading was obtained by numerically solving an approximate circuit model.[5,6] We found the current to be virtually flat under the *10* μm-wide contact stripe, and tapering to half maximum at approximately 5 μm from the contact stripe edges. Using the current distribution in the active layer, we can write the gain[7]

$$g(y) = 45\ J_{eff}(y)/d(y) - 190\ (cm^{-1}) \qquad (2)$$

where $J_{eff}(kA/cm^2)$ is the effective current density, and $d(y)$ is the active layer thickness. The gain affects both the imaginary and real parts of the dielectric constant[2]:

$$\delta\kappa_1(y) = 2n_1\delta n_1(y) + j\delta n_1\ g(y)/k_0 \qquad (3)$$

where $\delta n_1(y)$ is the gain-induced index change in the active layer. (It is proportional to the carrier injection.) Since $\delta n_1(y)$ is generally found to be negative we refer to it as gain-induced index depression. The net (*real*) effective index that characterizes the lateral field is

$$n_{eff}(y) = n_{eo}(y) + \Gamma(y)\ \delta n_1(y) \qquad (4)$$

If we assume that the background absorption coefficient α_0 in the unpumped active regions is *190* cm^{-1} we have for δn_1 the following *ad hoc* relationship

$$\delta n_1 = R\ (g(y) + 190)\ cm^{-1}\ /k_0 \qquad (5)$$

with *R* being the ratio of index changes to normalized gain changes, also known as antiguiding factor.[8,9] Finally, by using *(2)* and *(5)* we obtain

$$\delta n_1(y) = 45\ R\ J_{eff}(y)/k_0 d(y) \qquad (6)$$

The analysis was applied to two different high-power CDH-LOC structures. Active and guide-layer thicknesses were accurately measured in the lateral direction, over the range $10\ \mu m < y < 10\ \mu m$, by using 5^o angle-lapped stained cross-sections. The Al content of the various $Al_xGa_{1-x}As$ layers was determined from photoluminescence data. The layers varied laterally in thickness as shown in Fig. 1 (For one geometry the guide layer was asymmetric due to substrate misorientation effects on growth.[10]) With the structures fully characterized, the confinement factor $\Gamma(y)$ and the effective index $n_{eo}(y)$ are determined by solving for the transverse modes at each lateral data point. The $\Gamma(y)$ plots for the two structures are shown in Figs. 2 (a) and (c). In the same figures we plot the respective net effective refractive index profiles, $n_{eff}(y)$ (i.e., W-guides). Both the passive contribution $n_{eo}(y)$ and the active contribution, $\Gamma(y)\ \delta n_1(y)$, are considered. While n_{eo} and Γ were known, $\delta n_1(y)$ had to be deduced from fitting of theoretical far-field patterns to experimental ones (see Figs. 2 (b) and (d)). Thus we obtain for the two structures at threshold $\delta n_1(0)$ values of -0.028 and -0.02, which agree with δn_1 values determined by other workers[11,12] from different experiments. The gain in the active layer at threshold was set at $50\ cm^{-1}$ to offset end and internal cavity losses. Having generated the proper W-guides, we then solved the wave equation numerically for the lateral modes. Radiation patterns were determined from the Fourier Transform of the near fields.

As far as the discrimination against high-order mode oscillation, two features of Figs. 2 (a) and (c) are relevant: 1) $\Gamma(y)$ peaks at y = 0 and drops relatively fast across the lasing region (5-7 μm wide); and 2) $n_{eff}(y)$ profiles are W-guides. Both features favor oscillation in the fundamental mode over the first-order mode. It should be stressed that the

major effect of the gain-induced index depressions is to change the n_{eff} profile form a mild W-guide to a strong one. This result follows because the contribution of the gain-induced index depressions, $\delta n_1(y)$, to the net effective index (Eq. (4)) is weighted by the strongly varying $\Gamma(y)$ function. Thus, upon applying gain the center of the "built-in" W-guide is depressed more than its wings. In turn high-order modes are further suppressed. Since the $\Gamma(y)$ profile is virtually drive independent it follows that in CDH-LOC devices, we have a stable waveguide mode. By contrast, planar-stripe lasers do not have a built-in lateral variation in Γ, and thus are vulnerable to drive.

The far-fields were fitted by adjusting only one parameter: R(see Eq. (5). For run DB-208 (Fig. 2(b)) side lobes at 10^o, indicative of radiative leakage, could only be fit for R =-4. Run DB-181 (Fig. 2d) had no leakage for the fundamental mode since the central region of the W-guide was wide. Yet a lateral beamwidth of approximately 6^o could be fitted only for R values in the -3 to -4 range. Once R was determined, n_1 was obtained from (6), which in turn allows the generation of the actual W-guides.

The lateral modal content of the two structures for R values of practical interest and threshold mode gain of 50 cm^{-1} is as follows: only the fundamental mode for run DB-208; and three modes for run DB-181. Figure 2 (e) shows the threshold current density for the first two modes of DB-181 lasers as a function of the antiguiding factor R. We also plot the index depression at the center of the waveguide for various J_{eff} and R values. Note that the fundamental mode (i.e., Oth order mode) has a relatively constant threshold current density for all R values of practical interest. On the other hand, the first order mode has an abrupt

discontinuity at $R = -2.9$. Above that value the first order mode is being "pushed out" of the central index guiding region. Thus, the current density must be increased to large values in order to re-establish the mode. From a practical stand point we can consider the first-order mode to be cut off at $R = -2.9$. It is thus apparent that by varying the gain-induced index depression one can choose between multi-mode and fundamental-mode operation. Changes in n_1 can be incurred *via* changes in device length, facet(s) reflectivity and/or ambient temperature.

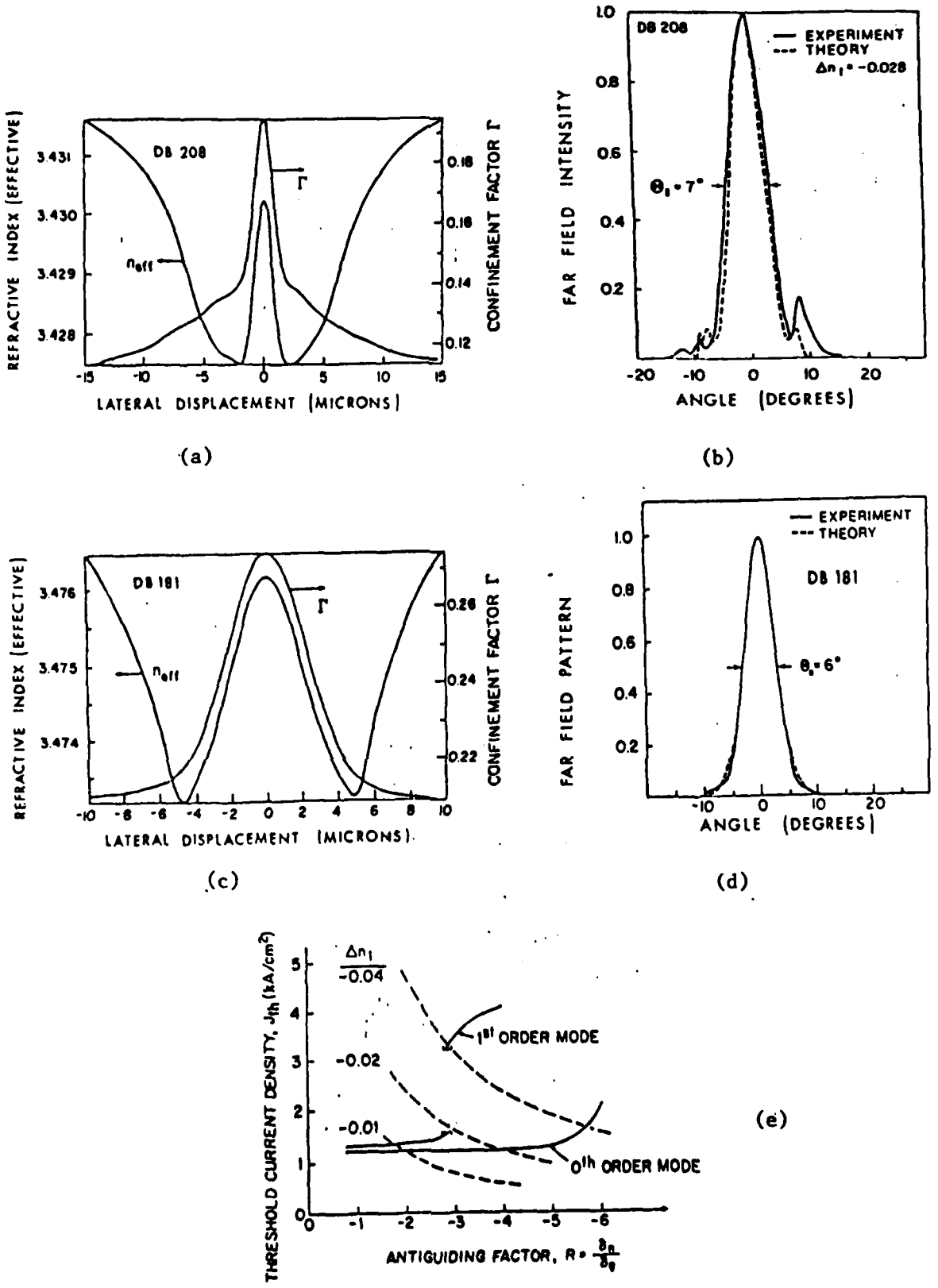

Fig. 2 Optical modes of CDH-LOC laser structures are calculated by the effective index method. (a) and (c) are for two different lasers. (b) and (d) show the experimental and theoretical far-field patterns. "Mode cutoff" conditions for DB 181 can be estimated from (e).

REFERENCES

1. D. Botez, "CW high-power single-mode operation of constricted double-heterojunction AlGaAs lasers with large optical cavity," *Appl. Phys. Lett.*, vol. 36, pp. 190-192, Feb. 1980.

2. J. K. Butler and D. Botez, "Mode characteristics of nonplanar double-heterojunction and large-optical-cavity laser structures," *IEEE J. Quantum Electron.*, vol. QE-18, pp. 952-961, June 1962.

3. H. Kressel and J. K. Butler, **Semiconductor Lasers and Heterojunction LED's**, Academic Press, New York, 1977.

4. D. Botez, J. K. Butler and J. C. Connolly, "Proc. 3rd International Conference on Integrated Optics and Optical Fiber Communications," Paper MB5, San Francisco, California, April 1981.

5. H. S. Sommers, Jr. and D. O. North, "Experimental and theoretical study of the spatial variation of junction voltage and current distribution in narrow stripe injection lasers," *J. Appl. Phys.*, vol. 48, pp. 4460-4467, Nov. 1977.

6. J. E. A. Whiteaway, "Theoretical analysis of current spreading in stripe-geometry injection lasers," *IEE Proc.*, Part I, vol. 129, pp. 89-95, June 1982.

7. F. Stern, "Calculated spectral dependence of gain in excited GaAs," *J. Appl. Phys.*, vol. 47, pp. 5382-5386, Dec. 1976.

8. J. K. Butler and J. B. Delaney, "A rigorous boundary value solution for the lateral modes of stripe geometry injection lasers," *IEEE J. Quantum Electron.*, vol. QE-14, pp. 507-513, July 1978.

9. J. Buus, "The effective index method and its application to semiconductor lasers," *IEEE J. Quantum Electron.*, vol. QE-18, pp. 1083-1089, July 1982.

10. D. Botez, "Constricted double-heterojunction AlGaAs diode lasers: structures and electrooptical characteristics," *IEEE J. Quantum Electron.*, vol. QE-17, pp. 2290-2309, Dec. 1980.

11. J. S. Manning and R. Olshansky, "Waveguiding in oxide-isolated stripe-geometry diode lasers," *J. Appl. Phys.*, vol. 53, pp. 840-842, Feb. 1982.

12. C. H. Henry, R. A. Logan and K. A. Bertness, "Spectral dependence of the change in refractive index due to carrier injection in GaAs lasers," *J. Appl. Phys.*, vol. 52, pp. 4457-4461, July 1981.

4. SUPPORTED PERSONNEL INVOLVEMENT

1. Dr. Jerome K. Butler, Principal Investigator.

2. Dr. Joseph B. Delaney, Doctoral Student, Received a Ph.D. in August 1980.

3. Dr. Alfredo Linz, Doctoral Student, Received a Ph.D. in May 1984.

4. Mr. George Hagicostas, Master Degree Student, Near completion of MSEE.

5. RESEARCH PROJECT PUBLICATIONS

1. J. K. Butler, and J. B. Delaney, "Field Solutions for the Lateral Modes of Stripe Geometry Injection Lasers," *IEEE J. Quantum Electron.*, Vol. QE-16, pp. 1326-1328, December 1980.

2. D. Botez, J. K. Butler and J. C. Connolly, "Single Mode Control in High-Power CDH-LOC Diode Lasers: The W-Shaped Lateral Waveguide," 1981 IOOC, San Francisco, California.

3. J. K. Butler and D. Botez, "Mode Characteristics of Nonplanar Double-Heterojunction and Large-Optical-Cavity Laser Structures," *IEEE J. Quantum Electron.*, Vol. QE-18, pp. 952-961, June 1982.

4. A. Linz and J. K. Butler, "Comparison of Numerical and Effective-Index Methods for a Class of Dielectric Waveguides," *1982 IEEE-MTTS Digest* (1982 International MTT Symposium), June 15-17, 1982, Dallas, Texas.

5. A. Linz and J. K. Butler, "Modal Solutions of Active Dielectric Waveguides by Approximate Methods," *IEEE Trans. Microwave Theory and Techniques*, Vol. MTT-30, December 1982.

6. J. B. Delaney, R. R. Shurtz, II and J. K. Butler, "Prediction of Transverse Mode Selection in Double Heterojunction Lasers by an Ambipolar Excess Carrier Diffusion Solution," *J. Appl. Phys.*, Vol. 54, pp. 540-549, February 1983.

7. A. Linz and J. K. Butler, "Application of a General Purpose Circuit Simulation Program to Semiconductor Laser Modeling - Part I: Electrical Analysis," Manuscript in Preparation, Abstract Attached.

8. A. Linz and J. K. Butler, "Application of a General Purpose Circuit Simulation Program to Semiconductor Laser Modeling _ Part II: Diffusion Analysis," Manuscript in Preparation, Abstract Attached.

9. A. Linz, J. K. Butler and K. W. Heizer, "An Integrated Electrical/Diffusion Model for the P-N Junction," Manuscript in Preparation, Abstract Attached.

APPENDIX A

PROGRESS REPORTS

PROGRESS REPORT

(TWENTY COPIES REQUIRED)

1. ARO PROPOSAL NUMBER: AMXRO-PRI-16436-EL

2. PERIOD COVERED BY REPORT: 1 May 1980 to 30 June 1980

3. TITLE OF PROPOSAL: Injection Laser Structure Design

---

4. CONTRACT OR GRANT NUMBER: DAAG29-80-K-004

5. NAME OF INSTITUTION: Southern Methodist University

6. AUTHOR(S) OF REPORT: Jerome K. Butler

7. LIST OF MANUSCRIPTS SUBMITTED OR PUBLISHED UNDER ARO SPONSORSHIP DURING THIS PERIOD, INCLUDING JOURNAL REFERENCES:
J. K. Butler and J. B. Delaney, "Field Solutions for the Lateral Modes of Stripe Geometry Injection Lasers," Sub. To IEEE J. Quan. El.

8. SCIENTIFIC PERSONNEL SUPPORTED BY THIS PROJECT AND DEGREES AWARDED DURING THIS REPORTING PERIOD:
J. K. Butler
J. B. Delaney

Dr. Jerome K. Butler 16436-El
Southern Methodist University
Department of Electrical Engineering
Dallas, TX 75275

BRIEF OUTLINE OF RESEARCH FINDINGS

The research carried out over this past period involved the exploration of the field solutions obtained by a rigorous method developed by the Principal Investigator. A highlight of our work shows that stripe geometry laser modes have characteristics that are similar to leaky waveguide modes. In our previous work we assumed that the dielectric profile in the injection laser had a parabolic functional variation along the lateral direction(parallel to the junction plane). Although the parabolic profile has been extensively used by previous investigators, it has definite realistic limitations. In our present work we are developing a model using a dielectric profile which can more accurately characterize the true one. For example, at large lateral distances (away from the current injecting contact) the dielectric constant must approach a limiting value; in the parabolic profile the dielectric constant continues increasing/decreasing dramatically with lateral distances.

PROGRESS REPORT

(TWENTY COPIES REQUIRED)

1. ARO PROPOSAL NUMBER: AMXRO-PRI-16436-EL

2. PERIOD COVERED BY REPORT: July 1, 1980 to December 31, 1980

3. TITLE OF PROPOSAL: Injection Laser Structure Design

4. CONTRACT OR GRANT NUMBER: DAAG29-80-K-004

5. NAME OF INSTITUTION: Southern Methodist University

6. AUTHOR(S) OF REPORT: Jerome K. Butler

7. LIST OF MANUSCRIPTS SUBMITTED OR PUBLISHED UNDER ARO SPONSORSHIP DURING THIS PERIOD, INCLUDING JOURNAL REFERENCES:

J. K. Butler and J. B. Delaney, "Field Solutions for the *Lateral Modes of Stripe Geometry Injection Lasers*," IEEE J. Quantum El. QE-16, p.1326, Dec. 1980.

D. Botez, J. K. Butler and J. C. Connolly, "Single-Mode Control in High-Power CDH-LOC Diode Lasers: The W-Shaped Lateral Waveguide," Submitted to IOOC Conf.1981, San Francisco.

8. SCIENTIFIC PERSONNEL SUPPORTED BY THIS PROJECT AND DEGREES AWARDED DURING THIS REPORTING PERIOD:

Jerome K. Butler
Joseph B. Delaney
Ph.D. awarded to J. Delaney.

Dr. Jerome K. Butler 16436-El
Southern Methodist University
Department of ELectrical Engineering
Dallas, TX 75275

PROGRESS REPORT

(TWENTY COPIES REQUIRED)

1. ARO PROPOSAL NUMBER: AMXRO-PRI-16436-EL

2. PERIOD COVERED BY REPORT: January 1, 1981 to June 30, 1981

3. TITLE OF PROPOSAL: Injection Laser Structure Design

4. CONTRACT OR GRANT NUMBER: DAAG29-80-K-004

5. NAME OF INSTITUTION: Southern Methodist University

6. AUTHOR(S) OF REPORT: Jerome K Butler

7. LIST OF MANUSCRIPTS SUBMITTED OR PUBLISHED UNDER ARO SPONSORSHIP DURING THIS PERIOD, INCLUDING JOURNAL REFERENCES:

D. Botez, J. K. Butler and J. C. Connolly, "Single-Mode Control in High Power CDH-LOC Diode Lasers. The W Shaped Lateral Waveguide," 1981 IOOC, San Francisco, Calif

8. SCIENTIFIC PERSONNEL SUPPORTED BY THIS PROJECT AND DEGREES AWARDED DURING THIS REPORTING PERIOD:

Jerome K. Butler
Alfredo Linz

Dr. Jerome K. Butler 16436-EL
Southern Methodist University
Department of Electrical Engineering
Dallas, TX 75275

BRIEF OUTLINE OF RESEARCH FINDINGS

The work during this past period has been aimed at an understanding of the lateral mode structure in CDH-LOC and stripe geometry lasers. The CDH-LOC devices are basic high power lasers with large optical cavities. Important cavity dimensions are: (1) thickness between heterojunctions that confine the light and (2) the width of the active region which is dictated by the injection current spread. The important results of the study during this period are that structures can be designed with varying cavity thicknesses aimed at the control of lateral modes. Ordinarily, lateral modes are not affected by cavity thicknesses.

We have had several verbal inquiries concerning the results of our recent publication in the Journal of Quantum Electronics. This publication is the first to predict how lateral mode structures are affected by thin optical waveguides. Previous publications have linked radiation pattern sidelobes to leaky modes while we have shown these lobes result from a "mode mixture", a requirement for a proper boundary value solution to the wave equation.

BRIEF OUTLINE OF RESEARCH FINDINGS

The work in this past period has been directed toward the extension of lateral mode analysis in constricted double heterojunction-large-optical (CDH-LOC) devices. These devices are fabricated in such a fashion that the active region as well as the optical mode confining region vary in thickness as a function of lateral position. These lasers are far superior in performance when compared to other injection laser devices. CDH-LOC lasers have excellent power output and spectral purity. (Device powers around 100 mwatts radiate in a single mode.) The Principal Investigator is presently preparing the analysis of CDH-LOC lasers in conjunction with the experimental program at RCA Laboratories.

Concurrent with the above work, we are extending the analysis of the exact mathematical solution of two dimensional modes in dielectric waveguides. It should be mentioned that there are published results for exact mode solutions only for (1) optical fibers, (2) dielectric waveguides of rectangular cross-section, and (3) slab waveguides with localized lateral gain distributions. (The latter work was previously reported by the PI.)

PROGRESS REPORT

(TWENTY COPIES REQUIRED)

1. ARO PROPOSAL NUMBER: AMXRO-PRI-16436-EL

2. PERIOD COVERED BY REPORT: 1 July, 1981 - 31 December, 1981

3. TITLE OF PROPOSAL: Injection Laser Structure Design

4. CONTRACT OR GRANT NUMBER: DAAG29-80-K-004

5. NAME OF INSTITUTION: Southern Methodist University

6. AUTHOR(S) OF REPORT: Jerome K. Butler

7. LIST OF MANUSCRIPTS SUBMITTED OR PUBLISHED UNDER ARO SPONSORSHIP DURING THIS PERIOD, INCLUDING JOURNAL REFERENCES:

   J.K. Butler and D. Botez, "Mode Characteristics of Non-Planar Double-Heterojunction and Large-Optical Cavity Laser Structures," I.E.E.E. J. Quan. Electron. (Accepted for publication)

   A. Linz and J.K. Butler, "Comparison of Numerical and Effective Index Methods for a Class of Dielectric Waveguides," Submitted to 1982 International Symposium of Microwave Theory and Techniques.

8. SCIENTIFIC PERSONNEL SUPPORTED BY THIS PROJECT AND DEGREES AWARDED DURING THIS REPORTING PERIOD:

   J.K. Butler

   A. Linz

Dr. Jerome K. Butler 16436-EL
Southern Methodist University
Department of Electrical Engineering
Dallas, TX 75275

BRIEF OUTLINE OF RESEARCH FINDINGS

During this past six months much effort has been spent on the development of : (1) an understanding of leaky wave structures found in contemporary high-power injection lasers, and (2) the integrity of the effective index method which is widely used in integrated optics.

The work reported in the first paper listed above contains extensive information on the analysis of leaky mode lasers. This work is the first to report and to properly analyze devices lasing in a true leaky mode. It was previously believed that leaky modes could not reach threshold because of their lossy nature.

The work reported in the second publication compares the modal solutions of a class of dielectric waveguides, obtained by exact and effective index methods. The waveguides studied are those which closely approximate actual guides designed for injection lasers. Our conclusion is that the effective index method is excellent for waveguide analysis.

MODE CHARACTERISTICS OF NON-PLANAR DOUBLE-HETEROJUNCTION AND LARGE-OPTICAL-CAVITY LASER STRUCTURES

J. K. Butler* and D. Botez
RCA Laboratories
Princeton, NJ 08540

Abstract

Mode behavior of non-planar double-heterojunction (DH) and large-optical-cavity (LOC) lasers is investigated using the effective index method to model the lateral field distribution. The thickness variations of various layers for the devices discussed are correlated with the growth characteristics of liquid-phase epitaxy over topographical features (channels, mesas) etched into the substrate. The effective dielectric profiles of constricted double-heterojunction (CDH)-LOC lasers show a strong influence on transverse mode operation: the fundamental transverse mode (i.e., in the plane perpendicular to the junction) may be laterally index-guided while the first (high)-order mode is laterally index-antiguided. The analytical model developed uses a smoothly varying hyperbolic cosine distribution to characterize lateral index variations. The waveguide model is applied to several lasers to illustrate conditions necessary to convert leaky modes to trapped ones via the active-region gain distribution. Theoretical radiation patterns are calculated using model parameters, and matched to an experimental far-field pattern.

This work has been partially supported by the U. S. Army Research Office under Grant No. DAAG29-80-K-004 and by NASA, Langley Research Center, Hampton, VA under Contract No. NAS1-15440.

*Permanent address: Southern Methodist University
Dallas, TX 75275

Comparison of Numerical and Effective Index Methods for a Class of Dielectric Waveguides*

A. Linz and J. Butler

Electrical Engineering Department

Southern Methodist University

Dallas, Texas 75275

Abstract

A numerical method and the effective-index method are applied to a three-layer dielectric waveguide with Eckart type dielectric constant variation in the active layer. The results of the 2 methods are compared in terms of the propagation constant γ.

* Supported by U.S. Army Research Office

PROGRESS REPORT

(TWENTY COPIES REQUIRED)

1. ARO PROPOSAL NUMBER: AMXRO-PRI-16436-EL

2. PERIOD COVERED BY REPORT: 1 January 1982 - 30 June 1982.

3. TITLE OF PROPOSAL: Injection Laser Structure Design

4. CONTRACT OR GRANT NUMBER: DAAG29-80-K-004

5. NAME OF INSTITUTION: Southern Methodist University

6. AUTHOR(S) OF REPORT: Jerome K. Butler

7. LIST OF MANUSCRIPTS SUBMITTED OR PUBLISHED UNDER ARO SPONSORSHIP DURING THIS PERIOD, INCLUDING JOURNAL REFERENCES:

   Attached

8. SCIENTIFIC PERSONNEL SUPPORTED BY THIS PROJECT AND DEGREES AWARDED DURING THIS REPORTING PERIOD:
   J. K. Butler
   A. Linz

Dr. Jerome K. Butler 16436-EL
Southern Methodist University
Department of Electrical Engineering
Dallas, TX 75275

BRIEF OUTLINE OF RESEARCH FINDINGS

In the work over the last period we have continued the investigation of approximate methods used for the analysis of mode characteristics of injection laser devices. We have reported that contemporary injection lasers with wide active regions can be accurately modelled with the effective index method. This is a very important result since many new lasers have non-planar layers; the effective index method affords a convenient mode analysis procedure. It should be noted however, that there are no exact methods for analyzing modes of non-planar laser structures. It is assumed that since approximate and exact calculations of mode character on planar structures produce almost identical results, that the approximate solutions are satisfactory for non-planar devices.

In our last publication we have theoretically predicted transverse mode operation of a multimode laser. Mode operation was predicted by calculation of the coupling between the optical field and injected charge density. We experimentally investigated mode switching by heating a diode laser; at low temperatures the device operated in the first high order mode while at high temperatures, fundamental mode operation was observed. The prediction of switching was tied to the fact that the optical field/charge distribution coupling are temperature sensitive.

7. J. K. Butler and D. Botez, "Mode Characteristics of Nonplanar Double-Heterojunction and Large-Optical-Cavity Laser Structures," IEEE J. Quantum Electron., Vol. QE-18, pp. 952-961, June 1982.

A. Linz and J. K. Butler, "Comparison of Numerical and Effective-Index Methods for a Class of Dielectric Waveguides," 1982 IEEE-MTTS Digest (1982 International MTT Symposium, June 15-17, 1982, Dallas, TX.

A. Linz and J. K. Butler, "Modal Solution of Active Dielectric Waveguides by Approximate Methods," IEEE Trans on Microwave Theory and Techniques, Submitted for publication.

J. B. Delaney, R. R. Shurtz, II, and J. K. Butler, "Prediction of Transverse Mode Selection in Double Heterojunction Lasers by an Ambipolar Excess Carrier Diffusion Solution," J. Appl. Phys., Submitted for publication.

Modal Solutions of Active Dielectric Waveguides by Approximate Methods

A. Linz and J.K. Butler
Electrical Engineering Department
Southern Methodist University
Dallas, Texas 75275

Abstract

Approximate methods are used to obtain the modal properties of stripe-contact semiconductor injection lasers using a planar three-layer waveguide model. The central active layer has a dielectric constant that varies smoothly along the direction parallel to the heterojunction boundaries. The complex dielectric constant under the stripe contact is dependent on the gain and approaches a constant value at large lateral distances. The two methods are compared in terms of their modal propagation constants. An application of the effective index method facilitates a physical understanding of dielectric waveguide modes as well as providing an efficient calculation procedure.

*Supported by the U.S. Army Research Office

PREDICTION OF TRANSVERSE MODE SELECTION IN DOUBLE HETEROJUNCTION LASERS BY AN AMBIPOLAR EXCESS CARRIER DIFFUSION SOLUTION*

by

Joseph B. Delaney
TRW Optron
Carrollton, Texas 75006

Richard R. Shurtz, II
Night Vision and Electro-optics Laboratory
Laser Division
Fort Belvoir, Virginia 22060

Jerome K. Butler
Southern Methodist University
Dallas, Texas 75275

ABSTRACT

Transverse mode selection is characterized for GaAs/AlGaAs double heterojunction lasers from optical field and electron/hole interaction. The electron/hole distribution determined from a solution of the ambipolar diffusion equation provides the necessary information about gain/mode coupling to predict the current at threshold. Lasing power out versus current solutions provide information about internal differential quantum efficiency. Theory is matched to experiment for a multimode laser with one heterojunction having a very small index step. It is found that the laser's characteristics over a temperature and current range are predicted by adjusting the active layer refractive index as determined from far field measurements.

* Supported in part by the U.S. Army Research Office.

PROGRESS REPORT

(TWENTY COPIES REQUIRED)

1. ARO PROPOSAL NUMBER: AMXRO-PRI-16436-EL

2. PERIOD COVERED BY REPORT: 1 July 1982 - 31 December 1982

3. TITLE OF PROPOSAL: Injection Laser Structure Design

4. CONTRACT OR GRANT NUMBER: DAAG29-80-K-004

5. NAME OF INSTITUTION: Southern Methodist University

6. AUTHOR(S) OF REPORT: Jerome K. Butler

7. LIST OF MANUSCRIPTS SUBMITTED OR PUBLISHED UNDER ARO SPONSORSHIP DURING THIS PERIOD, INCLUDING JOURNAL REFERENCES:

A. Linz and J. K. Butler, "Modal Solutions of Active Dielectric Waveguides by Approximate Methods," IEEE Trans. Microwave Theory and Techniques, Vol. MTT-30, December 1982

J. B. Delaney, R. R. Shurtz, II and J. K. Butler, "Prediction of Transverse Mode Selection in Double Heterojunction Lasers by an Ambipolar Excess Carrier Diffusion Solution," J. Appl. Phys, To Be Published, February 1982.

8. SCIENTIFIC PERSONNEL SUPPORTED BY THIS PROJECT AND DEGREES AWARDED DURING THIS REPORTING PERIOD:

J. K. Butler
A. Linz

Dr. Jerome K. Butler 16436-EL
Southern Methodist University
Department of Electrical Engineering
Dallas, TX 75275

BRIEF OUTLINE OF RESEARCH FINDINGS

The work over this last period has been concerned with both the theoretical and experimental characterization of high-power semiconductor laser devices. These lasers will have extensive applications in military communication and data processing systems. The particular devices modelled are the constricted-double-heterojunction large-optical-cavity (CDH-LOC) lasers which are fabricated at RCA Laboratories. These lasers have the highest output power (approximately 50 mW in continuous operation) of any contemporary injection laser. Furthermore, their operational range for single mode lasing is excellent. Our laboratory has developed the most comprehensive theoretical model of the modal characteristics of CDH-LOC devices.

Typically, reasonable theoretical/experimental performance comparisons are made via the far field radiation patterns. To augment our theory we have developed computer controlled apparatus for taking far-field data in two dimensions. For example, the attached figure shows the experimental pattern of a typical CDH-LOC laser where θ and ϕ are the two transverse angles in the far field. (The main lobe peaks at $\theta = \phi = 0$.)

We are now developing software to transmit the experimental data to a large computer for the purpose of theoretical/experimental comparisons. The addition of these laboratory experiments to our program will expedite our understanding of high-power injection lasers and thus improve our overall theoretical modelling capabilities.

DB 181 43

I_B = 100 mA

I_P = 10 mA

2.7 deg / slice

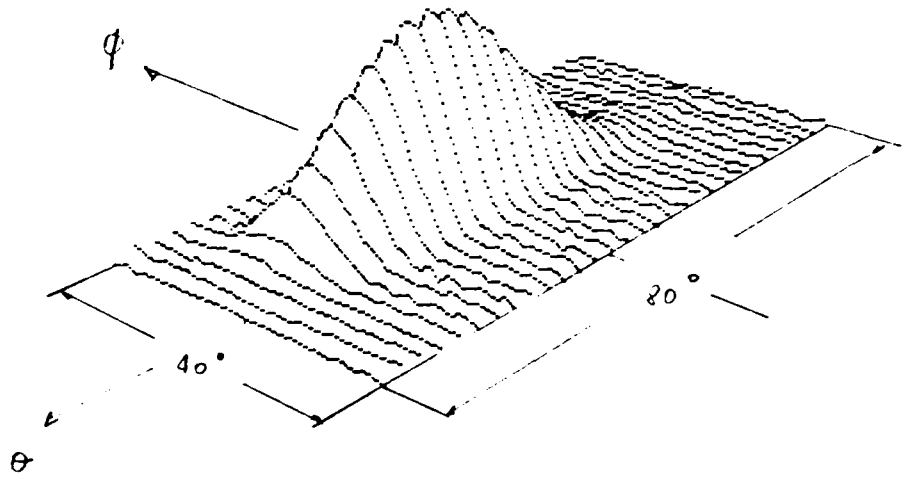

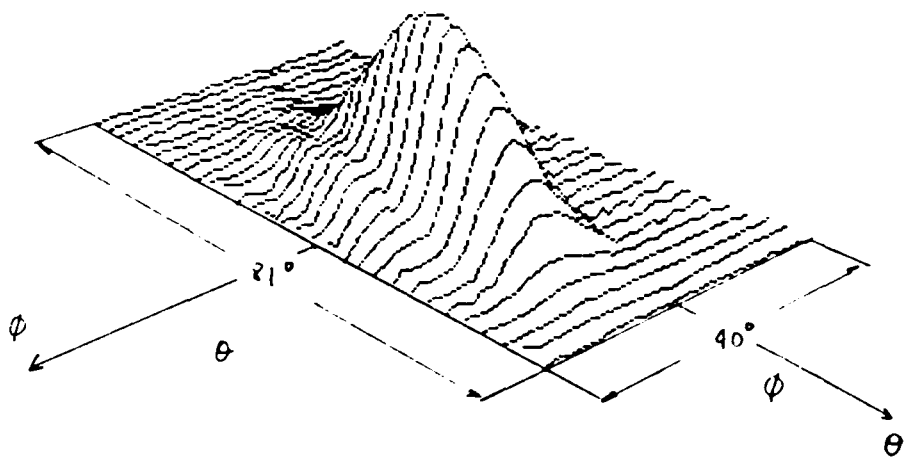

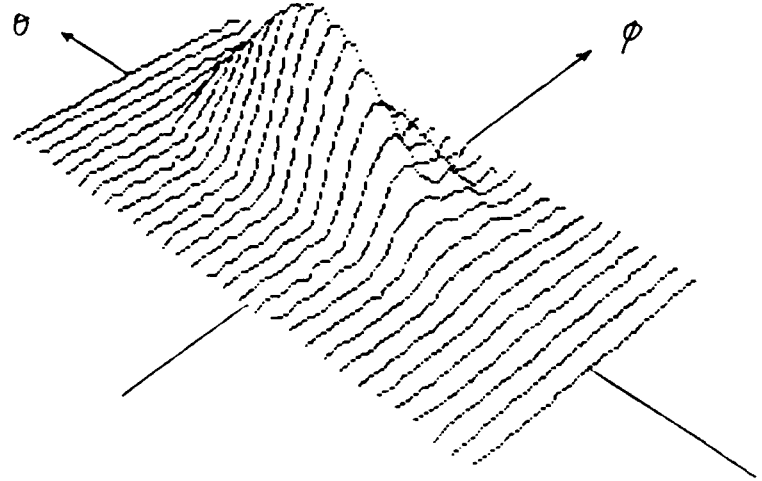

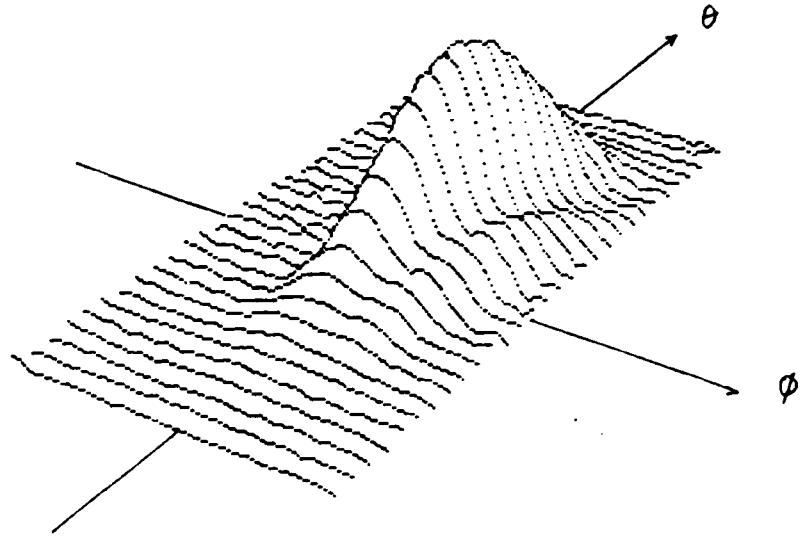

Modal Solutions of Active Dielectric Waveguides by Approximate Methods

A. Linz and J.K. Butler
Electrical Engineering Department
Southern Methodist University
Dallas, Texas 75275

Abstract

Approximate methods are used to obtain the modal properties of stripe-contact semiconductor injection lasers using a planar three-layer waveguide model. The central active layer has a dielectric constant that varies smoothly along the direction parallel to the heterojunction boundaries. The complex dielectric constant under the stripe contact is dependent on the gain and approaches a constant value at large lateral distances. The two methods are compared in terms of their modal propagation constants. An application of the effective index method facilitates a physical understanding of dielectric waveguide modes as well as providing an efficient calculation procedure.

PREDICTION OF TRANSVERSE MODE SELECTION IN DOUBLE HETEROJUNCTION LASERS BY AN AMBIPOLAR EXCESS DIFFUSION SOLUTION

by

J. B. Delaney
TRW Optoelectronics Division

R. R. Shurtz, II
Night Vision and Electro-optics Laboratory

J. K. Butler
Southern Methodist University

Abstract

Transverse-mode selection is characterized for GaAs/AlGaAs double heterojunction lasers from optical field and electron/hole interaction. The electron/hole distribution determined from a solution of the ambipolar diffusion equation provides the necessary information about gain/mode coupling to predict the current at threshold. Lasing power out versus current solutions provide information about internal differential quantum efficiency. Theory is matched to experiment for a multimode laser with one heterojunction having a very small index step. It is found that the laser's characteristics over a temperature and current range are predicted by adjusting the active-layer refractive index as detemined from far-field measurements.

APPENDIX B

PROJECT PUBLICATIONS

Field Solutions for the Lateral Modes of Stripe Geometry Injection Lasers

JEROME K. BUTLER, MEMBER, IEEE, AND JOSEPH B. DELANEY

Abstract—This paper compares the lateral mode patterns of stripe geometry lasers produced by two theories: 1) an approximate effective dielectric method and 2) an exact method. The exact method for calculating modes uses an expansion of Hermite-Gaussian functions. For small normalized frequencies and a depression of the refractive index under the stripe, the fundamental lateral mode shows structure usually associated with leaky waveguide modes.

A COMMON description of the lateral modes of a stripe geometry laser uses the Hermite-Gaussian (HG) function [1]-[8] while the transverse field dependence is dominated by the large index steps of the heterojunctions which sandwich the active layer. So far only two methods have been proposed to tie together the lateral and transverse field dependencies under the stripe. The first is the effective index method [7] and the second is an exact method [8]. The effective index method results in a single term lateral field description with appropriate "effective" parameters derived to account for the influence of the cladding layers on the lateral mode shape. The advantage of this representation is that a single term expression can easily be matched to such experimental observables as near- /far-field shapes and virtual waist positions. The exact description of the lateral mode takes into account the vertical geometry by matching the usual field quantities at the heterojunctions. The result is a lateral mode description by a linear combination of HG functions with appropriate weighting coefficients. This paper reports on a comparison of the two methods. A major difference between the two is the divergence of the modal shape when the lateral index is depressed under the stripe and the normalized frequency for the vertical geometry (see Fig. 1), $v = (d/2)\, k_0 (n_b^2 - n_a^2)^{1/2}$, is small. In general, the coefficients of the higher order HG functions rise in magnitude as more light escapes into the transverse cladding. For a negative depression in the lateral index, the higher order terms appear as shoulders on the near and far fields of the fundamental mode and the modal shape is deformed from the pure Gaussian. We begin with a brief recapitulation of the wave equation solutions of each method.

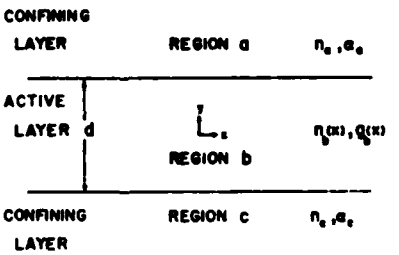

Fig. 1. Cross section of a stripe geometry laser.

The complex dielectric constant can be written as [7] (see Fig. 1)

$$\kappa(x,y) = \begin{cases} \kappa_b(x) = \kappa_0 - k_0^2 a^2 x^2, & |y| < \dfrac{d}{2} \\ \kappa_a = \kappa_c, & |y| > \dfrac{d}{2} \end{cases} \tag{1}$$

where κ_0 is the complex dielectric constant at $x = 0$, k_0 is the

Manuscript received October 1, 1979; revised August 4, 1980. This work was supported by the U.S. Army Research Office.

J. K. Butler is with Southern Methodist University, Dallas, TX 75275.
J. B. Delaney was with Southern Methodist University, Dallas, TX 75275. He is now with TRW Optron, Dallas, TX 75275.

0018-9197/80/1200-1326$00.75

free space wavenumber, and κ_a, κ_c are the dielectric constants of the cladding layers. The parameter "a" in (1) is defined as

$$a = \frac{(n_0 g_0)^{1/2}}{k_0 x_0} (2R + i10^{-4}/k_0)^{1/2} \tag{2}$$

$$R = \frac{\delta n}{\delta g} \text{ cm}. \tag{3}$$

x_0 is defined as the point at which gain has fallen to zero, i.e., $\delta g = g_0$. δn is the refractive index change at $x = x_0$. In the effective index method, the wave equation

$$\nabla_t^2 \Psi + [k_0^2 \kappa(x, y) + \gamma^2] \Psi = 0 \tag{4}$$

with

$$\Psi = \psi(x)\, \phi(y)\, e^{-\gamma z} \tag{5}$$

$$\frac{d^2\phi}{dy^2} = \begin{cases} -q^2\phi & |y| < \dfrac{d}{2} \\ p^2\phi & |y| > \dfrac{d}{2} \end{cases} \tag{6}$$

is multiplied by Ψ^* and integrated over $y\epsilon(-\infty, \infty)$ to yield an effective solution

$$k_0^2\kappa_0\Gamma + k_0^2\kappa_a(1-\Gamma) - q^2\Gamma + p^2(1-\Gamma) + \gamma^2 = k_0^2 a \Gamma^{1/2}(2l+1) \tag{7}$$

$$\psi(x) = H_l(a_{eff}^{1/2}\, k_0 x)\, e^{-1/2 a_{eff} k_0^2 x^2} \tag{8}$$

$$a_{eff} = \Gamma^{1/2} a \tag{9}$$

where Γ is the confinement factor

$$\Gamma = \int_{-d/2}^{d/2} \phi(y)\, \phi^*(y)\, dy \tag{10}$$

when $\phi^2(y)$ is normalized to unity, and

$$\phi(y) = A \begin{cases} \cos qy & |y| < \dfrac{d}{2} \\ \cos q\dfrac{d}{2}\, e^{p[(d/2)-|y|]} & |y| > \dfrac{d}{2}. \end{cases} \tag{11}$$

The quantities p and q are the eigenvalues of the slab waveguide. In [7], the equation corresponding to our (7) did not include the eigenvalue p. The integration over the y direction dictates an effective representation of $p^2(1-\Gamma) - q^2\Gamma$ as included in (7).

The exact method can be summarized [8]

$$\Psi = \sum_l A_l \cos(q_l y)\, H_l(a^{1/2} k_0 x)\, e^{-1/2 a k_0^2 x^2} \qquad |y| < \frac{d}{2}$$

$$= \int_0^\infty B(\chi) \cos \chi x \exp\left\{\left(\frac{d}{2} - y\right)(\chi^2 - k_0^2\kappa_a - \gamma^2)^{1/2}\right\} d\chi \qquad |y| > \frac{d}{2} \tag{12}$$

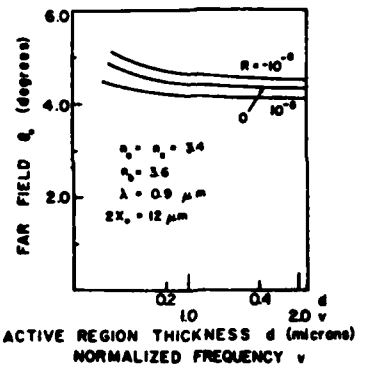

Fig. 2. Far field half-power full width $\theta_\perp$ versus normalized frequency v.

where $l = 0, 2, 4, \cdots$ for even modes. The vertical eigenvalue q_l satisfies

$$\gamma^2 = q_l^2 - k_0^2\kappa_0 + k_0^2 a(2l+1). \tag{13}$$

Parameters used in sample calculations are $n_a = n_c = 3.4$, $n_b(0) = 3.6$ $\lambda = 0.9$ μm, $G = 50$ cm^{-1}, and $\alpha_a = \alpha_c = 20$ cm^{-1}. Comparison of the two models begins with the gain. For the effective index method (7) can be used. The term $k_0^2(\kappa_0\Gamma + \kappa_a(1-\Gamma))$ is the effective dielectric constant, while $p^2(1-\Gamma) - q^2\Gamma$ represents an effective vertical eigenvalue. With $\gamma = -G/2 + i\beta$, the gain in the active region must include the mirror loss, losses in the cladding layers, and losses in the active layer represented by the right-hand side of (7). For instance, with $R < 0$, the gain region requires additional pumping to account for lateral refraction losses. Since these are the same losses accounted for by the exact technique, both methods calculate virtually the same peak gain values for all values of R investigated.

For $R > 0$, the near- and far-field structures coincide for both methods. A peculiarity of the patterns is the behavior as the normalized frequency v gets small ($d \to 0$). The far-field half-power full width $\theta_\perp$ is plotted in Fig. 2 versus active region width d. As the active region shrinks, peak gain values increase to satisfy additional losses. The parameter "a," as computed from (2), requires that the near field is pulled in and the far field spreads as the result of high cavity gain values.

The two methods diverge in modal shape for $R < 0$ and small normalized frequencies. For the refractive indexes of this work this corresponds to $d < 0.2$ μm. As power leakage to the cladding increases, the magnitude of the expansion coefficient A_2 increases as illustrated in Fig. 3. With $R < 0$, $|a_i| > |a_r|$, where $a = a_r + ia_i$, and shoulders develop on the fundamental mode patterns. An example of a far-field pattern evolution with $d = 0.1$ μm is shown in Fig. 4 where the dashed curve is the fundamental mode pattern for the effective method and the solid curve the fundamental mode pattern for the exact method. The negative value δn, computed from (3), is a measure of index change and antiguiding over the gain region. It can be seen that, for a value of $\delta n = -0.00185$ in Fig. 4(b), the shoulders on the far-field pattern are well developed. Since the Fourier transform of an HG function is an HG function, the near-field modal structure is theoretically similar to the shapes of Fig. 4. From Fig. 4(a) it would appear that there is no difference in the two models for $R = -10^{-6}$

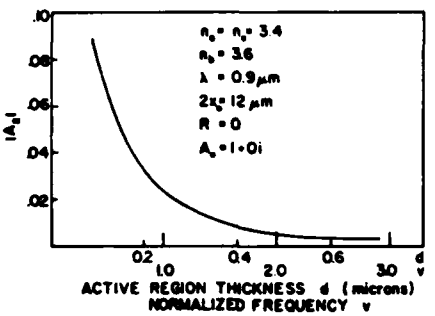

Fig. 3. Magnitude of the expansion coefficient A_2 versus normalized frequency v. As more light spreads vertically into the cladding layers, a larger percentage of higher order Hermite–Gaussian functions are needed to match appropriate fields at the heterojunctions.

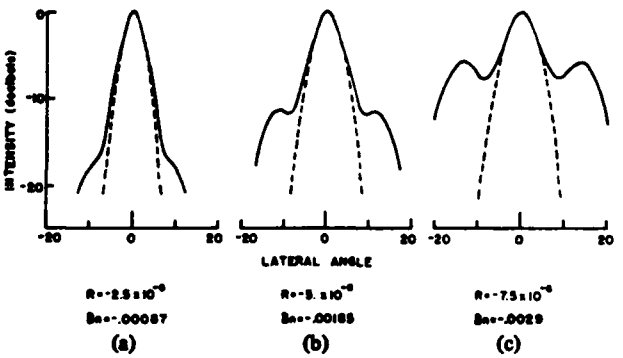

Fig. 4. Far-field lateral intensity of the fundamental mode. The dashed lines are for the effective method. For all curves $d = 0.1\,\mu m$, $n_a = n_c = 3.4$, $n_b = 3.6$.

and $d = 0.1\,\mu m$. In fact, since the modal shapes are so similar a curve for this case $R = -10^{-6}$ is included in Fig. 2. A final remark about Fig. 4 is that the position of the shoulders is predominately determined by the gain width $2x_0$ and not R. An index depression under the stripe, represented by a negative value of R, determines the intensity of the shoulders but not the lateral position.

In conclusion, we have briefly compared two solutions for a parabolic lateral dielectric constant in the active layer of a stripe geometry laser. Both solutions assume that the vertical dependence is due to the well defined index steps at the heterojunctions. The effective and exact methods predict the same peak gain values since both satisfy the same loss mechanisms. The two methods diverge in modal shape for the case of a depression in the refractive index in the gain region below the stripe and small normalized frequencies. Matching the fields at the vertical heterojunctions results in a fundamental modal shape that has shoulders on both the near- and far-field patterns in the case of lateral antiindexing guiding.

References

[1] T. H. Zachos and J. E. Ripper, "Resonant modes of GaAs junction lasers," *IEEE J. Quantum Electron.*, vol. QE-5, pp. 29–37, Jan. 1969.

[2] T. L. Paoli, J. E. Ripper, and T. H. Zachos, "Resonant modes of GaAs junction lasers II; High-injection level," *IEEE J. Quantum Electron.*, vol. QE-6, pp. 271–276, June 1969.

[3] F. R. Nash, "Mode guidance parallel to the junction plane of double-heterostructure GaAs lasers," *J. Appl. Phys.*, vol. 44, pp. 4696–4707, Oct. 1973.

[4] B. W. Hakki, "Carrier and gain spatial profiles in GaAs stripe geometry lasers," *J. Appl. Phys.*, vol. 44, pp. 5021–5028, Nov. 1973.

[5] D. D. Cook and F. R. Nash, "Gain-induced guiding and astigmatic output of GaAs laser," *J. Appl. Phys.*, vol. 46, pp. 1661–1672, Apr. 1975.

[6] P. A. Kirkby, A. R. Goodwin, C. H. B. Thompson, and P. R. Selway, "Observations of self-focusing in stripe geometry semiconductor lasers and the development of a comprehensive model of their operation," *IEEE J. Quantum Electron.*, vol. QE-13, pp. 705–719, Aug. 1977.

[7] T. L. Paoli, "Waveguiding in a stripe-geometry junction laser," *IEEE J. Quantum Electron.*, vol. QE-13, pp. 662–668, Aug. 1977.

[8] J. K. Butler and J. B. Delaney, "A rigorous boundary value solution for the lateral modes of stripe geometry injection lasers," *IEEE J. Quantum Electron.*, vol. QE-14, pp. 507–513, July 1978.

Jerome K. Butler (S'59–M'65) received the B.S.E.E. degree from Louisiana Polytechnic University, Ruston, LA, in 1960, and the M.S.E.E. and Ph.D. degrees from the University of Kansas, Lawrence, KS, in 1962 and 1965, respectively.

From 1960 to 1965 he was a Research Assistant at the Center for Research in Engineering Sciences, University of Kansas. His work was related to electromagnetic wave propagation and antenna arrays. In 1965 he joined the faculty of the Engineering School, Southern Methodist University, Dallas, TX, where he is now Professor of Electrical Engineering. He has been a member of the technical staff at RCA Laboratories, Princeton, NJ, during the summers from 1969 to 1977. His primary research areas include electromagnetic wave propagation in semiconductors, mode characterization of semiconductor lasers, integrated optical electronics, and quantum electronics. He has held consulting appointments with Texas Instruments, Incorporated, the Geotechnical Corporation of Teledyne, Inc., Earl Cullum Associates of Dallas, Texas, and the University of California Los Alamos Scientific Laboratory.

Dr. Butler is a member of Sigma Xi, Tau Beta Pi, and Eta Kappa Nu.

Joseph B. Delaney was born in Shreveport, LA, on July 16, 1950. He received the B.S.E.E. and M.S.E.E. degrees from Southern Methodist University, Dallas, TX, in 1973 and 1974, respectively. His Master's level work included fabrication of double-heterojunction GaAlAs lasers by solution growth techniques. He is presently working towards a doctoral degree in electrical engineering at Southern Methodist University.

D. BOTEZ, J. K. BUTLER, and J. C. CONNOLLY, RCA Laboratories, Princeton, N.J. 08540.

Of primary importance in many applications is the amount of cw power that can be delivered reliably from a diode laser into a single mode (spatially and in frequency). One approach toward the achievement of high-power mode-stabilized diodes is the use of large-optical-cavity (LOC) structures,[1-6] that is, structures in which the optical mode acquires gain from a thin (0.05–0.2-μm) active layer, while a sizable part of the mode energy propagates in thick (0.5–1.5-μm) guide layer(s) adjacent to the active layer. We have reported previously on high-power leaky-cavity CDH–LOC lasers.[6] Such devices provide single-mode cw operation up to 40 mW from one facet in beams of narrow transverse full width ($\theta_\perp$ = 25–30°) and in large lasing spots (1.5 × 6 μm). Here we report on a new type of CDH device: positive-index CDH–LOC, and we present a comprehensive treatment of lasing mode confinement and selection in CDH–LOC structures. Positive-index CDH–LOC devices have a relatively thick (0.20–0.35-μm) convex-lens-shaped active layer grown above a concave-lens-shaped guide layer. By comparison with leaky-cavity devices, (1) no radiation side lobes are observed in the lateral far-field pattern ($\theta_\parallel$ = 8°); (2) the transverse far field is still relatively narrow ($\theta_\perp \simeq$ 30°); (3) the threshold currents are lower (60–70 mA vs 90–130 mA) for the same device length; and (4) single-mode operation is achieved to only 12 mW/facet (cw) and 20 mW/facet (pulsed). Also the threshold currents are found to have record high-temperature coefficients for LOC-type structures: $T_0 \simeq$ 135°C in both pulsed and cw operation, while the difference in Al concentration between the active and guide layers is only 15%.

By using the effective-index method it is shown that in LOC structures the combination of a convex-lens-shaped active layer and a concave-lens-shaped guide layer provides a W-shaped lateral waveguide. Depending on the CDH–LOC structure geometry, these W-type guides support relatively large (5–7-μm) fundamental optical modes that can be (1) totally leaky (i.e., improper mode); (2) partially guided and partially leaky (i.e., guided-leaky mode); or (3) totally guided. Aside from bringing flexibility in the CDH–LOC single-mode laser design, W-type lateral guides, under certain conditions, strongly suppress oscillation of both high-order lateral and transverse modes, much more so than ridge guides[2-4,6,7] (local increase in index) or leaky guides[8] (local decrease in index). The theoretical treatment is backed by experimental results from CDH–LOC devices of various geometries. (12 min)

1. L. Figueroa and S. Wang, Appl. Phys. Lett. 32, 55 (1978).
2. N. Chinone, K. Saito, N. Shige, and K. Aiki, Appl. Phys. Lett. 35, 513 (1979).
3. T. Furuse, I. Sakuma, Y. Ide, K. Nishida, and F. Saito, in *Technical Digest, Fifth ECOC, Amsterdam, 1979*, paper 9.2.
4. R. D. Burnham, D. R. Scifres, W. Streifer, and S. Peled, Appl. Phys. Lett. 35, 734 (1979).
5. D. Botez, Appl. Phys. Lett. 36, 190 (1980).
6. R. L. Hartman, R. A. Logan, L. A. Koszi, and W. T. Tsang, J. Appl. Phys. 51, 1909 (1980).
7. W. Streifer, R. D. Burnham, and D. R. Scifres, Appl. Phys. Lett. 37, 121 (1980).
8. A. Yariv, *Quantum Electronics* (Wiley, New York, 1975).

Mode Characteristics of Nonplanar Double-Heterojunction and Large-Optical-Cavity Laser Structures

JEROME K. BUTLER, SENIOR MEMBER, IEEE, AND DAN BOTEZ, MEMBER, IEEE

Abstract—Mode behavior of nonplanar double-heterojunction (DH) and large-optical-cavity (LOC) lasers is investigated using the effective index method to model the lateral field distribution. The thickness variations of various layers for the devices discussed are correlated with the growth characteristics of liquid-phase epitaxy over topographical features (channels, mesas) etched into the substrate. The effective dielectric profiles of constricted double-heterojunction (CDH)-LOC lasers show a strong influence on transverse mode operation: the fundamental transverse mode (i.e., in the plane perpendicular to the junction) may be laterally index-guided, while the first (high)-order mode is laterally index-antiguided. The analytical model developed uses a smoothly varying hyperbolic cosine distribution to characterize lateral index variations. The waveguide model is applied to several lasers to illustrate conditions necessary to convert leaky modes to trapped ones via the active-region gain distribution. Theoretical radiation patterns are calculated using model parameters, and matched to an experimental far-field pattern.

I. Introduction

FABRICATION of semiconductor injection laser diodes over the past several years has progressed to a fairly sophisticated level in the sense that many contemporary devices are grown on substrate material that has been processed by the incorporation of various grooves and undulations at the substrate surfaces [1]-[15]. After the substrate has been properly processed, various layers of GaAs and AlGaAs compounds are grown over the grooves. The effects of grooves are to produce active layers as well as optical confining layers of relatively small lateral thickness variations, which tend to confine the optical radiation in the lateral direction defined by the grown layers. In this paper we discuss the performance of devices with grown layers as illustrated in Figs. 1 and 2. Specifically, we will discuss the character of the effective lateral refractive index and the resulting modes in several types of laser devices. Much of the previous work on laser structures has centered around double-heterojunction devices, where the active region is sandwiched between two optical confining layers, as illustrated in Fig. 1(a). We will discuss mainly the mode character of the fields in structures illustrated in Fig. 1(b) and in high-power LOC (large-optical-cavity) devices [11], where the majority of the optical field intensity is confined to a region adjacent to the active layer supplying optical power to the lasing mode. The LOC devices [10], [11] have been reported to exhibit stable lateral mode operation and high output powers. Basically, there are two types of LOC structures reported recently that exhibit stable lateral mode operation. These devices are derivatives of that illustrated in Fig. 2. In both cases the thickness of the active layer decreases as a function of distance with the maximum value occurring in the region where the optical field peaks. The adjacent layer which forms the large optical cavity, however, differs in the two structures; one [10] has the layer thickness decreasing with lateral distance, while the other [11], [15] has the layer increasing with lateral distance. Thus, the former structure has layers that act as convex lenses confining the optical radiation, while the latter has one layer causing convexity (i.e., guiding) but the other causing concavity (i.e., antiguiding).

After an initial discussion of the waveguide theory that pertains to nonplanar lasers, we will discuss the lateral mode character of lasers as they are influenced by lensing effects. We address how various layer thicknesses of LOC devices

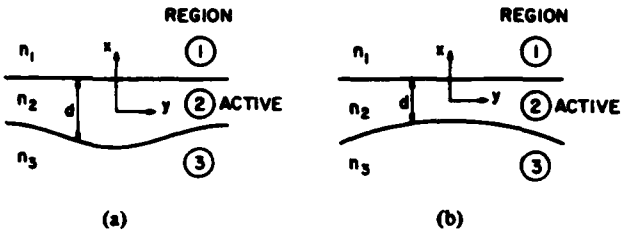

Fig. 1. Active layer grown of nonplanar double heterojunction lasers (a) convex and (b) concave waveguides.

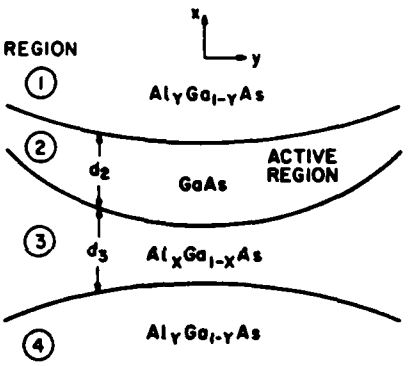

Fig. 2. Nonplanar large optical cavity (LOC) laser with a GaAs active region 2. The optical cavity includes both layers 2 and 3.

Manuscript received October 13, 1981; revised December 30, 1981. This work was supported in part by NASA, Langley Research Center, Hampton, VA under Contract NAS1-15440 and the U.S. Army Research Office under Grant DAAG-29-80-K-004.

J. K. Butler is with RCA Laboratories, Princeton, NJ 08540, on leave from Southern Methodist University, Dallas, TX 75275.

D. Botez is with RCA Laboratories, Princeton, NJ 08540.

0018-9197/82/0600-0952$00.75 © 1982 IEEE

affect transverse and lateral mode operation. For example, there exist combinations of thickness values d_2 and d_3, which determine whether the laser operates in the fundamental transverse mode or the first high-order one. We will present a series of design curves which facilitate the designs of fundamental transverse mode lasers. We also find that there exists a peculiarity that when the laser operates in the fundamental transverse mode, the mode sees a convex lateral index variation which, of course, tends to confine the mode. On the other hand, when the laser operates in the first-order transverse mode, that mode sees a concave lateral refractive index variation, which tends to defocus the mode.

To correlate effective dielectric variations with practical devices we present typical layer thickness variations in mode-stabilized DH and LOC structures grown on nonplanar substrates. Our particular emphasis will be on constricted-double-heterojunction (CDH) [6], [7], [13] and constricted-double-heterojunction large-optical cavity (CDH-LOC) [11], [15] lasers.

The lateral mode behavior is modeled using a hyperbolic cosine variation of the dielectric constant. This analytical model can be applied by-and-large to a broad number of nonplanar guides. Another useful aspect is the applicability of the model to leaky modes which might exist in index-antiguided structures. The incorporation of lateral gain in the model allows us to predict when leaky modes become trapped. (True leaky modes have lateral fields that increase without limit, while trapped modes have fields that decay to zero at infinite lateral distances.) After developing fundamental characteristics of the lateral modes found from the analytical field solutions, we apply our model to specific CDH and CDH-LOC lasers. The results indicate that most practical devices lase in trapped waveguide modes whether the mode is index-guided or index-antiguided. However, we address the possibility that some CDH lasers [6] might oscillate in a leaky mode. The infinite field strength that characterizes leaky modes never develops because of the scattering of energy into waveguide radiation modes at the facets.

Finally, the radiation patterns are given for the fundamental lateral mode found from analytical field solutions. The pattern of a CDH-LOC device is measured and compared with the theoretical pattern using the device parameters pertinent to the hyperbolic cosine variation of the dielectric constant.

II. Waveguide Theory

The analysis of waveguide modes in contemporary laser structures is typically effected in an approximate manner. Early approaches of analyzing two-dimensional waveguides other than those encountered in optical fibers are to treat the two perpendicular transverse directions independently [16]. More sophisticated approximate methods have been refined to what is generally now recognized as the effective index method [17], [19]. In laser structures we define two directions: x, the direction perpendicular to the grown epitaxial layers; and y, the direction along the various grown layers and in the plane of the mirror facet. The effective index method yields field solutions which accurately approximate the actual fields when the transverse dielectric variations are large compared to the lateral ones. In stripe geometry devices, the lateral dielectric dependencies are due to the lateral gain variations which affect the imaginary part of the dielectric constant, while temperature and carrier injection [20] affect the real part of the dielectric constant (local temperature rises increase the refractive index while carriers reduce it).

The dielectric constant in the grown layers is typically invariant with respect to position. However, in active devices, the dielectric constant of the active layer (region 2 in Fig. 1) must reflect the gain distribution. Then the active-layer dielectric constant κ_2 can be written as

$$\kappa_2(y) \simeq n_2^2 + ig(y)n_2/k_o \tag{1a}$$

$$\equiv \kappa_{02} + \kappa_{2v}(y) \tag{1b}$$

where n_2 is bulk refractive index of the active layer, $g(y)$ is the lateral gain distribution, k_o is the free-space propagation constant ($k_o = 2\pi/\lambda$), and $\kappa_{02} = n_2^2$. It should be noted that when index changes such as due to temperature occur, this small variation will be included in $\kappa_{2v}(y)$ as a real part. To make our analysis more general in nature, we write the dielectric constant of the ith layer as

$$\kappa_i(y) = \kappa_{oi} + \kappa_{vi}(y), \quad i = 1, 2, 3, 4 \tag{2}$$

where κ_{vi} contains only "lateral" variations.

Solutions to Maxwell's equations will be restricted to fields polarized along the junction plane and will be assumed $E(x, y) = \psi(x, y) \exp(i\omega t - \gamma z)$, where $\gamma = \alpha/2 + i\beta$ is the complex propagation constant. The wave equation is

$$\nabla_t^2 \psi + [k_o^2 \kappa(x, y) + \gamma^2]\, \psi = 0 \tag{3}$$

where $\kappa(x, y)$ defines the complex dielectric constant of all space and ∇_t^2 is the two-dimensional Laplacian operator. In the spirit of the effective index method, we write

$$\psi(x, y) = f(x, y)\, g(y) \tag{4}$$

where $f(x, y)$ describes the transverse fields and its y dependence appears there because of the layer thickness variations. The functional dependence of f is determined from the d_i's and κ_{oi}'s. Substituting (4) into (3) gives

$$g\frac{\partial^2 f}{\partial x^2} + f\frac{\partial^2 g}{\partial y^2} + [k_o^2 \kappa(x, y) + \gamma^2]\, fg = 0 \tag{5}$$

where we have neglected derivatives of f with respect to y (typically thickness variations are relatively slow in the y directions compared to dielectric variations in the x direction). Equation (5) is now multiplied by f^* and integrated on x in the range $(-\infty, \infty)$. This yields

$$\frac{\partial^2 g}{\partial y^2} + \gamma^2 g + \left\{\sum_i (k_0^2 \Gamma_i(y)\, \kappa_i - \Gamma_i(y)\, h_i^2(y))\right\} g = 0 \tag{6}$$

where

$$h_i^2(y) = -\frac{1}{f}\frac{\partial^2 f}{\partial x^2} \tag{6a}$$

and the overlap parameter $\Gamma_i(y)$ satisfies

$$\Gamma_i = \int_{i\text{th layer}} |f(x, y)|^2\, dx. \tag{6b}$$

The transverse functions $f(x, y)$ are normalized to unity along x so that $\Sigma_l \Gamma_l = 1$. In the effective index approach a propagation constant γ_0, which appears in a two-dimensional waveguide model, satisfies

$$\gamma_0^2 = h_l^2 - k_0^2 \kappa_{0l}. \tag{7}$$

Substituting (7) into (6) gives the differential equation describing the lateral fields

$$\frac{\partial^2 g}{\partial y^2} + \left[\gamma^2 - \gamma_0^2 + k_0^2 \sum_l \Gamma_l(y) \kappa_{vl}(y)\right] g = 0 \tag{8}$$

which is equivalent to the result derived by a more rigorous method [19]. It should be noted that for layered waveguides with no ohmic losses, the effective propagation constant $\gamma_0 = i\beta_0$ is imaginary for all proper modes. At this point we should note that there are mainly two types of contemporary lasers considered here: 1) double-heterojunction devices which have $d_3 = 0$ and $d_2 \sim 0.1$-0.3 μm, and 2) LOC structures with d_2 as above and with $d_3 \sim 1$-2 μm. Ordinarily, the former structure supports only a fundamental transverse "proper" (i.e., trapped) mode, while the latter can support high-order proper modes. In LOC devices the relative values of d_2 and d_3 should be chosen such that only the fundamental transverse mode oscillates, and thus the radiation is emitted in a single transverse lobe.

If we limit our discussion to devices that have $\kappa_{vl} = 0$ except for the active layer 2, then (8) assumes a form

$$\frac{\partial^2 g}{\partial y^2} + [\gamma^2 - \gamma_0^2 + k_0^2 \Gamma_2(y) \kappa_{v2}(y)]\, g = 0 \tag{9}$$

where $\Gamma_2(y)$ is the overlap or confinement factor of the mode power to the active layer. A similar equation was originally introduced by Paoli [21]. If $n_{e0} = -i\gamma_0/k_0$ is defined as the effective index in the absence of lateral index variations, then the net lateral effective index is

$$n_e^2 = (i\gamma_0/k_0)^2 + \Gamma_2(y) \kappa_{v2}(y). \tag{10}$$

In double-heterojunction devices $\Gamma_2(y)$ may be as low as 0.3 for narrow active layers, however, for LOC lasers Γ_2 might be less than 0.1.

III. Effective Index Variations of DH and LOC Structures

In this section the lateral variations of the effective index will be discussed for a variety of nonplanar DH lasers. These calculations have been reported earlier for DH [22], [23] and LOC [24] devices with convex curvature. We will give some approximations for DH lasers and extend the results to LOC devices with concave curvature of the heterojunction boundaries.

For simple DH structures with an active-layer thickness d (Fig. 1), the effective index in terms of the normalized width $D = k_0 d(n_2^2 - n_1^2)^{1/2}$ is [25]

$$n_{e0}^2 = b n_2^2 + (1 - b) n_1^2 \tag{11}$$

where

$$b \cong \frac{D^2}{4}\left(\frac{\sqrt{9 + 4D^2} - 1}{2 + D^2}\right)^2 \tag{12a}$$

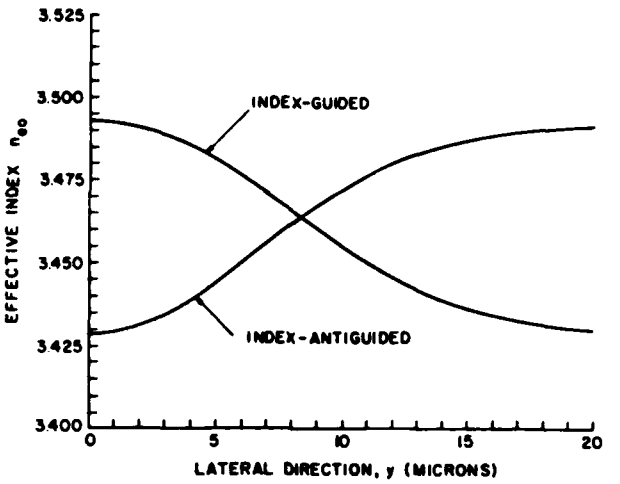

Fig. 3. The effective index variation in the lateral direction for both index and index antiguides. The active layer varies from 0.25 μm to 0.1 μm.

has been approximated from the confinement factor [26]

$$\Gamma(D) \cong \frac{D^2}{2 + D^2} \tag{12b}$$

and by using the relationship between b, Γ, and D [27]. The approximation formula for b is accurate within 3 percent over the interval $0 < D < 2.5$, which covers all cases of practical interest in AlGaAs/GaAs and InGaAsP/InP devices. Note that for InGaAsP/InP structures, where D is virtually independent of λ [28] (i.e., $D \cong 6.6d$), one obtains an approximation formula for b, which is a function of active-layer thickness alone.

In Fig. 3 we show the variation of the effective index n_{e0} as a function of y for both convex (index guided) and concave (index-antiguided) AlGaAs/GaAs structures. In the convex structure, the waveguide width varies from 0.25 μm to 0.1 μm, while the concave structure is of opposite variation; the refractive indexes of the various layers are $n_1 = 3.4$ and $n_2 = 3.6$ We have assumed that the thickness variation follows $d = d_e + (d_e - d_0) \exp(-y^2/y_0^2)$ with $y_0 = 10$ μm.

We now consider the waveguide parameters appropriate to the design of LOC structures. In Fig. 4 the confinement factors corresponding to the fundamental and the first-order transverse modes are shown for planar LOC structures with $d_3 = 1$ μm. The confinement factors of these transverse modes (i.e., modes in the plane perpendicular to the junction) play roles in transverse mode selection as well as in the determination of the lateral effective index variations as indicated in (9). At $y = 0$, the confinement factor of the fundamental transverse mode must be larger than that of the first-order transverse mode if the device is to operate in the fundamental mode. For example, if $d_2 = 0.2$ μm the Al concentration of layer 3 must be larger than 10 percent, since at the 10 percent point $\Gamma \sim 0.2$ for both transverse modes. The refractive indexes of the $Al_xGa_{1-x}As$ layers are assumed to follow $n_3 = 3.6 - 0.62x$.

A peculiarity of LOC structures is that *transverse* modes have lateral indexes with different functional dependencies. We will consider specifically a LOC device which is grown as a concave-lens-like structure. Fig. 5 shows the various regions

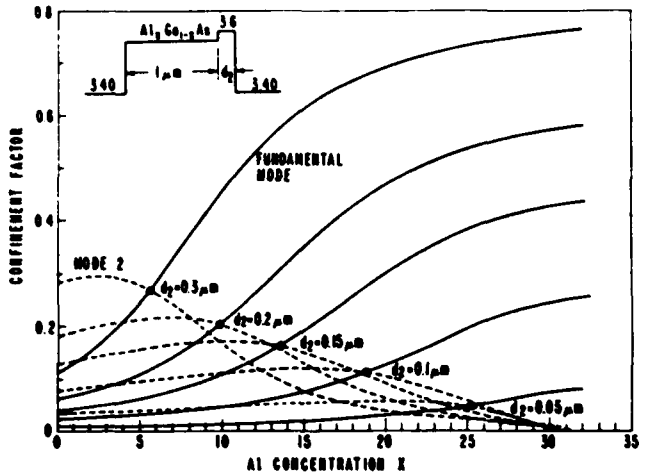

Fig. 4. Confinement factor Γ of optical power to the active region for the fundamental transverse mode (solid lines) and the first-order transverse mode (dashed lines) in LOC lasers as a function of Al concentration in region 3 of Fig. 2 (i.e., the guide layer). The graphs are drawn for a guide-layer thickness of 1 μm.

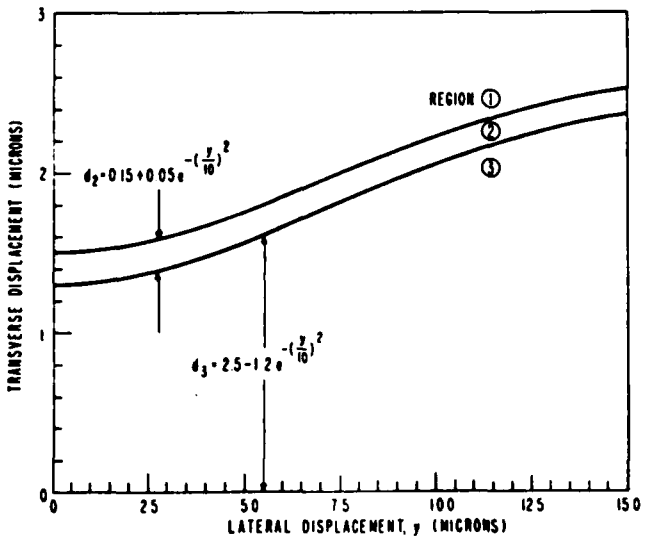

Fig. 5. A cross section of a typical nonplanar (CDH-LOC) laser. The active-layer thickness decreases with lateral position, whereas the guide-layer thickness increases. The effective index must reflect these opposite dependences on lateral displacement.

with thickness variations as a function of position, as discussed in the next section.

It should be noted that the effects of regions 2 and 3 on the effective index oppose each other, in the sense that one produces focusing while the other defocusing. As mentioned previously, the Al content of layer 3 affects lateral mode operation. In Fig. 6 we show the lateral index variations as a function of y for the fundamental transverse mode. In Fig. 6(a), where $x = 9.7$ percent, the lateral wave is index-antiguided when gain and losses are not considered. On the other hand, when $x = 11.3$ percent, the wave will be totally index guided. In going from concavity ($x < 9.7$ percent) to convexity ($x > 11.3$ percent) the intermediate x values produce the so-called W-shaped waveguide [29]. In Fig. 7 we show the lateral index variations as seen by the first-order transverse mode; note that this mode remains index-antiguided for all Al values listed. For $x = 11.3$ percent the fundamental

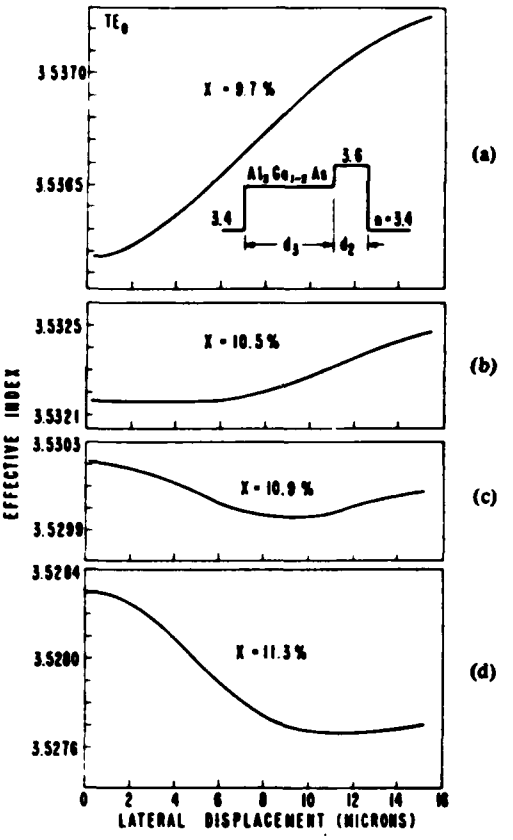

Fig. 6. The effective index as a function of lateral position for the fundamental transverse mode assuming the structure of Fig. 5. In (a) the lateral mode is index-antiguided, while in (d) it becomes index-guided.

transverse mode is laterally index-guided, while the first-order transverse mode in index-antiguided. Similar lateral index variations can be obtained while varying the layers' thicknesses at a fixed Al concentration [15], [29]. For instance, by increasing the active-layer thickness to 0.25–0.3 μm, CDH-LOC devices have been shown [15], [29] to become totally index-guided for the fundamental transverse mode.

IV. Lateral Wave Confining Structures Grown on Nonplanar Substrates

As discussed in the previous section, confinement of the optical mode can be realized by inducing thickness variations of the waveguiding layers along the plane of the junction. Such local variations in thickness can be generally achieved while depositing material by liquid-phase epitaxy (LPE) over nonplanar substrates [1]–[15]. We show in Fig. 8 three types of laser structures that can be obtained by LPE over topographical features etched into the substrate. The grown layers have variations in thickness due to two reasons: 1) a strong dependence of LPE growth on local surface curvature [2], [3], [30], [31], and 2) LPE-growth sensitivity to the degree of substrate misorientation [3], [30], [31].

Fig. 8 displays a DH-type device: the "ridge-guide" CDH laser [13], [31] [Fig. 8(a)], and two LOC-type devices: the nonplanar LOC laser [10] [Fig. 8(b)] and the CDH-LOC laser [11] [Fig. 8(c)]. In the DH device, as in most DH nonplanar-substrate devices [1]–[4], [6]–[8], [12]–[14], [32], the active-layer thickness variation solely determines lateral wave

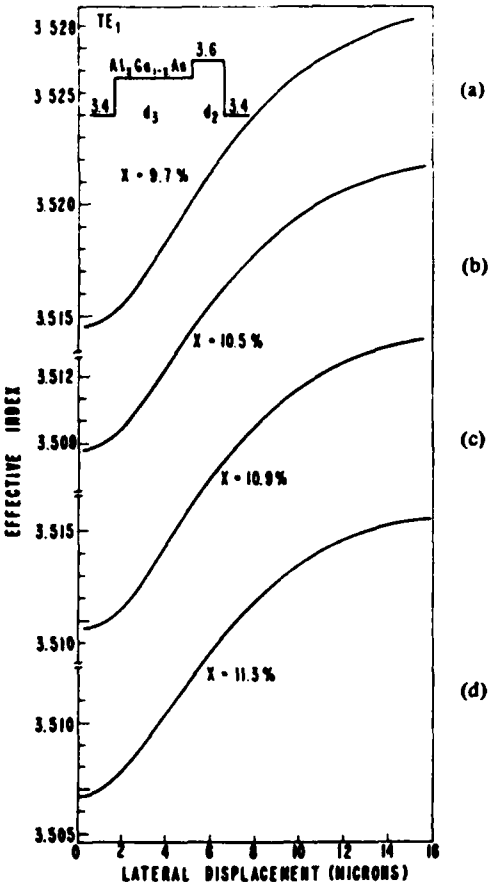

Fig. 7. The effective index as a function of lateral position for the first high-order transverse mode using the structure of Fig. 5. The waves are index-antiguided for all Al values considered.

confinement. By contrast, in LOC-type devices both the thickness variations of the active and guide layer play a role in mode confinement and selection. The nonplanar LOC structure [10] has convex-lens-shaped active *and* guide layers as a result of growth over a channel. A more complex situation is the CDH-LOC structure for which growth is performed above the mesa separating a pair of channels. Growth above the mesa is slow compared to growth in the planar areas outside the channels. Thus, after the growth of the *n*-AlGaAs confinement layer, one can obtain a shallow flat-bottomed channel. Then the guide layer assumes a concave-lens-like shape, and the subsequently grown active layer will assume a convex-lens-like shape.

It should be stressed that uniform current flow across the lasing area is "built-in" for CDH-type devices [Fig. 8(a) and (c)] since in such structures the lasing cavity is grown on the least resistive electrical path between the metallic stripe contact and the highly conductive substrate [31]. By contrast, in structures grown over channels [1]-[5], [9], [10], [32] [e.g., Fig. 8(b)], the current has the tendency to be focused towards the channel shoulders, and thus tight current confinement to the lasing area (e.g., very-narrow-stripes, preferential Zn-diffusion, back-biased junction) must be provided in order for the fundamental mode to be excited.

V. Lateral Mode Behavior

The analysis of the lateral mode structure has been accomplished by considering several types of dielectric profiles [33], [34]. These ad hoc profiles seldom describe the actual ones, but an understanding of the real modes can be realized by investigating the approximate models. In each of the lateral-index functions investigated above, it should be noted that with the assumed thickness variations the index is a smooth function of lateral position. Of all analytical profiles which have known field solutions, the hyperbolic cosine variation most closely matches our requirements of a smooth index profile. The index profile is then represented by the following variation of the dielectric constant κ:

$$\kappa(y) = \kappa_b + \frac{\kappa_a - \kappa_b}{\cosh^2\left(\frac{y}{y_0}\right)} \tag{13}$$

where $\kappa_a = n_a^2 = \kappa(0)$ and $\kappa_b = n_b^2 = \kappa(\infty)$; n_a, n_b are refractive index values at the center and edges of the distribution, respectively, and y_0 is a lateral displacement characteristic of the index lateral variation. (The values κ_a and κ_b may be complex.) It is interesting to note when κ_a and κ_b are real that if $\Delta\kappa = \kappa_a - \kappa_b > 0$, proper modes (trapped) exist, but if $\Delta\kappa < 0$, the fundamental mode as well as high-order modes are leaky. Our primary interest here is to understand both trapped and leaky modes in concave structures, as these devices have excellent power output and spectral character. Assuming that $\kappa_{v2} = 0$ and substituting (13) into (9), we have

$$\frac{\partial^2 g}{\partial x^2} + \left[k_0^2\kappa_b + \frac{k_0^2\Delta\kappa}{\cosh^2(y/y_0)} + \gamma^2\right] g = 0 \tag{14}$$

where $\kappa(y)$ is the effective dielectric constant. The solution to (14) is

$$g_s(y) = \cosh^{-b_s}\left(\frac{y}{y_0}\right) C_s^{b_s+(1/2)}\left(\tanh\frac{y}{y_0}\right), \qquad s = 0, 1, 2\cdots \tag{15}$$

where $b_s = b_0 - s$ and $b_0 = (k_0^2 y_0^2 \Delta\kappa + \frac{1}{4})^{1/2} - \frac{1}{2}$ and $C_s^{\lambda}(\zeta)$ are Gegenbauer polynomials, the first two of which are

$$C_0^{\lambda}(\zeta) = 1 \tag{16a}$$

and

$$C_1^{\lambda}(\zeta) = 2\lambda\zeta. \tag{16b}$$

The real value of $b_s = b_0 - s$ determines whether the s mode is proper or improper (leaky). Putting $b_s = b_s' + ib_s''$, the boundary that separates proper and improper modes occurs when $b_s' = 0$. From (15) it is seen that if $b_s' < 0$ the mode field strength increases without limit at large lateral distances, whereas $b_s' > 0$ gives $|g_s(y)| \to 0$ as $y \to \infty$. The boundary defined by $b_s' = 0$ is satisfied by [35]

$$\Delta'/\Delta'' = \frac{16s(s+1)(2s+1)^2 - (2k_0 y_0 \Delta''^{1/2})^4}{4(2s+1)^2 (2k_0 y_0 \Delta''^{1/2})^2} \tag{17}$$

where $\Delta\kappa = \Delta' + i\Delta''$. A similar result has been derived for

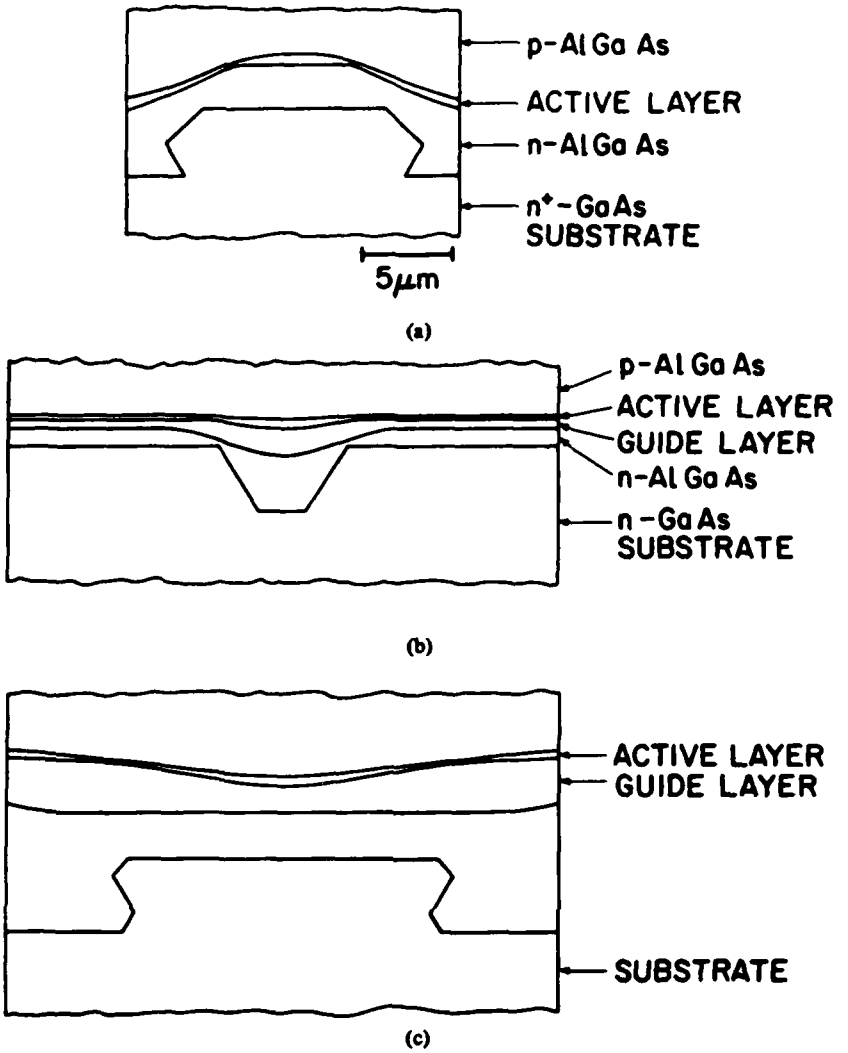

Fig. 8. (a) Nonplanar DH laser structure obtained by one-step liquid-phase-epitaxy: "ridge-guide" constricted double-heterojunction (CDH) laser [13], [31], nonplanar LOC laser structures obtained by one-step liquid-phase epitaxy, (b) nonplanar large-optical cavity (NP-LOC) laser [10], (c) constricted-double-heterojunction large-optical-cavity (CDH-LOC) laser [11].

step index variations [36]. Fig. 9 shows regions where the lateral modes are proper or leaky in terms of the complex dielectric step $\Delta\kappa$ and the width $2y_0$. The propagation constant is

$$\gamma^2 = -k_0^2[\kappa_b + b_s^2/(k_0 y_0)^2]. \tag{18}$$

If we neglect waveguide losses, index-antiguided modes have negative $\Delta\kappa$ values. The magnitude of the negative step influences both astigmatism and attenuation of the mode. Consider the fundamental $s = 0$ mode when $-\frac{1}{4} < k_0^2 y_0^2 \Delta\kappa < 0$, b_0 is real, and thus there is no phase variation of the field along the facet. Astigmatic leaky modes occur only when $k_0^2 y_0^2 \Delta\kappa < -\frac{1}{4}$. In most instances the attenuation of leaky modes is a direct reflection on power loss in the lateral directions so that in active devices a mode having a zero net attenuation occurs when power supplied by the active regions offsets the losses.

Let us now turn to waveguides in laser structures which have gain/losses. The lateral profile must be modified to include the dielectric variations occurring in the active layer. From (9) the profile is

$$\kappa(y) = \kappa_0(y) + \Gamma_2(y)\kappa_{v2}(y). \tag{19}$$

Neglecting temperature and strain effects

$$\kappa_{v2}(0) = ig(0)n_2/k_0 \tag{20a}$$

and

$$\kappa_{v2}(\infty) = -i\alpha_2 n_2/k_0 \tag{20b}$$

where it is assumed that $g(0)$ is the gain at $y = 0$ and $\alpha_2 = -g(\infty)$ is the absorption constant of layer 2 at large lateral distances. In the unpumped active layer, the absorption coefficient $\alpha_2 \sim 100 - 500\ \text{cm}^{-1}$. If we make the ad hoc assumption that $\Gamma_2(y)\kappa_{v2}(y)$ has a lateral dependence similar to $\kappa_0(y)$, then $\kappa(y)$ can be approximated to exhibit the hyperbolic cosine variation. The dielectric step becomes

$$\Delta\kappa = n_a^2 - n_b^2 + in_2[\Gamma_2(0)g(0) + \Gamma_2(\infty)\alpha_2]/k_0 \tag{21}$$

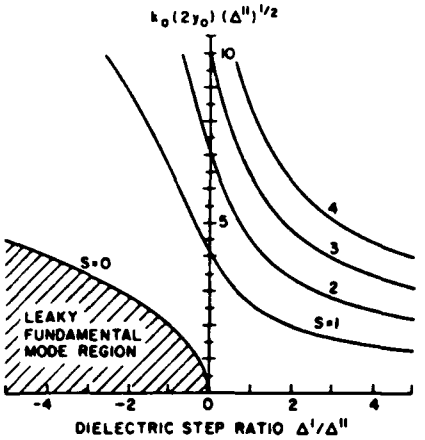

Fig. 9. Cutoff curves for the lateral modes as a function of the complex dielectric step and waveguide "width" y_0. In the cross-hatched region the fundamental mode is leaky or improper.

with

$$\Delta' = n_a^2 - n_b^2 \tag{22a}$$

and

$$\Delta'' = n_2 [\Gamma_2(0)\, g(0) + \Gamma_2(\infty)\, \alpha_2]/k_0. \tag{22b}$$

In (22b) the total value of the imaginary dielectric step is the sum of two positive terms because the gain is opposite in sign to the absorption so that the effective gain changes from $\Gamma_2(0)\, g(0)$ to $-\Gamma_2(\infty)\alpha_2$. In some devices the current distribution might tend to be uniform in the region containing the dielectric waveguide so that the gain in the active layer varies according to the thickness of the active layer d_2. If the current has inconsequential lateral variations along the lateral directions, the gain $g(\text{cm}^{-1})$ is written as [37] (neglecting lateral carrier diffusion)

$$g = 45(J_{eff}/d_2) - 190$$

where $J_{eff} = \eta_i J$ and η_i is the internal efficiency, $J(\text{kA/cm}^2)$ is the injection current density, and d_2 is dimensioned in microns. Now the imaginary part of the dielectric step becomes

$$\Delta'' = n_2 [\Gamma_2(0)\, g(0) - \Gamma_2(\infty)\, g(\infty)]/k_0. \tag{22c}$$

Devices exhibiting steps of the form (22c) are commonly found in constricted double-heterojunction structures unless tight current confinement is incorporated in the laser design.

VI. Device Calculations

Waveguide parameters will now be calculated for index-antiguided structures (CDH and CDH-LOC lasers) to illustrate the utility of the model.

A. "Leaky" CDH Laser [6]

It is well known that stripe geometry devices have modes supported by index antiwaveguides, and that the modes are essentially trapped because of the lateral gain distribution. The modes are not leaky, due to the fact that the optical field in the active layer is confined more or less to the region below the stripe contact. Other planar active-region devices such as the channel-substrate-planar laser [5] have only trapped lateral modes which lase; the structure is designed so that the real part of the lateral dielectric step is positive. In the CDH laser discussed here, the structure is fabricated with heterojunctions forming a concave waveguide [6] that has an active region thickness of $d_2 = 0.16\ \mu\text{m}$ at the lasing spot ($y = 0$) and $d_2 = 0.28\ \mu\text{m}$ at large lateral distances, defined in our formulation as $y = \infty$. Using the Al concentrations in the various layers, we have $n_a = 3.4866$ and $n_b = 3.5213$; calculations give $\Gamma(0) = 0.445$, $\Gamma(\infty) = 0.71$, $\Delta' = -0.243$, and $\Delta'' = (4.54 J_{eff} + 24) \times 10^{-4}$, where the gain distribution is estimated from the effective current density which is almost uniform over the waveguide vicinity. Assuming a value $y_0 = 6\ \mu\text{m}$, the condition for a proper mode $\Delta'' = (-\Delta')^{1/2}/k_0 y_0$ (crossing from the curve bounding the cross-hatched region of Fig. 9) gives $J_{eff} \sim 20\ \text{kA/cm}^2$ which corresponds to gain values $g(0) \sim 5000\ \text{cm}^{-1}$. Thus, it is not possible for this particular leaky device to reach the condition of a fundamental proper mode. On the other hand, using (18), the leaky mode propagating in the guide will reach threshold (assuming end losses $\sim 30\ \text{cm}^{-1}$) at $g(0) \sim 600\ \text{cm}^{-1}$ and $g(\infty) \sim 260\ \text{cm}^{-1}$; at these threshold gain values $b_0 = -0.33 + i22$ which would correspond to a very astigmatic mode; b_0', the real part of b_0 means the intensity increases without limit at large y values. However, experimental results showed that such devices lased with a very narrow spot ($\sim 2\ \mu\text{m}$) at the facet. There are two possible explanations for the discrepancy between our calculations and the experimental observations: 1) in the waveguide region at $y = 0$ the actual guide was relatively flat so that local ohmic heating in the region $|y| < 2\ \mu\text{m}$ produced an index increment, thus introducing a new waveguide parameter y_0 (the resulting structure would in fact be a W-guide), and 2) the possibility of "almost" total internal reflection of the mode at the waveguide facet. The problem with the first explanation is that the near field spread should be much larger than $2\ \mu\text{m}$ and, in fact, the laser should behave more like a stripe geometry device. The possibility of total internal reflection is more likely because of the large b_0'' values which are associated with the ray directions in the active layer. In particular, at large y values

$$g(y) \sim e^{-b_0 y/y_0} = e^{-b_0' y/y_0}\, e^{-ib_0'' y/y_0}. \tag{23}$$

The two plane wave components in region 2 which form the optical mode with respect to the x direction, are propagating at an angle with respect to the z axis. Thus, the net propagation vector $\hat{x}\beta_x + \hat{y}\beta_y + \hat{z}\beta_z$ of a single "plane wave" in the active layer has $\beta_x = k_0(n_2^2 - n_{eff}^2(y))^{1/2}$, $\beta_y = b_0''/y_0$, and $\beta_z = \text{Im}(\gamma)$, determined from (18). Combining the above components, rays in the active layer region with $d_2 = 0.28\ \mu\text{m}$ propagate at an angle (with respect to the z axis) $\theta \sim 14.2°$, which is near the critical angle for total internal reflection at the facet. Further, if these rays escape, it is doubtful that they entered the microscope. This explains why no radiation leakage was observed for the "leaky-guide" CDH device [6]. Only radiation propagating along the axis could be detected, and that provided a relatively narrow, centered beam ($\theta_{\|} \cong 20°$). As the width d_2 drops from $0.28\ \mu\text{m}$, the value of β_x increases and the corresponding ray angles increase. But near $y = 0$ the

plane waves change directions, thus increasing the possibility for light escaping from the facet.

B. CDH-LOC Lasers

The geometry of CDH-LOC devices is given in Fig. 5; we will use the structure with 9.7 percent Al in layer 3. This is an index-antiguided structure that can operate in a high-order transverse mode, but the fundamental is assumed. At $y = 0$, $d_2 = 0.2$ μm and $d_3 = 1.3$ μm, whereas at large y, $d_2 = 0.15$ μm and $d_3 = 2.5$ μm. The confinement factors are $\Gamma_2(0) = 0.157$ and $\Gamma_2(\infty) = 0.023$. The refractive indexes $n_a = 3.5363$ and $n_b = 3.5373$ are used to get $\Delta' = -0.007$. The value $y_0 = 5.3$ μm is estimated from lateral points where the refractive index changes go through one half of their total change, i.e., if y_h represents the point of half variation, $y_0 = 0.759\, y_h$. Assuming a uniform current distribution over the lasing portion of the waveguide, we find for a trapped or proper mode to exist, $J_{eff} \sim 2.5$ kA/cm^2 which corresponds to $g(0) \sim 370$ cm^{-1} and $g(\infty) \sim 560$ cm^{-1}. Even though $g(\infty) > g(0)$, the effective gains are modified by the confinement factors of the various lateral points. At $J_{eff} = 2.5$ kA/cm^2, the fundamental mode attenuation coefficient $\alpha_0 \sim 13$ cm^{-1}, but at threshold, $\alpha_0 = -30$ cm^{-1} and $J_{eff} \sim 3$ kA/cm^2, which give $g(0) = 485$ cm^{-1}, $g(\infty) = 710$ cm^{-1}, and $b_0 = 0.16 + i3.4$. At these small b_0'' values, the rays in the active layer are determined predominantly by β_x and β_z.

As a final example, we consider a CDH-LOC laser [15] that supports index-guided modes. This structure has $n_1 = 3.418$, $n_2 = 3.6$, $n_3 = 3.502$, and $n_4 = 3.44$ and $d_2 \sim 0.27$ μm, $d_3 \sim 1.8$ μm at $y = 0$ and $d_2 \sim 0.2$ μm, $d_3 \sim 2.1$ μm at $y \sim 10$ μm. Computations give $n_a = 3.5297$, $n_b = 3.5153$, $\Gamma(0) = 0.6157$ and $\Gamma(\infty) = 0.4282$. From geometrical estimates, $y_h \sim 7$ μm giving $y_0 \sim 5.3$ μm. Again assuming a uniform current distribution, threshold occurs when $g(0) \sim 60$ cm^{-1} and $g(\infty) \sim 150$ cm^{-1}. At these gain values, $b_0 = 12.3 - i\,0.076$. Actually, the gain distribution in this structure plays little or no role in the lateral mode shape. Nevertheless, the large charge density differential between the points $y = 0$ and $y = 10$ μm will cause a relatively large diffusion current directed toward $y = 0$. It is interesting to note that our model holds for cases such as when the gain is suppressed at $y = 0$ and increases with y; this is opposite to the CDH structure discussed above.

VII. Radiation Patterns

The optical radiation pattern can be determined once the near field distribution is known. The most elementary approach and the one given here is to calculate the Fourier transform of the near field mode. This method is reasonably accurate for proper modes where there is little internal mode conversion at the facet. In the case of the "leaky" CDH device [6] discussed earlier, portions of the fundamental mode in the regions $y > y_0$ might see a very high reflection coefficient at the facet. Thus, little light would escape from the device, with most coming from the region around $y = 0$. Under these conditions, much of the reflected light would be distributed in the waveguide radiation modes and be dissipated internally.

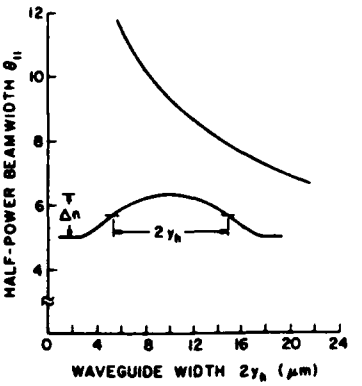

Fig. 10. The half-power beamwidth $\theta_{\parallel}$ as a function of the waveguide width $2y_h$ for the CDH-LOC laser of [15].

Since the near field is separated into $f(x, y)$ and $g(y)$ via the effective index method, the far field can be similarly divided into independent perpendicular angle dependencies. We concentrate here on the lateral pattern $F(\theta)$ given by

$$F(\theta) = \int_{-\infty}^{\infty} g(y)\, e^{i\chi y}\, dy \tag{24}$$

where $\chi = k_0 \sin\theta$ and θ defines the lateral angle from the facet normal. (The obliquity factor has been dropped.) For the sake of briefness, we consider only the fundamental mode pattern in the lateral direction. Using $g(y) = \cosh^{-b_0}(y/y_0)$

$$F(\theta) = \frac{2^{b_0-2} y_0}{\Gamma(b_0)} \Gamma(b_0/2 + iy_0\chi/2)\, \Gamma(b_0/2 - iy_0\chi/2) \tag{25}$$

where $\Gamma(w)$ is the gamma function [*not the confinement factor* in (6), (9), (12a), and (19)]. Contour and relief maps [38] of the gamma function with complex arguments can be used to analyze the behavior of the far field patterns. The gamma function $\Gamma(w)$ has a pole at $w = 0$. If we put $w = u + iv$ with u = constant and vary v, the gamma function peaks at $v = 0$ and varies monotonically from $v = 0$. In the far field pattern of the fundamental mode, the two gamma functions actually form different peaks at symmetrical positions about $k_0 \sin\theta = 0$. If the value b_0'' is sufficiently small the two peaks combine to form a single peak at $\theta = 0$. But in the case when the two peaks can be separated and b_0'' is large, peaks occur at

$$\sin\theta = \pm\frac{b_0''}{k_0 y_0}. \tag{26}$$

As the value of $b_0' \to 0$ from the positive side, the two peaks increase without limit. The value of b_0'' is dependent upon the dielectric step $\Delta\kappa$ and $k_0 y_0$. If Re $[\Delta\kappa]$ is positive and large, $b_0'' \sim 0$, but if Re $[\Delta\kappa]$ is large and negative, then for $k_0 y_0 \gg 0$, $b_0'' \sim k_0 y_0 (n_b^2 - n_a^2)^{1/2}$ so that far field peaks occur at

$$\sin\theta = \pm(n_b^2 - n_a^2)^{1/2} \tag{27}$$

which allows us to estimate the index step for index-antiguided modes. For large b_0' values, Stirling's approximation for the gamma function can be employed.

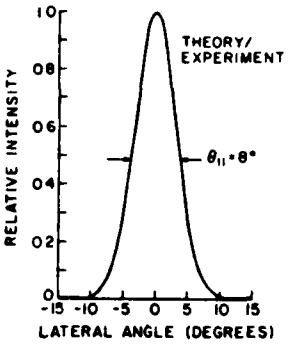

Fig. 11. Theoretical experimental pattern of the CDH-LOC laser of [15]. The optimum fit occurs at $y_0 = 6.25\ \mu m$.

To illustrate the use of (25), we calculate the radiation pattern of the index-guided CDH-LOC [15] discussed earlier. Using the index calculation, Fig. 10 shows the half-power beamwidth of the fundamental lateral mode as a function of $2y_h$. At $2y_h \sim 14\ \mu m$ we find that $\theta_{\parallel} \sim 8°$, which is in good agreement with the experimental patterns. In Fig. 11 we plot both theory and experiment.

VIII. Conclusion

The effective index method has been applied to both CDH and CDH-LOC lasers to analyze their lateral mode behavior. The LOC devices have shown that lateral mode behavior is strongly influenced by transverse mode operation when the optical cavity contains AlGaAs layers with relatively large aluminum concentrations. This occurs in geometries where the optical cavity increases in thickness laterally. In devices with relatively small active layer thicknesses all transverse modes are index-antiguided in the lateral direction.

Lateral modes are analyzed using the smoothly varying hyperbolic cosine distribution. The effects of the active region gain are included in the model to indicate when leaky waveguide modes become proper.

Acknowledgment

The authors gratefully acknowledge discussions with M. Ettenberg and J. C. Connolly.

References

[1] R. D. Burnham and D. R. Scifres, "Etched buried heterostructure GaAs/GaAlAs injection lasers," *Appl. Phys. Lett.*, vol. 27, pp. 510–511, Nov. 1975.

[2] D. Botez, W. Tsang, and S. Wang, "Growth characteristics of GaAs-$Ga_{1-x}Al_xAs$ structures fabricated by liquid-phase epitaxy over preferentially etched channels," *Appl. Phys. Lett.*, vol. 28, pp. 234–237, Feb. 15, 1976.

[3] P. A. Kirkby and G.H.B. Thompson, "Channeled substrate buried heterostructure GaAs-(GaAl)As injection lasers," *J. Appl. Phys.*, vol. 47, pp. 4578–4589, Oct. 1976.

[4] L. Figueroa and S. Wang, "Inverted-ridge-waveguide double-heterostructure injection laser with current and lateral optical confinement," *Appl. Phys. Lett.*, vol. 31, pp. 45–47, July 1, 1977.

[5] K. Aiki, M. Nakamura, T. Kuroda, J. Umeda, R. Ito, N. Chinone, and M. Maeda, "Transverse mode stabilized $Al_xGa_{1-x}As$ injection lasers with channel-substrate-planar structures," *IEEE J. Quantum Electron.*, vol. QE-14, pp. 89–97, Feb. 1978.

[6] D. Botez and P. Zory, "Constricted double-heterostructure (AlGa)As diode lasers," *Appl. Phys. Lett.*, vol. 32, pp. 261–263, Feb. 15, 1978.

[7] D. Botez, "Single-mode CW operation of 'double-dovetail' constricted DH (AlGa)As diode lasers," *Appl. Phys. Lett.*, vol. 33, pp. 872–874, Nov. 15, 1978.

[8] T. Sugino, K. Itoh, M. Wada, H. Shimizu, and I. Teramoto, "Fundamental transverse and longitudinal mode oscillation in terraced substrate GaAs-(GaAl)As lasers," *IEEE J. Quantum Electron.*, vol. QE-15, pp. 714–726, Aug. 1979.

[9] T. Furuse, I. Sakuma, Y. Ide, K. Nishida, and F. Saito, "Transverse mode stabilized AlGaAs DH laser having a built-in planoconvex waveguide," in *Proc. 5th European Conf. on Opt. Commun.*, Amsterdam, The Netherlands, Sept. 1979, paper 2.2.

[10] R. D. Burnham, D. R. Scifres, W. Streifer, and S. Peled, "Nonplanar large optical cavity GaAs/GaAlAs semiconductor laser," *Appl. Phys. Lett.*, vol. 35, pp. 734–737, Nov. 15, 1979.

[11] D. Botez, "CW high-power single-mode operation of constricted double-heterojunction AlGaAs lasers with a large optical cavity," *Appl. Phys. Lett.*, vol. 36, pp. 190–192, Feb. 1, 1980.

[12] K. Kishino, Y. Suematsu, Y. Takahashi, T. Tanbunek, and Y. Itaya, "Fabrication and lasing properties of mesa substrate buried heterostructure GaInAsP/InP lasers at 1.3 μm wavelength," *IEEE J. Quantum Electron.*, vol. QE-16, pp. 160–165, Feb. 1980.

[13] D. Botez and J. C. Connolly, "Low-threshold high-T_o constricted double heterojunction AlGaAs diode lasers," *Electron. Lett.*, vol. 16, pp. 942–944, Dec. 1980.

[14] E. Oomura, H. Higuchi, R. Hirano, H. Namizaki, T. Murotani, and W. Susaki, "Transverse mode control in InGaAsP/InP buried crescent diode lasers," *Electron. Lett.*, vol. 17, pp. 83–84, Jan. 1981.

[15] D. Botez and J. C. Connolly, "Single-mode positive-index guided CW CDH-LOC AlGaAs lasers with low threshold-current temperature sensitivity," *Appl. Phys. Lett.*, vol. 38, pp. 658–660, May 1, 1981.

[16] E.A.J. Marcatilli, "Dielectric rectangular waveguide and directional coupler for integrated optics," *Bell Syst. Tech. J.*, vol. 45, pp. 2071–2102, Sept. 1969.

[17] G. B. Hocker and W. K. Burns, "Mode dispersion in diffused channel waveguides by the effective index method," *Appl. Opt.*, vol. 16, pp. 113–118, Jan. 1977.

[18] J. Buus, "Detailed field model for DH stripe lasers," *Opt. Quantum Electron.*, vol. 10, pp. 459–474, 1978.

[19] W. Streifer and E. Kapon, "Application of the equivalent-index method to DH diode lasers," *Appl. Opt.*, vol. 18, pp. 3724–3725, Nov. 15, 1979.

[20] J. S. Manning and R. Olshansky, "Carrier induced index change in AlGaAs double-heterostructure lasers," *Electron. Lett.*, vol. 17, pp. 506–507, July 9, 1981.

[21] T. L. Paoli, "Waveguiding in a stripe-geometry junction laser," *IEEE J. Quantum Electron.*, vol. QE-13, pp. 662–668, Aug. 1977.

[22] W. Streifer, D. R. Scifres, and R. D. Burnham, "Above-threshold analysis of double-heterojunction diode lasers with laterally tapered active regions," *Appl. Phys. Lett.*, vol. 37, pp. 877–879, Nov. 15, 1980.

[23] K. Moriki, K. Wakao, M. Kitamura, K. Iga, and Y. Suematsu, "Single transverse mode operation of terraced substrate GaInAsP/InP lasers at 1.3 μm wavelength," *Japan. J. Appl. Phys.*, vol. 19, pp. 2191–2196, Nov. 1980.

[24] W. Streifer, R. D. Burnham, and D. R. Scifres, "Analysis of diode lasers with lateral spatial variations in thickness," *Appl. Phys. Lett.*, vol. 37, pp. 121–123, July 15, 1980.

[25] J. Buus and M. J. Adams, "Phase and group indices for double heterostructure lasers," *Solid-State Electron. Devices*, vol. 3, pp. 189–195, Nov. 1979.

[26] D. Botez, "Analytical approximation of the radiation confinement factor of the TE_0 mode of a double heterojunction laser," *IEEE J. Quantum Electron.*, vol. QE-14, pp. 230–232, Apr. 1978.

[27] W. O. Schlosser, "Gain-induced modes in planar structures," *Bell Syst. Tech. J.*, vol. 52, pp. 887–905, July–Aug. 1973.

[28] D. Botez, "InGaAsP/InP double-heterojunction lasers: Simple expressions for wave confinement, beamwidth, and threshold current over wide ranges in wavelength (1.1–1.65 μm)," *IEEE J. Quantum Electron.*, vol. QE-17, pp. 178–186, Feb. 1981.

[29] D. Botez, J. K. Butler, and J. C. Connolly, "Mode control in high-power CDH-LOC diode lasers: The *W*-shaped lateral waveguide," in *Proc. 3rd Int. Conf. on Integrated Opt. and Opt. Fiber Commun.*, San Francisco, CA, Apr. 27–29, 1981, pp. 10–11, paper MB5.

[30] D. Botez, "Planar and inverted-ridge GaAs waveguide lasers: Device characteristics and studies of liquid-phase epitaxy growth," Ph.D. dissertation, Univ. of California, Berkeley, Dec. 1976.
[31] —, "Constricted double-heterojunction AlGaAs diode lasers: Structures and electro-optical characteristics," *IEEE J. Quantum Electron.*, vol. QE-17, pp. 2290–2310, Dec. 1981.
[32] P. A. Kirkby, "Channelled-substrate narrow-stripe GaAs/GaAlAs injection laser with extremely low threshold currents," *Electron. Lett.*, vol. 15, pp. 824–825, Dec. 1979.
[33] P. M. Asbeck, D. A. Cammack, and J. J. Daniele, "NonGaussian fundamental mode patterns in narrow-stripe-geometry lasers," *Appl. Phys. Lett.*, vol. 33, pp. 504–506, Sept. 1978.
[34] W. Streifer, D. Scifres, and R. Burnham, "Analysis of gain-induced waveguiding in stripe geometry diode lasers," *IEEE J. Quantum Electron.*, vol. QE-14, pp. 418–427, June 1978.
[35] F. Srobar, unpublished.
[36] J. B. Delaney and J. K. Butler, "The effect of device geometry on lateral mode content of stripe-geometry lasers," *IEEE J. Quantum Electron.*, vol. QE-15, pp. 750–755, Aug. 1979.
[37] F. Stern, "Calculated spectral dependence of gain in excited GaAs," *J. Appl. Phys.*, vol. 47, p. 5382, Dec. 1976.
[38] E. Jahnke and F. Emde, *Tables of Functions*. New York: Dover, 1945, p. 12.

Jerome K. Butler (S'59–M'65–SM'78) was born in Shreveport, LA, on September 27, 1938. He received the B.S. degree from Louisiana Polytechnic University, Ruston, in 1960, and the M.S. and Ph.D. degrees from the University of Kansas, Lawrence, in 1962 and 1965, respectively.

From 1960 to 1965 he was a Research Assistant at the Center for Research in Engineering Sciences, University of Kansas, Lawrence. His research was related to electromagnetic-wave propagation and to the optimization and synthesis techniques of antenna arrays. In 1965, he joined the staff of the School of Engineering and Applied Science, Southern Methodist Univeristy, Dallas, TX, where he is now Professor of Electrical Engineering. His primary research areas are solid-state injection lasers, radiation and detection studies of lasers, communication and imaging systems, integrated optics and the application of integrated optical circuits, and quantum electronics. In the summer from 1969 to 1981 he was a member of the Technical Staff, RCA Laboratories, Princeton, NJ, where he did research concerned with electromagnetic-wave propagation in solid-state injection lasers. Dr. Butler is coauthor of the book *Semiconductor Lasers and Heterojunction LED's* (New York: Academic). He has held consulting appointments with the Central Research Laboratory, Texas Instruments, Inc., the Geotechnical Corporation of Teledyne, Inc., Earl Cullum Associates, Dallas, TX, and the University of California Los Alamos Scientific Laboratory.

Dr. Butler is a member of Sigma Xi, Tau Beta Pi, Eta Kappa Nu, and is a Registered Professional Engineer in the State of Texas.

Dan Botez (S'71–M'79), for a photograph and biography, see p. 870 of the May 1982 issue of this JOURNAL.

Prediction of transverse-mode selection in double heterojunction lasers by an ambipolar excess carrier diffusion solution

Joseph B. Delaney
TRW, Optoelectronics Division, Carrollton, Texas 75006

Richard R. Shurtz, II
Night Vision and Electro-optics Laboratory, Laser Division, Fort Belvoir, Virginia 22060

Jerome K. Butler
Southern Methodist University, Dallas, Texas 75275

(Received 6 July 1982; accepted for publication 23 September 1982)

Transverse-mode selection is characterized for GaAs/AlGaAs double heterojunction lasers from optical field and electron/hole interaction. The electron/hole distribution determined from a solution of the ambipolar diffusion equation provides the necessary information about gain/mode coupling to predict the current at threshold. Lasing power out versus current solutions provide information about internal differential quantum efficiency. Theory is matched to experiment for a multimode laser with one heterojunction having a very small index step. It is found that the laser's characteristics over a temperature and current range are predicted by adjusting the active-layer refractive index as determined from far-field measurements.

PACS numbers: 42.55.Px, 42.60.By

I. INTRODUCTION

In recent years, there has been considerable effort spent fabricating various semiconductor laser-device geometries for control of mode operation. In GaAs/AlGaAs devices, the transverse-mode operation is usually governed by the growth of various layer thicknesses and index steps at the grown heterojunctions. Double heterojunction lasers which confine the optical field to the thin active layers usually operate in the fundamental mode. Furthermore, the lasing mode is independent of drive because small index changes due to injection have negligible effects on mode selection. While transverse-mode lasing can be well controlled by epitaxial heterojunctions, lateral-mode operation in contemporary lasers is drive sensitive. Stripe-contact devices[1–3] have lateral guides defined only by the current density which affects the gain distribution while more sophisticated structures[4–7] have grown layers whose thicknesses are functions of lateral positions. Thus, in these devices the lateral modes are shaped by the lateral effective index as well as gain variations.

Because the gain distribution plays a major role in defining mode stability in lasers, it is important to understand the mechanisms of electron/hole transport in active layers. In this paper, we discuss the transverse-mode operation of lasers which are affected by the electron/hole distribution. For the first time the ambipolar diffusion equation is solved for the active layer in an injection laser. The direct consequence of this solution is the ability to predict crossover of competing modes in the active layer. In contrast to ambipolar diffusion, assuming simple electron injection does not explain this phenomena in sufficient detail.

In this work we investigate mode selection from the standpoint of the exact selection process. This includes mode gain coupling and differential quantum efficiency. We concentrate on the transverse (perpendicular to the junction plane) modes in a double heterojunction laser. The excess carrier distribution is assumed ambipolar and a complete solution is obtained. From mode/gain coupling, it is possible to predict the threshold, and from the slope efficiency, it is possible to predict mode crossover.

The laser we apply this to is a broad-area double heterojunction GaAs device with a small index step at one of the heterojunctions. The laser is heated over a temperature range and the first two modes are investigated. It is found that cavity-mode preference is very sensitive to temperature and current level. Application of the diffusion equation is used to describe the crossover of the first two modes and it is established that the mode with the highest slope efficiency will dominate. Far-field patterns are described by standard multilayer waveguide techniques. Finally, a calculation is made to estimate the effect of free carriers on the refractive index in the material.

II. THEORY

A. Approach

Excess carrier movement in the active layer of an injection laser is described using the ambipolar diffusion equation. Quasi-Fermi level continuity as well as electron and hole current continuity is imposed at each interface. The quasi-Fermi level location is calculated using a nonparabolic Γ_{1C} extremum, and parabolic X_{1C} and Γ_{15V} extrema. The boundary condition is set up in such a way as to eliminate the need for a solution within the space charge layer surrounding each interface. The spontaneous recombination lifetime is calculated without imposing quasimomentum conservation for parabolic bands. Above threshold, a stimulated recombination term is included in the ambipolar diffusion equation and the gain is assumed to be pinned at the threshold value. The lasing modal shape for the transverse modes (perpendicular to the metallurgical junctions) is calculated by solving Maxwell's equations for a multilayer dielectric wave guide.

B. The excess carrier distribution

The diffusion equation evolves along the standard route. We demand, as is customary, that each carrier type

 0021-8979/83/020540-10$02.40

satisfies the continuity equation[8]

$$D_p \nabla^2 p - \mu_p \nabla\cdot(p\bar{E}) + g_p - p/\tau_p = \partial p/\partial t, \tag{1a}$$

$$D_n \nabla^2 n + \mu_n \nabla\cdot(n\bar{E}) + g_n - n/\tau_n = \partial n/\partial t, \tag{1b}$$

where n, p = total electron, hole carrier density; D_n, D_p = electron, hole diffusion constant; g_n, g_p = electron, hole generation rate; and τ_n, τ_p = electron, hole mean recombination time. We further demand that Poisson's equation be satisfied:

$$\nabla\cdot\bar{E} = (4\pi\rho/\epsilon), \tag{2}$$

where ρ is the space charge density and ϵ is the dielectric constant.

Rather than solve Eqs. (1) and (2) exactly, we take an approximate route where we assume that the internal field between the electron and hole charge densities is strong enough to guarantee charge neutrality. Although this condition is violated in the space charge layer surrounding the heterojunctions, we can formulate the problem in such a way that only diffusion processes outside the heterojunctions need be considered. Under this assumption, the excess electron and hole densities, δn and δp, respectively, must be equal:

$$\delta n = n - n_0 = p - p_0 = \delta p. \tag{3}$$

Here, n_0, p_0 designate the thermal-equilibrium carrier densities. If we take $(\partial n_0)/(\partial x) - (\partial p_0)/(\partial x) = 0$, we can substitute Eq. (3) into Eq. (1) to obtain two equations for the two unknowns δp and $\bar{E}$. The terms involving $\nabla\cdot\bar{E}$ can be eliminated by multiplying Eq. (1a) by $n\mu_n$ and Eq. (1b) by $p\mu_p$ and adding to obtain[9]

$$D^*\nabla^2(\delta p) - \mu^*\bar{E}\cdot\nabla(\delta p) + g' - \frac{\delta p}{\tau} = \frac{\partial(\delta p)}{\partial t}, \tag{4}$$

where

δp = excess carrier density,

$$D^* = \frac{n\mu_n D_n + p\mu_p D_p}{n\mu_n + p\mu_p},$$

$$\mu^* = \frac{\mu_n\mu_p(n_0 - p_0)}{n\mu_n + p\mu_p}, \quad g' = g'_n = g'_p,$$

$$\frac{\delta p}{\tau} = \frac{p_0 + \delta_p}{\tau_p} - \frac{p_0}{\tau_{p_0}} = \frac{n_0 + \delta n}{\tau_n} - \frac{n_0}{\tau_{n_0}},$$

g'_n, g'_p = excess carrier generation rates, and

τ = excess carrier recombination lifetime.

We have implicitly assumed that the net recombination rate $(\delta p)/\tau$ is the same for electrons as for holes, as it must be. We have further assumed that the equilibrium generation rate is equal to the equilibrium recombination rate for both electrons and holes.

For the ambipolar diffusion Eq. (4), observe that the ambipolar diffusion rate for excess carriers is determined by the average value of D_n and D_p, weighted by $n\mu_n$ and $p\mu_p$. In other words, the two oppositely charged clouds interact with each other through the internal field in such a way as to satisfy Poisson's equation and must then diffuse at a naturally acceptable rate. This is crucial because of the very large injected charge densities encountered in injection lasers ($\sim 2\times 10^{18}$ cm^{-3}).

The electric field in Eq. (4) refers to both the internal and applied fields. Under the conditions encountered in an injection laser, these fields exert only a small direct influence on carrier distribution, and as such can be ignored in Eq. (4). In other words, the electric field does not alter the actual excess carrier spatial distribution, but rather only causes carriers to drift. This is the case if the drift length is much less than the diffusion length, i.e.,

$$\mu^* E\tau \ll (D^*\tau)^{1/2}. \tag{5}$$

This condition is met in the solutions ultimately obtained. The major effect of the internal field, that of charge neutrality, is still accounted.

If we assume the only excess carrier drain, other than spontaneous recombination $\delta p/\tau$, is stimulated recombination, then for an infinitely long cavity and time-averaged values[10]

$$r = \frac{\partial(\delta p)}{\partial t} = \frac{1}{\eta_s}\frac{gP(x)}{h\nu}, \tag{6}$$

where $P(x)$ = time-averaged power density, g = gain, η_s = stimulated quantum efficiency, and $h\nu$ = photon energy. For 100% carrier confinement, η_s is the internal differential quantum efficiency. In these calculations we put $\eta_s = 1$. Equation (4) becomes

$$D^*\nabla^2(\delta p) - (\delta p)/\tau = r, \tag{7}$$

where D^* = ambipolar diffusion constant, τ = spontaneous recombination lifetime, and r = stimulated recombination rate. The value r is equated to zero in the region where $g < 0$. The spontaneous recombination lifetime is

$$\tau = 1/[B(n_0 + p_0 + \delta p)], \tag{8}$$

where B is 1.3×10^{-10} cm^3/sec.[11,12]

C. The boundary conditions

At each boundary within the device there exists a space charge layer with a width severely reduced under conditions of forward bias. Because quasicharge neutrality is violated within this layer, we match across the layer under the assumptions it is is thin enough and internal fields are strong enough that carriers are swept through without significant recombination. Hence, we demand that the electron and hole current densities be the same on each side of the space charge layer. These densities are written

$$\bar{J}_n = qn\mu_n\bar{E} + qD_n\nabla(\delta p), \tag{9a}$$

$$\bar{J}_p = qp\mu_p\bar{E} - qD_p\nabla(\delta p). \tag{9b}$$

Here, $\bar{E}$ is the total field and q is the electron charge. Although $\bar{E}$ can be ignored in Eq. (7), where it has a small effect, it must be included in the boundary conditions because both drift and diffusion terms are significant.

In addition to continuity of current densities, we also impose continuity of hole and electron quasi-Fermi levels across each layer interface. Although it is clear this alignment of Fermi levels implies band bending, i.e., space charge, we assume an abrupt heterojunction and ignore such effects.

D. The electromagnetic field distribution

The standard multilayer slab dielectric waveguide model is used to describe the transverse far-field patterns.[13,14] Standard calculations yield propagation constants $\gamma = \alpha + j\beta$ and fields. For instance, for a TE mode, we can express the mth-mode field distribution for the ith layer as

$$E'_m(x) = E_m \cos(h'_m x + \phi'_m), \tag{10}$$

where h'_m is the complex eigenvalue and x is the coordinate across the active region. The overall field solution is obtained by matching the field components at each interface. The far-field pattern then becomes proportional to the Fourier transform of the near field on a lasing facet.

E. The diffusion-equation solution

Assume a three-layer device with the central layer active (see Fig. 3). Also, assume the mode is propagating down the z axis with x perpendicular to the guide. The excess carrier diffusion equations for this case become

$$\frac{d^2(\delta p)}{dx^2} - \frac{\delta p}{(L_i^*)^2} = 0, \quad i = 1,3, \tag{11a}$$

$$\frac{d^2(\delta p)}{dx^2} - \frac{\delta p}{(L_i^*)^2} = \frac{g(x)P_m(x)}{\eta_s h\nu}, \quad i = 2, \tag{11b}$$

where $L_i^* = (D^{*i}\tau^i)^{1/2}$, $g(x)$ is the localized gain and $P_m(x)$ is the optical Poynting vector component along the propagation direction.

These equations are linearized by replacing $g(x)$ with its weighted average within the active region[10]

$$g = \frac{\int_{-\infty}^{\infty} g(x)E_m^2(x)\,dx}{\int E_m^2(x)\,dx} = \frac{g_m N_m}{T_m}, \tag{12}$$

where N_m is the field normalization constant and T_m is the mode intensity integrated over the active layer. It should be noted that $g(x) = 0$ outside the active region. Further, assuming no losses in layers external to the active region, g_m represents the propagation gain of the mth mode. With D^* and τ assumed to be piecewise constant layer-to-layer, Eq. (11b) becomes

$$\frac{d^2(\delta p)}{dx^2} - \frac{\delta p}{(L_2^*)^2} = \beta_m \cos^2(h_m^2 x + \phi_m^2), \tag{13}$$

where

$$\beta_m = \frac{g_m P_m E_m^2}{D^* T_m h\nu\eta_s},$$

$$P_m = \int_{-\infty}^{\infty} P_m(x)\,dx.$$

Ignoring the minor effect of the layer 3-4 interface on the carrier distribution, the solution to the diffusion equation in the various layers becomes

$$\delta p_3(x) = G_3 \cosh(x/L_3^*) + F_3 \sinh(x/L_3^*), \tag{14a}$$

$$\delta p_2 = G_2 \cosh(x/L_2^*) + F_2 \sinh(x/L_2^*) - \beta_m (L_2^*)^2/2\left(1 + \frac{\cos^2(h_m^2 x + \phi_m^2)}{1 + (2h_m^2 L_2^{*2})^2}\right), \tag{14b}$$

$$\delta p_1(x) = G_1 \cosh(x/L_1^*) + F_1 \sinh(x/L_1^*). \tag{14c}$$

With these eigenfunctions, the solution follows directly from matching the current density and quasi-Fermi levels at each interface. The Fermi-level continuity condition is applied using Kane's nonparabolicity for the Γ_{1C} minimum and a parabolic expression for both Γ_{15V} and the X_{1C} minima. The effect of aluminum concentration on carrier mobility, effective mass, and band gap is included. The volume recombination rate is related to the optical gain of the laser in linear fashion using coefficients obtained by integrating over parabolic bands without quasimomentum conservation. The recombination lifetime is found in a similar manner. The diffusion coefficients are calculated using the generalized Einstein equation. The complete formulation of the problem is presented elsewhere.[15] The necessary roots are calculated on a computer using a real-root searching routine. The final solution provides current-voltage curves, power output-current curves, threshold current density of each mode, and finally electron and hole injection efficiencies into the active layer.

F. Validation of numerical results

This theory has been applied to double heterojunction lasers, single heterojunction lasers, and separate electron-optical confinement lasers. Close agreement has been found with experimental values. Two typical results for a double heterojunction laser are shown in Figs. 1 and 2. The first shows threshold current density as the active region thickness is reduced, and the second shows threshold as a function of the aluminum concentration in the passive regions. The slope of Fig. 1 is 5.2 kA/cm^2 μm, a value which compares closely with available data.[16,17]

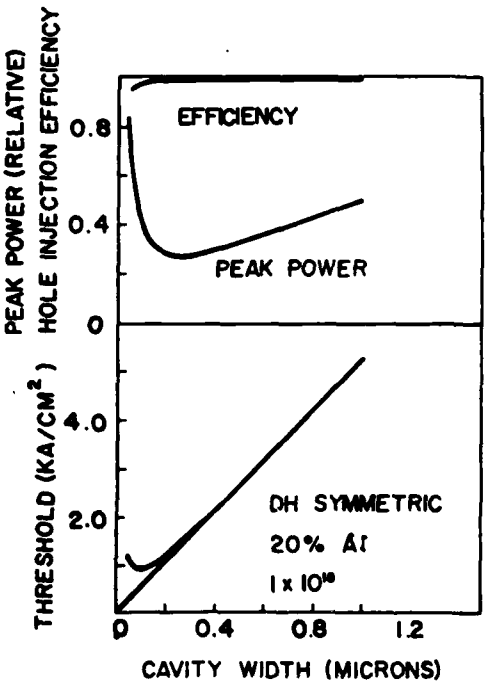

FIG. 1. Calculated hole injection efficiency, relative peak power, and threshold current density of a symmetric DH laser as a function of cavity width. The active layer doping is p-10^{17} cm^{-3} and the passive n-layer doping is 10^{18} cm^{-3}. The passive p layer has a 5×10^{18} cm^{-3} doping level. The AlAs percentage in the outer layers is 20%.

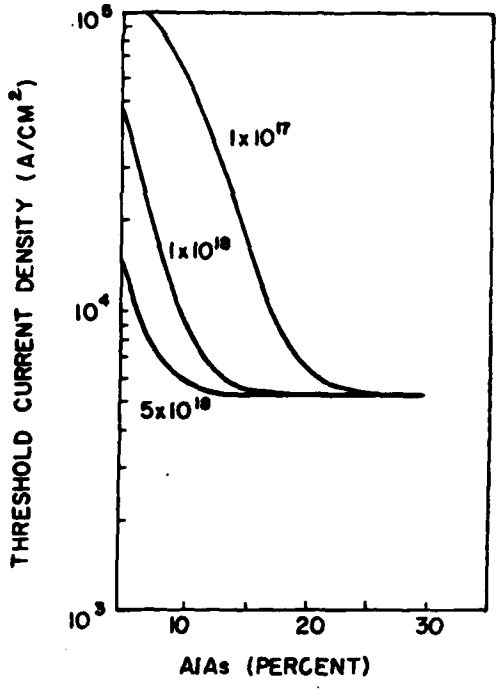

FIG. 2. Calculated threshold current density as a function of AlAs percentage in the GaAlAs passive p layer of a symmetric DH laser with a 1-μm wide GaAs (p-10^{17} cm^{-3}) active layer. Three passive p-layer doping levels are shown. The passive n-layer doping level is 1×10^{18} cm^{-3}.

III. EXPERIMENT

The lasers characterized in this experiment are broad-area double heterojunction lasers grown by liquid phase epitaxy methods. Figure 3 gives the geometry of one such laser, PL174-1-31. Other lasers of this type were characterized, but PL174-1-31 was selected for its transverse modal behavior with temperature due to the small refractive index step at one heterojunction. Estimating the refractive index of the aluminum layers is accomplished using experimental data[18,19] at a lasing wavelength $\lambda = 9000$ Å. This gives $\Delta\eta = 0.62x$, where x is the fraction of aluminum in the solid. The laser has a cross section of 214×356 μm, where the latter is the cavity length. The chip thickness is 77 μm. The

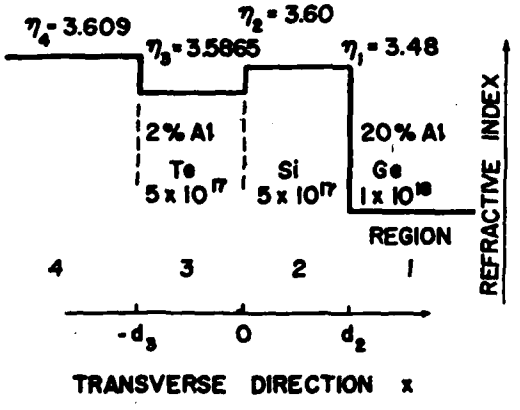

FIG. 3. Geometry of PL174-1-31. For the excess carrier calculation, only layers 1, 2, and 3 are used.

laser is mounted p-side up on the header and has no reflective coating on the facets.

The device is driven with 250-nsec pulses with a 0.01% duty cycle to minimize internal heating. While driven, the laser is heated over temperature range of 20–40 °C. The temperature/current-drive characteristics of the laser are characterized by its far- and near-field dependence.

To measure the far field, the laser is placed on a rotating platter with an axis turned by a 2-rph timing motor. The laser's output is collected by monochromator and amplified by an RCA 7102 photomultiplier tube (PMT). Typical measurement parameters are 2-Å slit width and 750-V bias for the PMT. The output of the PMT is fed to a lock-in amplifier triggered by a reference signal from the pulser. An HP 7560 A log converter and HP 2470 A×10 dc multiplier process the signal for the y axis of a chart recorder. An impedance matching network allows the y axis to be calibrated to three decibels per inch deflection. The calibration is good for over five decades of response. The speed of the x axis, combined with the 2-rph timing motor presents 24° rotation per inch deflection for the x axis. An alternative presentation is to load the PMT with a 50-Ω terminator and display the output pulse on a sampling oscilloscope with a 50-Ω input. This provides a time decomposition of the light-output pulse for ready comparison to the current-input pulse. Patterns were typically made with $J = 1.1J_{th}$.

The measurement scheme for the near field is accomplished by attaching the laser mount to a micropositioner which has a three-dimensional adjustment. A microscope objective with 160 magnification is mounted opposite the laser facet and a video camera collects the output of the objective lens and displays the image on a monitor.

Peak threshold current values for laser PL174-1-31 are shown in Fig. 4. Triangles denote the fundamental mode whereas crosses mark the second. In the heat-sink temperature range 20–28 °C, only the second mode is present; for 28–42 °C, both fundamental and second modes are present; and above 42 °C, only the fundamental mode propagates. The lasing wavelengths for the two modes are shown in Fig. 5.

The multilayer waveguide model is used to describe the transverse far-field patterns of the modes. Figure 6 is an example of a match of the second mode at 20 °C. The solid curve is the measured pattern, and the dashed curve is the match. The bump on one shoulder at 21.6° of Fig. 6 is the result of light coupling to the lossy substrate. This bump can be accurately positioned to match the experimental pattern by applying Snell's law at the substrate-air interface. The internal angle from the normal to the facet θ' is given by $\tan\theta' \simeq \theta' \simeq h_4''/\beta \simeq \eta_4 \sin\theta$. Here, h_4'' is the imaginary part of h_4, the real propagation constant $\beta = \mathrm{Im}\{\gamma\}$, θ is the external angle to the normal to the facet, and η_4 is the refractive index of the substrate. The relative intensity or amplitude of the bump is adjusted by the separating width d_3.

θ_{pp} is defined as the angle separating the two major lobes of the second mode. The solid line in Fig. 7 shows how θ_{pp} changes over the temperature range. The dashed line in Fig. 7 is the multilayer θ_{pp} versus the active-region refractive index η_2. Over the entire range 20–42 °C the active-region index depression necessary to match experimental evidence

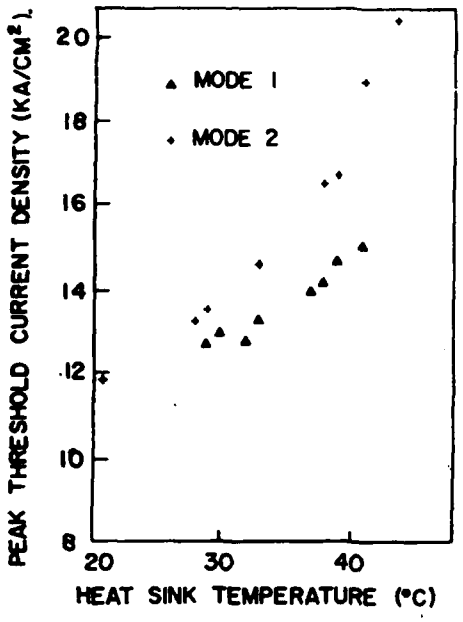

FIG. 4. Peak threshold current vs heat-sink temperature. The triangles are data points for the fundamental mode and the crosses for the second mode of PL174-1-31.

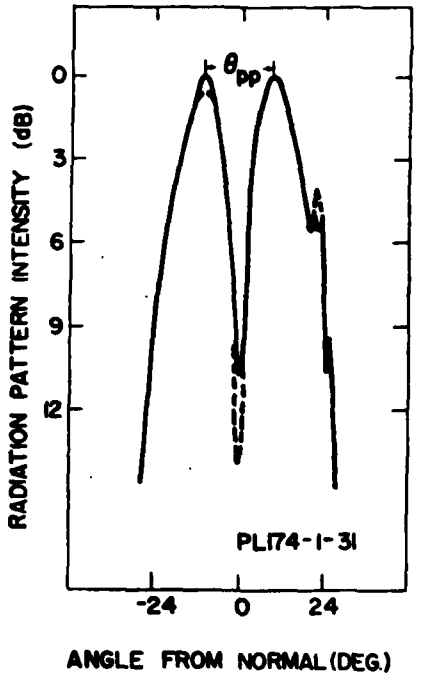

FIG. 6. Experimental (solid line) and theoretical (dashed line) far-field patterns for the second mode of PL174-1-31 at 20°.

is $\delta\eta = -0.002$. The fundamental mode also is marked by this refractive index decrease over the temperature range. The half-power full-width of the fundamental transverse mode $\theta_\perp$ decreased over 28–42 °C in a manner consistent with the $\delta\eta$ calculated for the second mode. The second-mode lobe-separation angle θ_{pp} was chosen for calculations for better accuracy.

An interesting feature of this laser is the cavity selection of modes at an intermediate temperature of 38 °C, where Fig. 4 suggests both lower-order modes may exist during a current pulse. In Figs. 8(d) and 8(e) the far field is filtered with the monochromator and the output of the photomultiplier is fed into the sampling scope with a 50-Ω termination. The top pulse of each picture is the current pulse while the lower is the optical pulse of the laser. It was established during the experiment, from output pulses as in Fig. 8 and from near-field pictures, that the laser switched modes during the current pulse. The discussion to follow explains this multimode switching with current magnitude at an intermediate temperature. Theoretical results accompanying the experiment

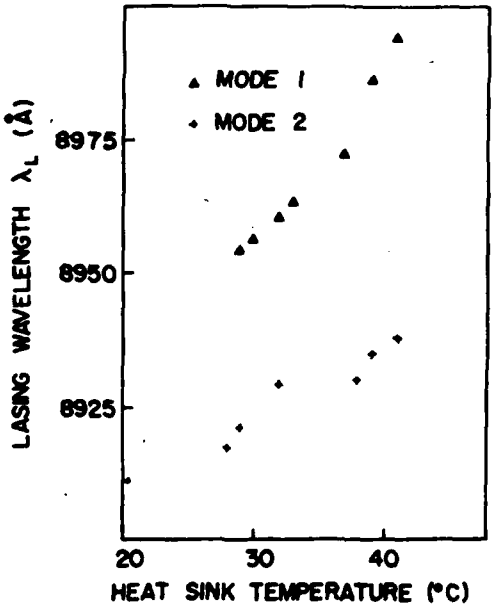

FIG. 5. Lasing wavelength vs heat-sink temperature of PL174-1-31.

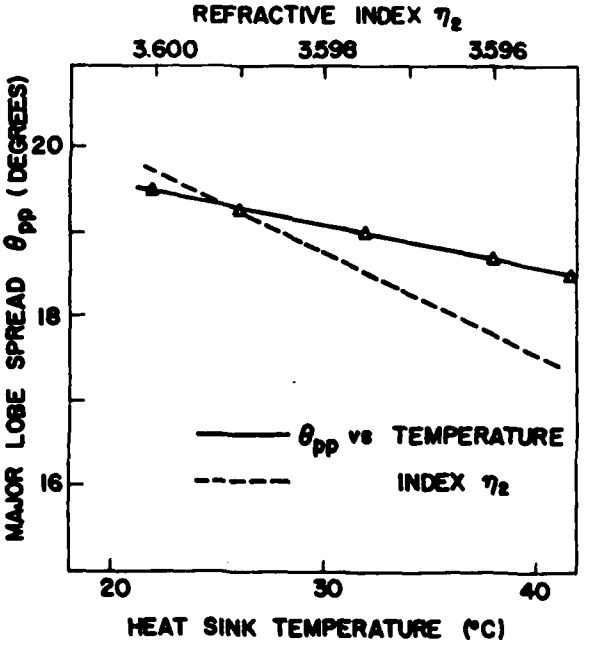

FIG. 7. Experimental θ_{pp} (solid line) vs heat-sink temperature and five-layer waveguide calculated θ_{pp} (dashed line) vs active-region index.

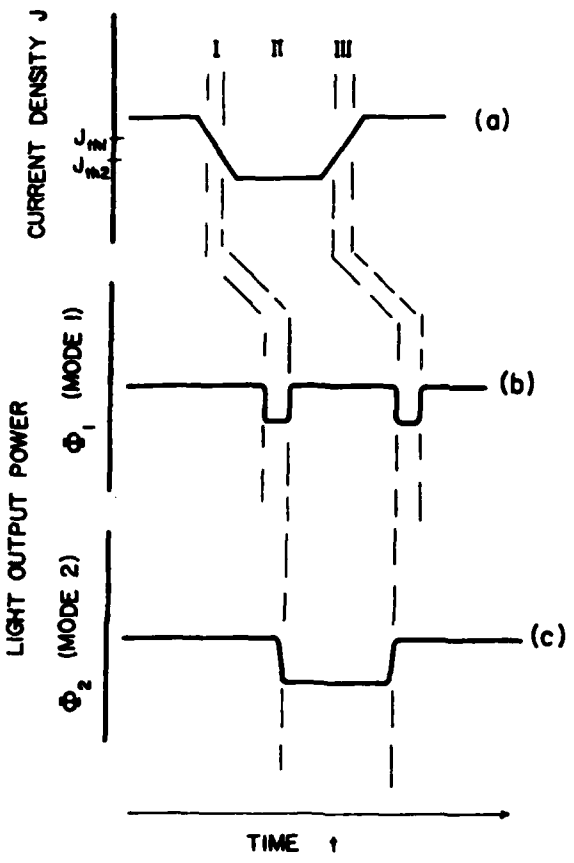

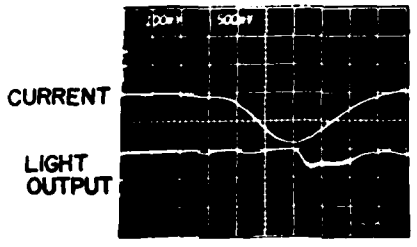

(d) MODE 1

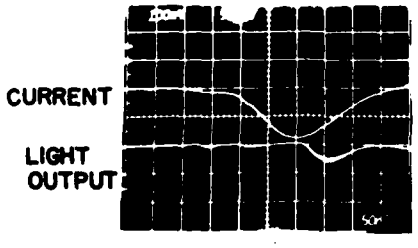

(e) MODE 2

FIG. 8. Time display of input laser current and optical output. In (a) an input current pulse is drawn. J_{th_1} and J_{th_2} are the threshold current densities of the first two modes, respectively. In (b), optical flux Φ_1 at the fundamental mode wavelength is shown to exist in regions I and III. In (c), the second mode optical flux Φ_2 is detected in region II at the second mode wavelength. In (d), the experimental output pulse is shown in the lower trace at the fundamental mode wavelength. The top pulse is the input current. In (e), the lower trace is the second-mode output at its wavelength.

show the cavity selection is sensitive to gain/mode profile coupling and index change with excess carrier injection.

IV. DISCUSSION

The data from Fig. 3 were used with the data from Table I for a multilayer waveguide analysis of the transverse modes. This method was used first to check the accuracy of material parameters. In Fig. 6, the dashed line shows a close fit with the solid measured curve of the far field. The pip on one shoulder is a leaky wave coupling to the substrate layer. As previously mentioned, Snell's law dictates a fixed refractive index for the substrate. It was noticed in the experiment that the pip remained stationary in angular displacement with temperature change 20–40 °C and with current drive. Also, the pip remains about 4 dB below the main lobes over temperature and current variations. This means the thickness and refractive index of layer 3 in Fig. 2 should be fixed in order to hold the pip stationary. The only feature to change for the second mode is the angular separation of the major lobes designated as θ_{pp}. These data are represented in Fig. 7 and will be discussed subsequently.

The only way to match the θ_{pp} change with temperature is to slightly decrease the active-layer refractive index with increased current drive. The increase in threshold current of a mode with temperature occurs due to a modal confinement change, internal quantum-efficiency decrease, or a carrier-lifetime or absorption-coefficient change.[20] Near-field measurements did not show a shift of the transverse mode with temperature. The refractive-index change of each layer with temperature $\delta\eta/\delta T$ can be shown to be 1.5×10^{-4}/°K.[21] For a twenty-degree range, 20–40 °C, $\delta\eta\simeq0.003$. On the other hand, the index change due to dispersion[21] for a layer is $\delta\eta/\delta E\simeq0.8$/eV. For $\delta\lambda = 20$ Å from Fig. 5 (the first high-order mode), it can be shown that $\delta\eta\simeq -0.003$/Å.

The dispersion and heating effects on refractive index of each layer tend to cancel. Therefore, with the evidence that the near field remains constant with temperature, the pip on the shoulder of the far field remains stationary and dispersion and heating effects tend to cancel, it is assumed that the dominant refractive-index change is that of the active layer

TABLE I. Typical values for the physical constants used in the ambipolar diffusion solution.[a]

	Layer 1	Layer 2	Layer 3
Doping	p-10^{-18}	p-5×10^{17}	n-5×10^{17}
Al concentration	20%	0	2%
η	3.48	variable	3.5865
Absorption	5	20.8	2.4
Width	...	2.65×10^{-4}	...
μ_n	3132	3649	3649
μ_p	138	167	167
D_n	81.0	198	128
D_p	3.67	4.65	4.33
τ	7.69×10^{-9}	3.59×10^{-9}	8.46×10^{-9}
D^*	80.6	15.6	6.8
L^*	7.87×10^{-4}	2.37×10^{-4}	2.4×10^{-4}

[a] All quantities are in cgs units, with the exception of mobility which is in the mixed units cm^2/V sec and absorption which is in cm^{-1}.

TABLE II. Calculated values for threshold current density, modal absorption and internal differential quantum efficiency obtained from the ambipolar diffusion solution

	Mode 1	Mode 2
Threshold current density (kA/cm^2)	15.58	16.93
Modal absorption (cm^{-1})	19.74	6.38
Internal differential quantum efficiency (%)	66.8	72.8

due to injection level. The data of Tables I and II and Fig. 3 are used to find the solution to the ambipolar diffusion equation. A rise in temperature is represented by a reduction in refractive index as required in matching the far-field pattern of Fig. 6.

With the relevant material parameters listed in Fig. 3, a solution was found for the ambipolar diffusion equation. In Fig. 9 the threshold current density for the first two modes is plotted as a function of the active-region refractive index. For larger η_2 values (corresponding to a larger index step) the second mode has the lowest threshold due to superior coupling to the excess carrier distribution. But as the active-region index is lowered and the second mode approaches cutoff, its coupling efficiency diminshes and the fundamental mode emerges with the lowest threshold.

Typical material parameters calculated (fundamental mode at $\eta_2 = 3.5948$) are shown in Table I. Since many of the parameters depend on injection levels, the quantities in Table I vary slightly over the graphs presented. With these calculated values, the usefulness of the ambipolar equation can be shown for the active layer. The calculated hole-injection efficiency is 99.4% and the electron-injection efficiency is 86% for this case. This calculation predicts a crossover point at a slightly lower η_2 value than the multilayer mode range in Fig. 7. This is because in the multilayer model, the presence of the substrate with a relatively high refractive index increases the active-region eigenvalue. For instance, if the buffer-layer thickness d_3 were decreased, the active-layer eigenvalue would shift even more.

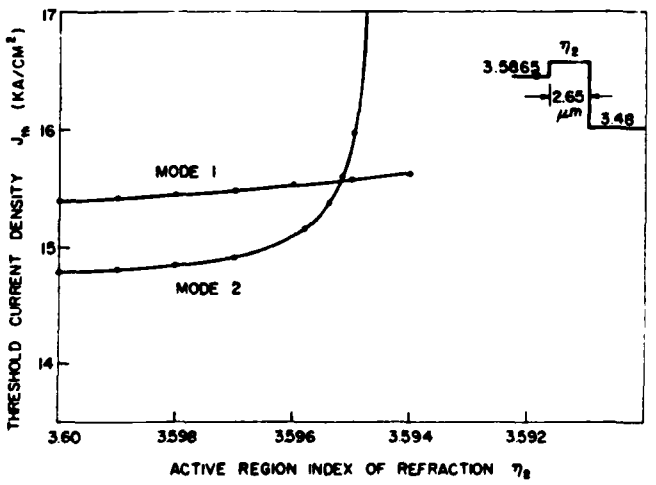

FIG. 9. Ambipolar diffusion solution. Threshold current density for the first-and second-order modes is plotted against the active-region index η_2.

Figure 9 is useful in interpreting the phenomena shown in Fig. 4. The fundamental mode does not occur below 30 °C. At 20 °C, the second mode has a threshold current density of about 12 kA/cm^2. However, abruptly above 30 °C, the fundamental mode appears. From Fig. 8, a slight change in η_2 on the order of $\delta\eta_2 = -0.002$ is sufficient to cause a crossover in threshold currents between the two modes. Both Figs. 4 and 9 show that the second-mode threshold increases sharply after the crossover. Threshold current densities predicted by the ambipolar solution are in fair agreement with experimental values.

Modal output power as a function of current density is plotted in Fig. 10. Because the linear theory of gain is assumed, only one mode at a time is calculated. At power levels above threshold, the modal gain is assumed pinned at its threshold value. Note that the second mode, despite higher threshold current density and reduced coupling efficiency, has a higher internal differential quantum efficiency than the fundamental mode. Thus, for a sufficient overdrive beyond threshold, the second mode will eventually be the more efficient overall and will dominate. An explanation for this higher internal differential quantum efficiency can be seen in Table II. The modal absorption of the second mode is low because a significant portion of its energy is propagating outside the lossy active region whereas most of the fundamental mode is well confined to the active region. Since modal loss dominates slope efficiency, the second mode has the higher value. This higher value, in conjunction with a higher threshold due to poorer coupling efficiency, causes the mode efficiency crossover point.

With these results, the phenomena of mode crossover in this laser can be understood. At 20 °C the second mode has the lower threshold and higher efficiency and consequently only the second mode appears. At an intermediate temperature, the second mode will appear at high-enough current overdrive due to better slope efficiency. Above 42 °C, the threshold for the second mode becomes prohibitive. Figure 8 depicts a time resolution between the two modes at an intermediate temperature. Figure 8(a) represents an input drive pulse. The two threshold current densities for the two modes are labeled J_1 and J_2. As the current pulse rises above J_1 the first mode turns on in region I. Output flux Φ_1 for the first mode is represented in Fig. 8(b). As the input current progresses to J_2, region II is entered. The second mode turns on, as shown in Fig. 8(c), as Φ_2. Finally, with the drop of input current, region III is entered and first mode reappears. As shown in Figs. 8(d) and 8(e), this situation is observed experimentally. In Fig. 8(d), the monochromator is set on the first-mode wavelength and the lower pulse is the output power. Reviewing the two output pulses, it can be seen the two modes have a time separation during a current pulse. This is explained by the fact that, from Fig. 9, the second-mode threshold can still be reached slightly after crossover. From Fig. 10, the second mode clearly is predicted to dominate the first mode if threshold can be reached, due to better efficiency.

Theoretical mode and excess carrier coupling for the laser is shown in Fig. 11, where the excess carrier profile is plotted across the active layer for the two modes operating at

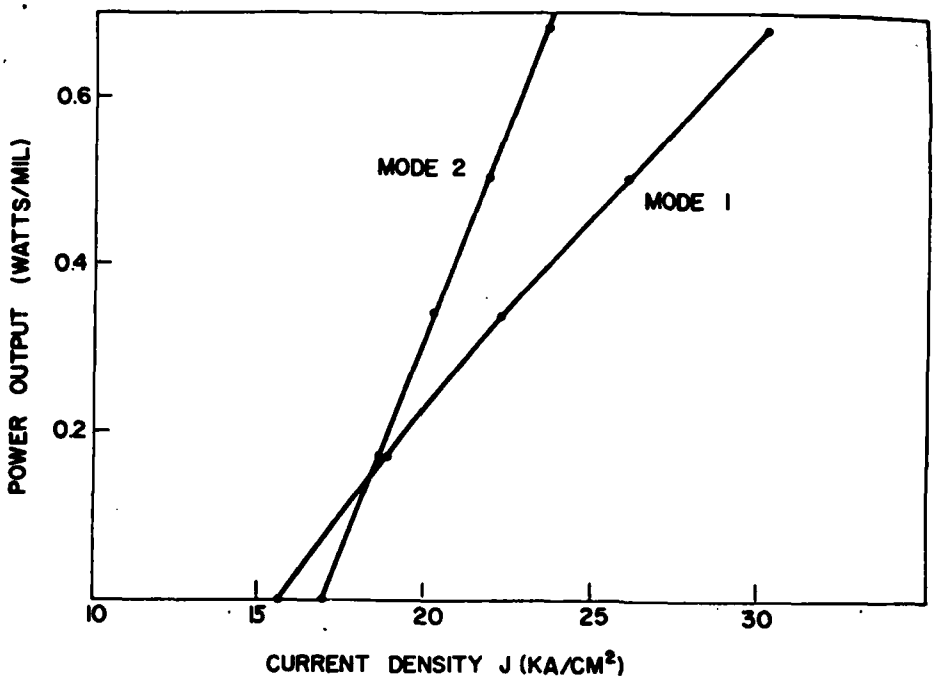

FIG. 10. Ambipolar diffusion solution. Output power is plotted against threshold current density for the first two modes. The slight curvature in the mode 1 curve is caused by carrier redistribution. The index $\eta_2 = 3.5948$.

two power-output levels (threshold and 0.67 w/mil.). Included on the carrier plot is the normalized modal distribution. Several factors should be noted. First, the second-mode distribution is clearly penetrating the passive n layer, indicating a near cutoff situation and a modal loss dominated by the n-layer absorption. With all curves normalizd, a simple product of δp and E^2, integrated over the active region, shows the fundamental mode better coupled than the second, as expected. Second, it can be seen that the carrier profile peaks on the side where holes are injected. This profile contradicts the notion that electron injection dominates and the peak occurs on the n side. Since the charge cloud is ambipolar, it must accommodate the low-hole mobility to maintain quasi-charge neutrality. Hence, the profile is skewed toward the hole injection or p side of the active layer. As expected, carrier profiles change shape with current density.

As a final note, we use the refractive-index dependency of the active region on temperature and hence current density to estimate the free-carrier effect. The influence of free carriers on the refractive index in a material is determined from the classical theory of dispersion. The refractive index in the presence of free carriers η is related to the refractive index in the absence of carriers $\bar{\eta}$ by

$$\eta^2 = \bar{\eta}^2\left(1 - \frac{4\pi N q^2}{m^* \omega^2 \bar{\eta}^2}\right). \tag{15}$$

Here, m^* is the effective mass of the carrier, q is the charge of an electron, N is the carrier density, $\omega = 2\pi c/\lambda$, and ϵ_0 is the vacuum permittivity. Since the change in index is much smaller than $\bar{\eta}$, Eq. (15) can be rearranged to

$$\delta\eta_{fc} \simeq \frac{2\pi N q^2}{m^* \omega^2 \bar{\eta}}. \tag{16}$$

In other words, the change in index due to free carriers is directly proportional to the concentration of free carriers

$$\delta\eta_{fc} = K N, \tag{17}$$

where K is a constant we wish to determine. By plotting refractive-index change versus carrier increase, the constant K would be the slope at a particular point

$$d(\delta\eta_{fc}) = K\, d(N) \tag{18}$$

or

$$K = \frac{d(\delta\eta_{fc})}{d(N)}. \tag{19}$$

A change in a particular parameter, say lifetime τ, with injection would be reflected in Eq. (17) having a nonzero second derivative. We take $\delta\eta_{fc}$ from Fig. 7 and conclude that this index change is very nearly a linear function of temperature. However, we find from Fig. 4, carrier concentration N, related to the peak threshold current, is not quite a linear function with temperature. Therefore, under the assumption the free-carrier effect is the dominant cause of observed pattern change, the constant K would be precisely

$$K = \frac{d(\delta\eta_{fc})/dT}{d(N)/dT}.$$

This expression contains the information that K is not a true "constant" but is itself a slight function of injection level. Nevertheless, it is instructive to estimate K using Eq. (19) to compare with conventional theory. Using

$$N = \frac{J\tau}{q d_2}$$

and a straight line approximation to $d(N)$ over the temperature range 20–42 °C we get

$$K = -3.1 \times 10^{-21}\ \text{cm}^3, \quad \tau = 3\ \text{nsec}$$

and

$$K = -6.2 \times 10^{-21}\ \text{cm}^3, \quad \tau = 2\ \text{nsec}.$$

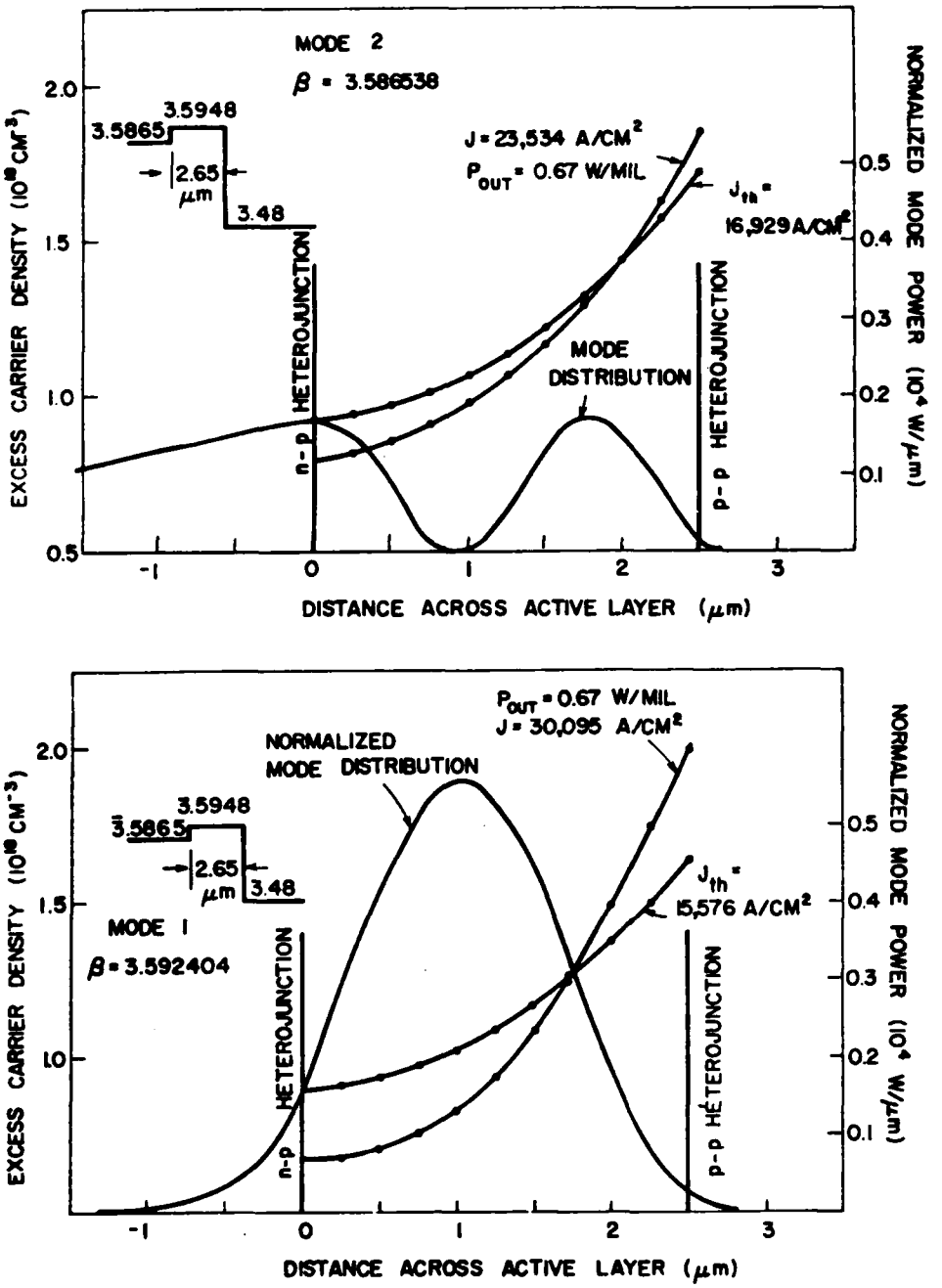

FIG. 11. Excess carrier densities plotted across the active region for the ambipolar diffusion equation. In (a), the second-mode distribution is plotted. In (b), the first-mode distribution is shown. Note in (a) that the second mode "tail" extends into the *n* cladding.

These results can be compared to $K = -4\times10^{-21}$ cm^3 from Thompson[22] and $K = -(5\text{–}11)\times10^{-21}$ cm^3 from Selway.[23] Thompson used $\tau = 3$ nsec for his calculation. Several other values for K have recently been reported. Olsson and Tang[24] report $K = -(4.9\pm0.4)\times10^{-21}$ for $\tau = 2.2$ nsec. Henry *et al.*[25] report $K = -(1.8\pm0.4)\times10^{-21}$ for lasers with carrier densities estimated at 1.02×10^{18} cm^{-3}.

V. CONCLUSION

A solution for the ambipolar diffusion was presented for the active region of a double heterojunction laser. Along with the solution of modes from Maxwell's equations in a multilayer waveguide, this combined description was applied to a broad-area heterojunction laser. The refractive-index change of the active region with temperature was estimated from far-field pattern matching of the transverse modes. Transverse-mode-selection conditions were predicted with the diffusion equation and compared with the transverse-mode selection of the sample laser.

Mode threshold was shown to depend on coupling efficiency between excess carriers and modal distribution in the active layer. The differential internal quantum efficiency depends primarily on mode absorption and injection efficiency. Mode crossover occurs when the mode with the highest threshold also has the highest slope efficiency.

Carrier transport in a semiconductor laser is an ambipolar diffusion process which can be described using the relaxation time approximation. In bulk regions, quasi-charge

neutrality is satisfied because of the strong internal field between electrons and holes. The active region of a semiconductor laser undergoes double injection: hole injection from the p side and electron injection from the n side. In devices with good injection efficiencies, the injected carrier profile is higher at the p-p, rather than at the p-n, interface because of low hole mobility.

The device modeled here shows a distinct peak of carriers on the p-p interface. The slope of the carrier profile increases with increased current density. Since these carrier profiles demonstrate significant skewing, it is clear that this can affect mode selection if the modal shape couples poorly with the carrier concentration.

ACKNOWLEDGMENTS

The lasers used in this study were supplied by E. Mehal. This work was supported in part by the U.S. Army Research Office.

[1]J. C. Dyment, Appl. Phys. Lett. **10**, 84 (1967).
[2]J. E. Ripper, J. C. Dyment, L. A. D'Asaro, and T. L. Paoli, Appl. Phys. Lett. **18**, 155 (1971).
[3]J. C. Dyment, L. A. D'Asaro, J. C. North, B. I. Miller, and J. C. Ripper, Proc. IEEE **60**, 726 (1976).
[4]R. D. Burnham and D. R. Scifres, Appl. Phys. Lett. **27**, 510 (1975).
[5]D. Botez, W. Tsang, and S. Wang, Appl. Phys. Lett. **28**, 234 (1976).
[6]P. A. Kirkby and G. H. B. Thompson, J. Appl. Phys. **47**, 4578 (1976).
[7]K. Aiki, M. Nakamura, T. Karoda, J. Omeda, R. Ito, N. Chinone, and M. Maeda, IEEE J. Quantum Electron. **QE-14**, 89 (1978).
[8]J. P. McKelvey, *Solid State and Semiconductor Physics* (Harper & Row, New York, 1966).
[9]W. Van Roosbroeck, Phys. Rev. **91**, 282 (1953).
[10]B. W. Hakki, J. Appl. Phys. **45**, 288 (1974).
[11]F. Stern, IEEE J. Quantum Electron. **QE-9**, 290 (1973).
[12]G. W. 'tHooft, Appl. Phys. Lett. **39**, 389 (1981).
[13]J. K. Butler, J. Appl. Phys. **42**, 4447 (1971).
[14]M. Cross, IEEE J. Quantum Electron. **QE-9**, 517 (1973).
[15]R. R. Shurtz, *Mode and Recombination Control in Semiconductor Lasers*, Ph.D. Dissertation, University Microfilms International, No. 76-3782, (1975).
[16]E. Pinkas, B. I. Hayashi, and P. W. Foy, J. Appl. Phys. **43**, 2877 (1972).
[17]J. C. Dyment, F. R. Nash, C. J. Hwang, C. A. Rozonyi, R. C. Hartman, H. M. Marcos, and S. F. Haszky, Appl. Phys. Lett. **24**, 481 (1974).
[18]H. Kressel, H. F. Lockwood, and J. K. Butler, J. Appl. Phys. **44**, 4095 (1973).
[19]H. C. Casey, Jr., D. D. Sell, and M. B. Panish, Appl. Phys. Lett. **24**, 63 (1974).
[20]H. Kressel and J. K. Butler, *Semiconductor Lasers and Heterojunction LED's*, (Academic, New York, 1977).
[21]F. Stern, Phys. Rev. **133**, A1653 (1964).
[22]G. H. B. Thompson, Opto-Electron. **4**, 257 (1972).
[23]P. R. Selway, G. H. B. Thompson, G. D. Henshall, and J. E. A. Whiteway, Electron. Lett. **10**, 453 (1974).
[24]A. Olsson and C. L. Tang, Appl. Phys. Lett. **39**, 24 (1981).
[25]C. J. Henry, R. A. Logan, and K. A. Bertness, J. Appl. Phys. **52**, 4457 (1981).

COMPARISON OF NUMERICAL AND EFFECTIVE-INDEX METHODS FOR A CLASS OF DIELECTRIC WAVEGUIDES*

H-2

A. Linz and J.K. Butler
Electrical Engineering Department
Southern Methodist University
Dallas, Texas 75275

Abstract

A numerical method and the effective-index method are applied to a three-layer, constant thickness dielectric waveguide with smoothly varying dielectric constant inside the active layer and constant permittivity in the confining layers. The results of the two methods are compared in terms of the propagation constant γ calculated by each method. Application of the effective-index method facilitates a physical understanding of dielectric waveguide modes as well as providing an efficient approximate method for calculating mode behavior.

*Supported by the U.S. Army Research Office.

Introduction

Several papers [1-3] have analyzed mode propagation in dielectric waveguides with spatially varying refractive index, usually approximated by parabolic or $\tanh^2$ functions, which go to infinity at large distances from the reference point $x = 0$. We will use the approximation [4]

$$\kappa = \kappa_S + \Delta\kappa/\cosh^2(x/x_0) \tag{1}$$

to describe the variation of κ. This is in closer correspondence with the physical situation and leads to equations with known solutions. The disadvantage in this case is the fact that the field solutions consist of a finite (possibly empty) set of confined (trapped) modes, an infinite set of diverging "leaky" modes and a continuum of solutions that will be designated as "radiation" modes.

The 2-dimensional character of the problem due to the variation of the refractive index in the lateral (x) and transverse (y) directions requires the use of approximate methods or numerical solutions. Among the former, the effective index method is the most popular ([2], [4] - [8]). Direct numerical integration is possible, but the computation time required is much larger than that needed for other methods like the one used in [1], which we will apply in this paper.

The following sections describe the class of waveguides considered, the numerical method and the application of the effective-index method to our problem, ending with conclusions.

Description of Structures

Figure 1 shows the structure considered in this paper. The confining layers A and C are assumed identical, their refractive indices being described by

$$\kappa_A = \kappa_C = n_A^2 - i\,\alpha_A n_A/k_0 \tag{2}$$

α_A describes the power loss in these layers and is constant with distance. The active layer has a constant thickness d, with a refractive index

$$\kappa(x) = n^2(x) - i\,\alpha(x)\,n(x)/k_0 \tag{3}$$

whose dependence with x is considered to be reasonably well-approximated by (1). In that equation,

$$\Delta\kappa = \kappa_0 - \kappa_S \tag{4a}$$

$$\kappa_0 = \kappa(0) = n_0^2 + i\,g_0\,n_0/k_0 \tag{4b}$$

$$\kappa_S = n_S^2 - i\,\alpha_S\,n_S/k_0 \tag{4c}$$

x_0 is a parameter related to the width of the stripe contact in the case of a semiconductor laser. The values of power attenuation coefficient and refractive index inside the active region far away from the stripe are α_S and n_S, respectively. The quantity g_0 represents the peak power gain under the stripe ($x = 0$), where the refractive index is n_0. For $\Delta n = n_0 - n_S > 0$ the mode will be index-guided, while for $\Delta n < 0$ it will be index anti-guided, and this latter effect can eventually offset the guiding effect of the gain distribution.

Numerical Solution

We follow the method used in [1]. Maxwell's equations are solved for both the active and the confining layers, requiring as boundary conditions that the general solutions inside and outside the active layer and their normal derivatives match at the interfaces $y = \pm d/2$. We also demand that these solutions vanish at $x = \pm\infty$, $y = \pm\infty$. Application of the method of separation of variables results in a vertical field solution inside the active region of the form

$$\phi(y) = \begin{Bmatrix}\sin \\ \cos\end{Bmatrix} qy \tag{5}$$

and a differential equation

$$\frac{d^2\psi}{dx^2} + \left[k_0^2\kappa_S + \gamma^2 - q^2 + k_0^2\,\frac{\Delta\kappa}{\cosh^2(x/x_0)}\right]\psi = 0 \tag{6}$$

where q is the separation constant. Equation (6) possesses solutions of the form

$$\psi_\ell(x) = [\cosh(x/x_0)]^{\ell - b_0}\, C_\ell^{b_0 - \ell + \frac{1}{2}}(\tanh[x/x_0]) \tag{7}$$

where $C_\ell^\lambda(z)$ are Gegenbauer polynomials [9] and

$$b_0 = -\tfrac{1}{2} + (\tfrac{1}{4} + k_0^2 x_0^2\,\Delta\kappa)^{\frac{1}{2}} \tag{8}$$

To satisfy the boundary conditions we require

$$\mathrm{Re}\{b_0 - \ell\} > 0 \tag{9}$$

For $\mathrm{Re}\{b_0\} > 0$, the fundamental mode ($\ell = 0$) is trapped. Modes of order ℓ such that $\mathrm{Re}\{b_0 - \ell\} < 0$ are still solutions of (6) but diverge as $|x| \to \infty$ and will be designated as "leaky". Radiation modes would be described by other solutions of (6) for arbitrary (non-integer) eigenvalues [9]. The general solution will be a linear combination of the few discrete trapped

0149-645X/82/0000-0107 $00.75

modes (8) satisfying (9), plus an integral over the continuum, and the leaky modes must be excluded if the field has to vanish for $|x| \to \infty$. The importance of the continuum can be expected to decrease as the number of trapped modes increases. Since this number is relatively large for structures with modal gains that are high and not very sensitive to the refractive index step $\Delta n = n_0 - n_s$, this continuum will be neglected. Hence, the general even solution inside the active region is approximated by

$$\psi_b(x,y) \approx \sum_{\ell=0,2,\ldots}^{\bar{\ell}_{max}} A_\ell \, \psi_\ell(x) \cos(q_\ell \, y) \qquad (10)$$

where $\bar{\ell}_{max}$ is the maximum even value of ℓ for which $\psi_\ell(x)$ is confined. Solution of the wave equation for the confining layers proceeds as in [1]. Matching the functions and their derivatives with respect to y at the boundary $y = d/2$ and applying the orthogonality relation for the trapped modes results in a finite system of homogeneous linear equations

$$(\Omega^T - I)\bar{A} = 0 \qquad (11)$$

where $A^{-T} = (A_0, A_2, \ldots, A_{\bar{\ell}_{max}})$, I is the unit matrix, and the matrix elements of Ω are given by

$$\Omega_{\ell\ell'}(\gamma) = \frac{4 \cos(q_\ell \, d/2) \sqrt{N_\ell}}{\pi x_0 \, q_{\ell'} \sin(q_{\ell'} \frac{d}{2}) \sqrt{N_{\ell'}}} \, I_{\ell\ell'}(\gamma) \qquad (12)$$

where $$I_{\ell,\ell'}(\gamma) = \int_0^\infty \bar{\psi}_\ell(\chi) \, \bar{\psi}_{\ell'}(\chi) \, (\chi^2 - \gamma^2 - k_a^2)^{\frac{1}{2}} \, d\chi \qquad (13)$$

$\bar{\psi}_\ell(\chi)$ being the normalized Fourier cosine transform of $\psi_\ell(x)$, and $\ell, \ell' = 0, 2, \ldots, \bar{\ell}_{max}$. The q_ℓ satisfy

$$q_\ell^2 = \gamma^2 + k_0^2 \kappa_s + (b_0 - \ell)^2 / x_0^2 \qquad (14)$$

The system of equations (11) has a non-trivial solution only if $\det(\Omega - 1) = 0$. Numerical computation of the roots yields the possible values of the propagation constant γ.

Numerical Results

The method was applied to a structure described by the following parameters:

$n_A = 3.38$, $\alpha_A = 50\ cm^{-1}$, $\alpha_S = 50\ cm^{-1}$, $g_0 = 200 cm^{-1}$

$n_0 = 3.595$, $x_0 = 6\mu m$.

Direct solution of (11) involves computation of the $\Omega_{\ell\ell'}$. In general, $\Omega_{\ell\ell'} = \Omega_{\ell'\ell}$, but $I_{\ell\ell'} = I_{\ell'\ell}$. Values of the modal loss = $\mathrm{Re}(\gamma)$ were computed by evaluating $I_{\ell\ell'}(\gamma)$ using the exact expression (13). This has to be done once for every value of γ. Instead of solving the complete system (11), we start with a 1x1 matrix, go on to a 2x2 matrix, etc., and observe that the result converges relatively fast for a 2x2 case, which is considered sufficient for our approximation. In spite of this, the computation time is still impractically high. An increase in speed by nearly two orders of magnitude while still maintaining good accuracy is achieved expanding the radical in (13) using the binomial theorem (which results in integrals that do not depend on γ) and retaining the first three terms.

Figure 2 shows plots of the modal loss = $\mathrm{Re}(\gamma)$ as a function of Δn with g_0, the gain under the stripe, as a parameter. We notice that, for each value of g_0, Δn can be decreased up to a certain value beyond which the fundamental mode becomes leaky.

Effective-Index Calculation

The effective-index method consists basically of reducing a two-dimensional problem to an equivalent one-dimensional one. In our case, the two-dimensional character of the problem is given by the dependence of the dielectric constant on x and y. As a first approximation, the variation in one direction (in our case, x) is neglected; this is justified if this variation is much less than that in the y direction. This is equivalent to approximating the waveguide with a simple 3-layer guide whose dielectric constants do not vary with x. The solution of this problem yields the transverse or vertical variation of the field. Next, the original equation describing the 2-dimensional equation in x can be solved for the lateral variation of the field, and the overall solution is approximated by the product of this lateral field and the vertical field found from the 3-layer problem. We start with the wave equation in 2 dimensions:

$$\nabla_t^2 \psi + [\gamma^2 + k_0^2 \kappa(x,y)] \psi = 0 \qquad (15)$$

For the simple 3-layer guide we assume $\kappa(x) = \kappa_0$ inside the active layer. Now, we transform (15) making $\Psi(x,y) = \psi(x) \, \phi(y)$, multiplying it by $\phi^*(y)$ and integrating it over y from $-\infty$ to ∞, and obtain

$$\frac{d^2\psi}{dx^2} + [\gamma^2 - q_{eff}^2 + k_0^2 \kappa_{S\,eff} + k_0^2 \frac{\Delta\kappa_{eff}}{\cosh^2(x/x_0)}]\psi = 0 \qquad (16)$$

with
$$q_{eff}^2 = \Gamma k_0^2 x_0 - p^2 - k_0^2 \kappa_A \qquad (17a)$$

$$\kappa_{S\,eff} = \Gamma \kappa_S \qquad (17b)$$

$$\Delta\kappa_{eff} = \Gamma \Delta\kappa \qquad (17c)$$

where Γ is the filling or confinement factor.

Equation (16) has the same form as eq. (6). It will also have polynomial solutions similar to (7) that represent trapped modes:

$$\psi_\ell(x) = [\cosh(x/x_0)]^{\ell - b_{0\,eff}} \, C_\ell^{b_{0\,eff} - \ell + \frac{1}{2}} (\tanh \frac{x}{x_0}) \qquad (18)$$

$$\ell = 0, 1, 2, \ldots$$

where $b_{0\,eff}$ is defined as in (8) with $\Delta\kappa$ replaced by $\Gamma \Delta\kappa$ and p is the eigenvalue of the simple 3-layer problem. For the fundamental mode, $\ell = 0$, and we obtain

$$\gamma^2 = -k_0^2 \kappa_A - (b_{0\,eff}^2 / x_0^2) - (p^2 - k_0^2 \Gamma \Delta\kappa) \qquad (19)$$

for the propagation constant.

Discussion

Values of γ obtained using (19) are compared with those obtained with the numerical method in fig. 3. Solutions are very close for all values of Δn for which the mode exhibits a gain which is relatively high and with low sensitivity to Δn. The results differ most in the range of Δn for which the mode has a net loss or has a relatively low gain with higher sensitivity to Δn.

Figure 4 gives the required value of the peak power gain g_0 under the stripe to obtain a given modal gain G, as a function of Δn, using the effective-index method.

Also included is the region for which the fundamental mode becomes leaky. The vertical confinement factor Γ did not vary appreciably with Δn; a typical value for the case considered was $\Gamma = 0.4963$. We see that lateral variations in the refractive index affect the gain much more by altering the lateral field distribution than by affecting the vertical variation.

The effective-index method is seen to be a fast and relatively accurate way to obtain the field distributions for the class of waveguides considered, for which the numerical method we used is not practical for extensive modeling due to its long computation time in spite of all approximations. The remarkable agreement between the effective-index method and experimental results found by other workers ([10]) increases our confidence in this powerful approximate method.

References

1. J.K. Butler and J.B. Delaney, "A Rigorous Boundary Value Solution for the Lateral Modes of Stripe Geometry Injection Lasers", IEEE J. Quantum Electron., Vol. QE-14, pp. 507-513, 1978.

2. T.L. Paoli, "Waveguiding in a Stripe-Geometry Junction Laser", IEEE J. Quantum Electron., Vol. QE-13, pp. 662-668, 1977.

3. W. Streifer, D. Scifres, R. Burnham, "Analysis of Gain-Induced Waveguiding in Stripe-Geometry Injection Lasers", IEEE J.Q.E. Vol. QE-14, No. 6, June, 1978 pp. 418-427.

4. P.M. Asbeck, D.A. Cammack, and J.J. Daniele, "Non-gaussian Fundamental Mode Patterns in Narrow-Stripe-Geometry Lasers", Appl. Phys. Lett., Vol. 33, pp. 504-506, 1978.

5. R.M. Knox and P.P. Toulios, "Integrated Circuits for the Millimeter Through Optical Frequency Range", Proc. MRI Symp. on Submillimeter Waves, J. Fox, Ed. (Polytechnic Press, Brooklyn, 1970).

6. W. Streifer and E. Kapon, "Application of the Equivalent-Index Method to DH Diode Lasers", Appl. Opt. Vol. 18, pp. 3724-3725, 1979.

7. J. Buus, "A Model for the Static Properties of DH Lasers", IEEE Electron., Vol. QE-15, pp. 734-739, 1972.

8. J.K. Butler and J.B. Delaney, "Field Solutions for the Lateral Modes of Stripe Geometry Injection Lasers", IEEE J. Quantum Electron., Vol. QE-16, pp. 1326-1328, 1980.

9. Erdelyi, Magnus, Oberhettinger, Tricomi, "Higher Transcendental Functions", Vol. I-Bateman Manuscript Project - McGraw-Hill, 1953, Sections 3.15, 3.16.

10. J.K. Butler, D. Botez, "Mode Characteristics of Non-Planar Double-Heterojunction and Large-Optical Cavity Laser Structures", to be published.

Figures

1. Waveguide structure considered
2. Modal loss as a function of Δn with peak power gain g_0 as a parameter. Regions at left of vertical lines correspond to leaky fundamental mode.
3. Modal loss $\mathrm{Re}(\gamma)$ as a function of Δn for numeric (1x1 matrix) and effective-index methods.
4. Peak power gain under contact stripe (g_0) as a function of Δn with modal gain as a parameter. Shaded area shows region corresponding to leaky fundamental mode.

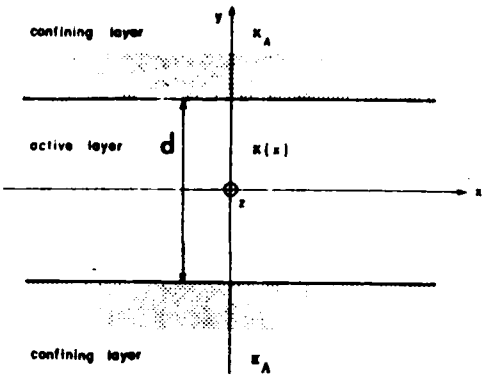

Figure 1

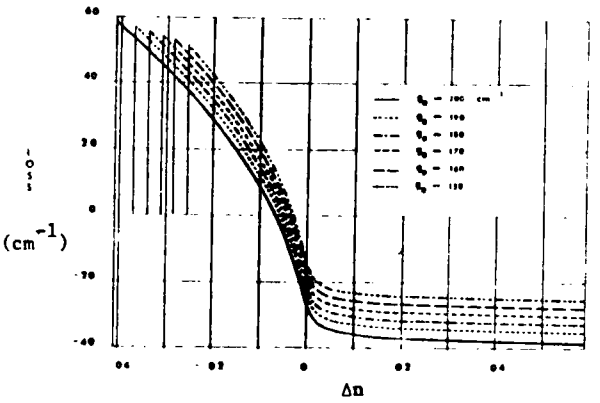

Figure 2

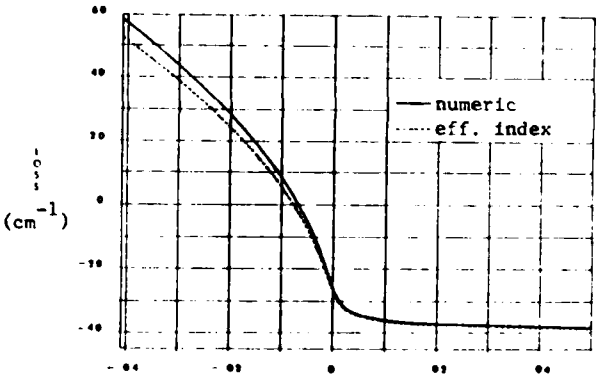

Figure 3

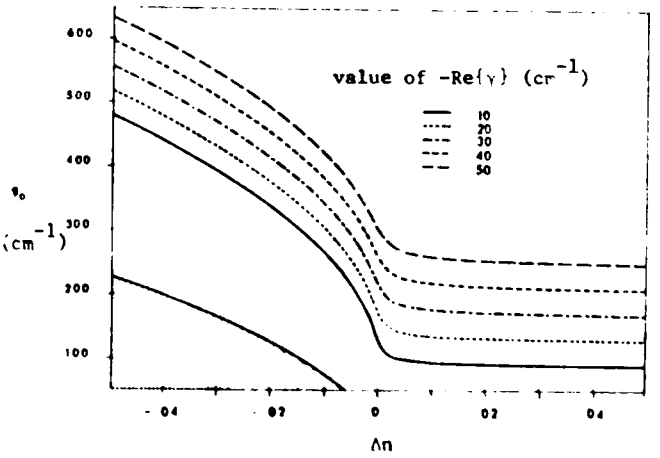

Figure 4

Modal Solutions of Active Dielectric Waveguides by Approximate Methods

A. LINZ, MEMBER, IEEE, AND J. K. BUTLER, SENIOR MEMBER

Abstract — Approximate methods are used to obtain the modal properties of stripe-contact semiconductor injection lasers using a planar three-layer waveguide model. The central active layer has a dielectric constant that varies smoothly along the direction parallel to the heterojunction boundaries. The complex dielectric constant under the stripe contact is dependent on the gain and approaches a constant value at large lateral distances. The two methods are compared in terms of their modal propagation constants. An application of the effective index method facilitates a physical understanding of dielectric waveguide modes as well as providing an efficient calculation procedure.

I. Introduction

ANALYSIS OF mode propagation in dielectric waveguides with a spatially varying refractive index has been the subject of several papers [1]–[3]. Typically, the variation of the dielectric constant with distance has been approximated with a parabolic profile [1], [2] or a function of the form $\kappa = -\kappa_0 + \kappa_3 \tanh^2(x/x_0)$ [3]. Both approximations have the disadvantage that the value of κ goes to infinity at large distances from the point $x = 0$, which corresponds to the axis of lateral symmetry of the structure. In the case of a semiconductor laser, this corresponds to the region below the center of the contact stripe. Another approximation that eliminates this disadvantage is the use of a function of the form [4]

$$\kappa = \kappa_S + \Delta\kappa/\cosh^2(x/x_0) \qquad (1)$$

to describe the variation of κ. This is in closer correspondence with the physical situation, since κ now acquires the value κ_S for $x \gg x_0$. Even if this particular form of variation of κ does not describe the actual variation very closely, it retains the most important features, and leads to equations with known solutions. The disadvantage in this case is the fact that the field solutions consist of a finite (possibly empty) set of confined trapped modes, an infinite set of discrete, diverging "leaky" modes, and a continuum of solutions that will be designated as "radiation" modes, as opposed to an infinite set of discrete trapped modes only, as in the parabolic and $\tanh^2(x/x_0)$ profiles. Mode analysis is a two-dimensional problem, since the refractive index varies in both lateral (x) and transverse (y) directions. Therefore, numerical or approximate methods need to be applied. The most popular and effective approximation method is the "effective-index" solution, whereby the two-dimensional problem is reduced to an equivalent, one-dimensional one [2], [4]–[8]. Numerical methods have also been developed. For example, in [1] the parabolic variation is used. Maxwell's equations are solved both for the active layer and the confining layers, and then superposition is applied to both types of solutions to form a general expression for the field. These solutions and their derivatives are matched at the boundaries of the active layer, yielding an infinite system of linear homogeneous equations, whose solutions, numerically obtained, are the expansion coefficients for the mode in terms of the eigenfunctions of the active layer problem. Of course, direct numerical integration of the two-dimensional wave equation is possible, but the computation times are long compared to those required by the algorithm discussed in this paper.

For the type of variation considered here, a general field in the active layer must be expressed as a superposition of the few confined discrete modes plus an integral over the continuum. Leaky modes cannot be included in the expansion if the field is to decrease to zero for large distances from the stripe.

Direct application of the numerical method used in [1] results in a finite set of linear equations (due to the finite number of trapped modes) coupled with an integral equation (due to integral over the continuum). For the case in which only one trapped mode exists (the fundamental mode), an integral equation results, which can in principle be solved. However, these cases will be seen to correspond to structures with net modal loss or low gains very sensitive

Manuscript received May 6, 1982; revised June 22, 1982. This work was supported by the U.S. Army Research Office.

The authors are with the Department of Electrical Engineering, Southern Methodist University, Dallas, TX 75275.

0018-9480/82/1200-2139$00.75 ©1982 IEEE

Leaky modes ($l > l_{max}$) cannot be used when expressing a general confined field as a superposition of modes. This results in a finite discrete eigenvalue spectrum, and the need arises for a continuum in order to have a complete orthogonal set of functions. We will seek an approximate solution neglecting the continuum. For the trapped modes, the product solutions will be of the form

$$\psi_l(x)\cos(q_l y) \tag{24}$$

and the general solution will be approximated by

$$\Psi_b(x,y) \cong \sum_{l=0,2,\cdots,}^{\bar{l}_{max}} A_l \psi_l(x)\cos(q_l y) \tag{25}$$

for a field even in x, where $\bar{l}_{max}$ is the maximum even value of l for which ψ_l is confined. The trapped modes satisfy the orthogonality relation

$$\frac{1}{x_0}\int_{-\infty}^{\infty} \psi_l(x)\psi_{l'}(x)\,dx = N_l \delta_{l,l'}. \tag{26}$$

The first few normalization constants are

$$N_0 = \frac{\sqrt{\pi}\,\Gamma(b_0)}{\Gamma(b_0+\frac{1}{2})} \tag{27a}$$

$$N_1 = \frac{2(b_0-\frac{1}{2})^{1/2}}{(b_0-1)}\sqrt{\pi}\,\frac{\Gamma(b_0)}{\Gamma(b_0+\frac{1}{2})} \tag{27b}$$

$$N_2 = \frac{2\sqrt{\pi}\,(b_0-3/2)^2(b_0-\frac{1}{2})\Gamma(b_0)}{(b_0-2)\Gamma(b_0+\frac{1}{2})} \tag{27c}$$

where $\Gamma(z)$ is the factorial function. An analytic but lengthy expression for the N_l exists but is not given here.

Solution of (8) for the confining layers proceeds as in [1]. Separation of variables is applied to (8); the lateral solution is of the form $\cos(\chi x)$ whereas the vertical solution is a decreasing exponential. Superposition is then applied; this results in an integral since no boundary conditions are available that would result in a discrete spectrum. The general solution will be

$$\Psi_a(x,y) = \int_0^{\infty} B(\chi)\cos(\chi x) \cdot \exp\left[(\chi^2-\gamma^2-k_a^2)^{1/2}(d/2-y)\right]d\chi \tag{28}$$

where

$$k_a^2 = k_0^2\kappa_A.$$

Now, (25) and (28) and their normal derivatives have to be matched at $y = \pm d/2$, the boundaries of the active layer. Matching ψ_a and ψ_b results in an expression for $B(\chi)$

$$B(\chi) = \frac{2}{\pi}\sum_{l=0,2,\cdots,}^{\bar{l}_{max}} A_l\sqrt{N_l}\cos\left(q_l\frac{d}{2}\right)\bar{\psi}_l(\chi) \tag{29a}$$

where

$$\bar{\psi}_l(\chi) = \int_0^{\infty}\frac{\psi_l(x)}{\sqrt{N_l}}\cos(\chi x)\,dx. \tag{29b}$$

Matching the derivatives respect to y at $y = d/2$ and applying the orthogonality relation (26) yields, after using (29a)

$$\frac{4}{\pi x_0}\sum_{l=0,2,\cdots,}^{\bar{l}_{max}} A_l\sqrt{N_l}\cos\left(ql\frac{d}{2}\right)I_{l,l'}(\gamma) = A_{l'}q_{l'}\sin\left(q_{l'}\frac{d}{2}\right)\sqrt{N_{l'}} \tag{30}$$

with $l, l' = 0,2,\cdots,\bar{l}_{max}$ and

$$I_{l,l'}(\gamma) = \int_0^{\infty}\bar{\psi}_l(\chi)\bar{\psi}_{l'}(\chi)(\chi^2-\gamma^2-k_a^2)^{1/2}d\chi \tag{31}$$

$$\bar{\psi}_l(\chi) = \frac{1}{\sqrt{N_l}}\sum_{m=0}^{l/2} 2^{(l-2m)}\frac{(-1)^m\Gamma(b_0+\frac{1}{2}-m)}{\Gamma(b_0-l+\frac{1}{2})m!(l-2m)!} \cdot \sum_{k=0}^{\frac{l}{2}-m}\left\{\frac{(-1)^k\left(\frac{l}{2}-m\right)!}{\left(\frac{l}{2}-m-k\right)!k!}\cdot t(\chi, b_0+2k-l, x_0)\right\} \quad (l \text{ even}) \tag{32}$$

where

$$t(\chi,\lambda,x_0) = \frac{2^{\lambda-2}x_0}{\Gamma(\lambda)}\Gamma\left(\lambda+i\frac{\chi x_0}{2}\right)\Gamma\left(\lambda-i\frac{\chi x_0}{2}\right). \tag{33}$$

This is a finite system of linear homogeneous equations of the form

$$(\Omega^T - I)\bar{A} = 0 \tag{34}$$

where $\bar{A}^T = (A_0, A_2, \cdots, A_{\bar{l}_{max}})$, I is the unit matrix, and the matrix elements of Ω are given by

$$\Omega_{ll'}(\gamma) = \frac{4\cos(q_l d/2)\sqrt{N_l}}{\pi x_0 q_{l'}\sin\left(q_{l'}\frac{d}{2}\right)\sqrt{N_{l'}}}I_{ll'}(\gamma). \tag{35}$$

The q_l satisfy, from (12a) and (12b)

$$q_l^2 = \gamma^2 + k_0^2\kappa_S + \frac{(b_0-l)^2}{x_0^2}. \tag{36}$$

The system of equations (34) has a nontrivial solution only if $\det(\Omega - I) = 0$. Numerical computation of the roots yields the possible values of the propagation constant γ.

IV. Numerical Results

The method was applied to a structure described by the following parameters:

$n_A = 3.38$	$g_0 = 200\ \text{cm}^{-1}$
$\alpha_A = 50\ \text{cm}^{-1}$	$n_0 = 3.595$
$\alpha_S = 50\ \text{cm}^{-1}$	$x_0 = 6\ \mu\text{m}$.

Direct solution of (34) involves computation of the $\Omega_{ll'}$. In general, $\Omega_{ll'} \neq \Omega_{l'l}$, but $I_{ll'} = I_{l'l}$.

Values of the modal loss = $\text{Re}\{\gamma\}$ were computed first by evaluating $I_{ll'}(\gamma)$ using the exact expression (31). This required one computation of this integral for every value of

boundaries $y = \pm d/2$, and demand that Ψ_a and Ψ_b decrease to zero as $x \to \pm\infty$, and also that $\Psi_a \to 0$ as $|y| \to \infty$. These boundary conditions are homogeneous, so we can apply separation of variables.

First we consider the solution inside the active layer making

$$\Psi_b(x, y) = \psi(x)\phi(y). \tag{9}$$

Substitution in (7) results in a vertical solution of the form

$$\phi(y) = \begin{pmatrix} \sin \\ \cos \end{pmatrix} qy \tag{10a}$$

and a differential equation

$$\frac{d^2\psi}{dx^2} + \left[k_0^2\kappa_S + \gamma^2 - q^2 + k_0^2\frac{\Delta\kappa}{\cosh^2(x/x_0)}\right]\psi = 0 \tag{10b}$$

where q is the separation constant. The substitutions

$$\xi = \tanh(x/x_0) \tag{11a}$$

$$\psi = (1-\xi^2)^{B/2}W(\xi) \tag{11b}$$

$$b_0(b_0+1) = k_0^2x_0^2\Delta\kappa \tag{12a}$$

$$B^2 = (q^2 - \gamma^2 - k_0^2\kappa_S)x_0^2 \tag{12b}$$

in (10b) result in

$$(1-\xi^2)W'' - (2\lambda+1)\xi W' + \alpha(\alpha+2\lambda)W = 0 \tag{13}$$

with

$$\lambda = B + \tfrac{1}{2} \tag{14a}$$

$$\alpha = b_0 - \lambda + \tfrac{1}{2}. \tag{14b}$$

Several solutions exist for (13). When α is an integer $l = 0, 1, 2, \cdots$, we have polynomial solutions, which are the ultraspherical or Gegenbauer polynomials $C_l^\lambda(\xi)$. Physically, they give rise to an infinite number of discrete modes, of which some may be trapped. The radiation modes would be described by other solutions that satisfy (13) for arbitrary α (see [9]).

We will now examine the polynomial solutions $W(\xi) = C_l^\lambda(\xi)$ in detail. For α an integer l

$$\lambda = b_0 - l + \tfrac{1}{2} \tag{15a}$$

$$B_l = b_0 - l, \qquad l = 0, 1, 2, \cdots. \tag{15b}$$

The $C_l^\lambda(\xi)$ are defined by

$$C_0^\lambda(\xi) = 1 \tag{16a}$$

$$C_1^\lambda(\xi) = 2\lambda\xi \tag{16b}$$

$$(l+1)C_{l+1}^\lambda(\xi) = 2(l+\lambda)\xi C_l^\lambda(\xi) - (l+2\lambda-1)C_{l-1}^\lambda(\xi). \tag{16c}$$

Using (11a) and (11b) we obtain the expression for the modes

$$\psi_l(x) = [\cosh(x/x_0)]^{l-b_0}C_l^{b_0-l+\frac{1}{2}}(\tanh[x/x_0]) \tag{17}$$

where, from (12a)

$$b_0 = -\tfrac{1}{2} + \left(\tfrac{1}{4} + k_0^2x_0^2\Delta\kappa\right)^{1/2}. \tag{18}$$

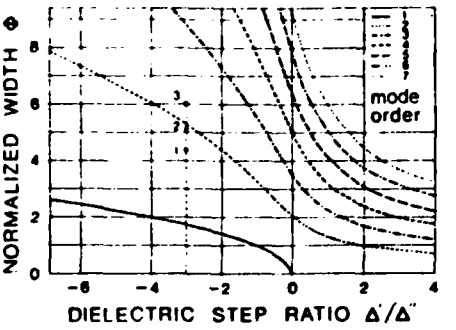

Fig. 4. Confinement curves (Φ versus Δ'/Δ'') for several mode orders.

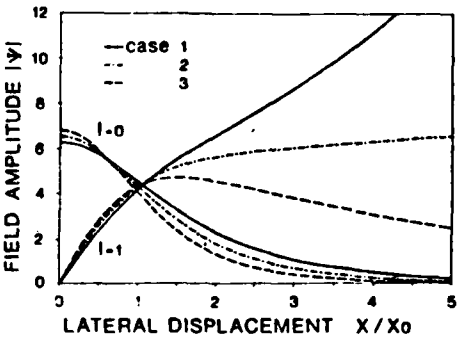

Fig. 5. Field amplitude versus lateral displacement for modes of order 0 and 1 for the 3 cases shown in Fig. 4. The curves for $l = 1$ are magnified five times.

For $x \gg x_0$, (17) becomes

$$\psi_l(x) \simeq 1/2 \exp\left[-(x/x_0)(b_0 - l)\right]\cdot C_l^{b_0-l+1/2}(1). \tag{19}$$

So to satisfy the boundary conditions, we require

$$\mathrm{Re}(b_0 - l) > 0. \tag{20}$$

For a given b_0, if $\mathrm{Re}\{b_0\} > 0$ there exists at least one mode that decreases as $x \to \pm\infty$, for $l = 0$ (the fundamental mode). Modes of order l such that $\mathrm{Re}\{b_0 - l\} < 0$ are still solutions of (10b) but diverge as $|x| \to \infty$, and will be designated as "leaky". Notice that, if $\mathrm{Re}\{b_0\} < 0$, even the fundamental mode becomes leaky. Condition (20) can be expressed in terms of the real and imaginary parts of $\Delta\kappa$ defining the quantities

$$\delta = \Delta'/\Delta'' \tag{21a}$$

$$\Phi = 2k_0x_0(\Delta'')^{1/2} \tag{21b}$$

where $\Delta\kappa = \Delta' + i\Delta''$. We obtain

$$\delta \geq \frac{(2l+1)^2l(l+1) - \Phi^4}{\Phi^2(2l+1)^2} \tag{22}$$

as the region for lateral confinement. Fig. 4 shows Φ as a function of δ for several values of l. Fig. 5 shows the behavior of the $|\psi_l|$ for sets of parameters resulting in the (δ, Φ) points marked in Fig. 4. In particular, notice the behavior of $|\psi_1|$ when we go from "1" to "2" to "3".

The $\psi_l(x)$ will diverge for $l > l_{\max}$, where

$$l_{\max} = INT[\mathrm{Re}\{b_0\}]. \tag{23}$$

to the dielectric step size. For structures that exhibit higher, stable gain, several discrete trapped modes exist, and we achieve reasonable convergence with the first few modes, so that considering the continuum is not necessary. We also apply the effective-index method and compare it with the approximate numerical method in terms of the propagation constant γ, which is calculated as a function of the dielectric step size in the active layer $\Delta n = n_0 - n_S$, where n_0 and n_S are the values of refractive index under the stripe and far away from it. The results of the two methods practically coincide for the cases in which several trapped modes exist. They differ appreciably only for that range of Δn for which only one trapped mode exists. The discrepancy may be possibly due to the continuum, but this paper does not investigate this matter further. The following sections will consist of a description of the class of waveguides considered, followed by a description of the approximate numerical method, ending with the application of the effective-index method to this problem and conclusions.

II. Description of Structures

Fig. 1 shows the structure considered in this paper. The confining layers A and C are assumed identical, their refractive indices being described by

$$\kappa_A = \kappa_C \cong n_A^2 - i\alpha_A n_A / k_0. \tag{2}$$

α_A describes the power loss in these layers, and is constant with distance. The active layer has a constant thickness d, with a refractive index

$$\kappa(x) = n^2(x) - i\alpha(x)n(x)/k_0 \tag{3}$$

whose dependence with x is considered to be reasonably well approximated by

$$\kappa(x) = \kappa_S + \Delta\kappa/\cosh^2(x/x_0) \tag{4}$$

where

$$\Delta\kappa = \kappa_0 - \kappa_S \tag{5a}$$

$$\kappa_0 = \kappa(0) = n_0^2 + ig_0 n_0/k_0 \tag{5b}$$

$$\kappa_S = n_S^2 - i\alpha_S n_S/k_0. \tag{5c}$$

x_0 is a parameter related to the width of the stripe. The values of power attenuation coefficient and refractive index inside the active region far away from the stripe are α_S and n_S, respectively. The quantity g_0 represents power gain under the stripe, where the refractive index is n_0, and $k_0 = 2\pi/\lambda$.

Using (4) and (5), we can obtain expressions for the variation of the refractive index n and the loss α (or gain $-\alpha$) as a function of distance. Figs. 2 and 3 show $n(x)$ versus x/x_0 and $\alpha(x)$ versus x/x_0. For $\Delta n = n_0 - n_S > 0$, the mode will be index-guided, while for $\Delta n < 0$, it will be index-antiguided. In this latter case, it will still be confined because of the gain distribution, but the field will be more spread and the modal gain will be low (eventually we may have a net power loss). If Δn is negative enough, the guiding effect is lost and the modes become leaky. The condition $\Delta n > 0$ results in strong confinement and high and stable values of modal gain.

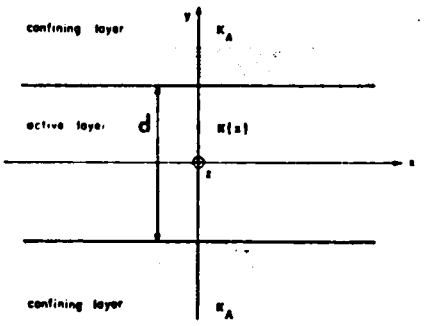

Fig. 1. Waveguide structure considered.

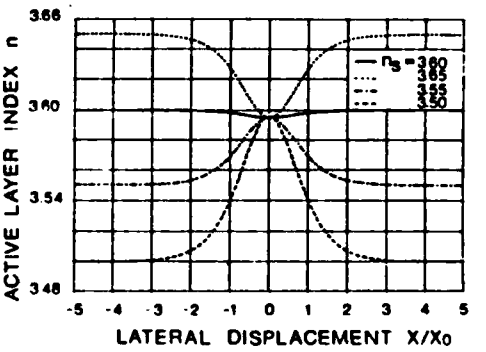

Fig. 2. Refractive index of active layer versus lateral displacement for $\alpha_S = 50\ \text{cm}^{-1}$, $g_0 = 200\ \text{cm}^{-1}$, $n_0 = 3.595$ for different values of n_S.

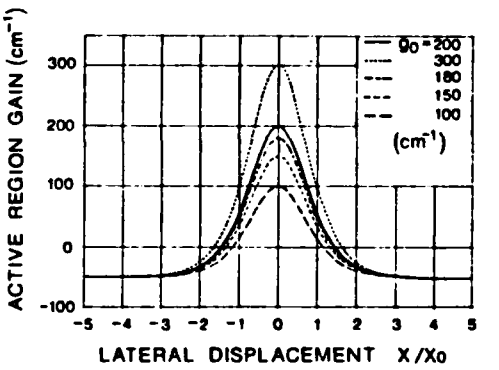

Fig. 3. Power gain $-\alpha$ for active region versus lateral displacement for $\alpha_S = 50\ \text{cm}^{-1}$, $n_0 = 3.595$, $n_S = 3.6$ for different values of g_0.

III. Numerical Solution

We assume an electric field of the form

$$E_x = \Psi(x, y). \tag{6}$$

Following [1], we apply Maxwell's equations to the structure in Fig. 1, and obtain inside the active layer

$$\nabla_t^2 \Psi_b + \left[\gamma^2 + k_0^2 \kappa(x)\right]\Psi_b = 0 \tag{7}$$

and outside the active layer

$$\nabla_t^2 \Psi_a + \left[\gamma^2 + k_0^2 \kappa_A\right]\Psi_a = 0 \tag{8}$$

where $\kappa(x)$ is given by (4). We require the functions Ψ_a and Ψ_b and their normal derivatives to be continuous at the

γ, i.e., every iteration in the solution of (34). This resulted in unacceptably high computation times, in part because $\bar{\psi}_l$ involves repeated use of a gamma-function routine and also because the integrand is an oscillating function of χ. In order to improve speed, instead of solving the complete system (34) we start with a 1×1 matrix, go on to a 2×2 matrix, etc., and observe the convergence of the result. Fig. 6 shows $\mathrm{Re}(\gamma)$ versus Δn for 1×1 and 2×2 matrices. We see that the result converges relatively fast, so a 2×2 matrix is sufficient for our approximation. This holds for the case $\bar{l}_{\max} \geq 2$. For $\bar{l}_{\max} = 0$, we are limited to the 1×1 case. In Fig. 6, for $\Delta n < -0.01$, $\bar{l}_{\max} = 0$. For $\Delta n > -0.01$, $\bar{l}_{\max}$ increases as shown in the figure.

In spite of this, even for $\bar{l}_{\max} = 0$, the computation time is impractically high. An increase in speed is achieved recognizing that (31) can be written as

$$I_{ll'}(\gamma) = \left(-\gamma^2 - k_a^2\right)^{1/2} \int_{-\infty}^{\infty} \left[1 + \frac{\chi^2}{-\gamma^2 - k_a^2}\right]^{1/2} \cdot \bar{\psi}_l(\chi)\bar{\psi}_{l'}(\chi)\, d\chi. \quad (37)$$

For common values of k_a^2 and γ, $|\chi^2/(-\gamma^2 - k_a^2)| \ll 1$ in the range of values of χ for which $\bar{\psi}_l(\chi)$ and $\bar{\psi}_{l'}$ are appreciably different from zero. This allows us to expand the radical in (37) using the binomial theorem and retaining only a finite number of terms. This results in

$$I_{ll'}(\gamma) = \left(-\gamma^2 - k_a^2\right)^{1/2} \left\{ \int_{-\infty}^{\infty} \bar{\psi}_l \bar{\psi}_{l'}\, d\chi + \frac{1}{2\left(-\gamma^2 - k_a^2\right)} \cdot \int_{-\infty}^{\infty} \chi^2 \bar{\psi}_l \bar{\psi}_{l'}\, d\chi - \frac{1}{8\left(-\gamma^2 - k_a^2\right)^2} \cdot \int_{-\infty}^{\infty} \chi^4 \bar{\psi}_l \bar{\psi}_{l'}\, d\chi + \cdots \right\}. \quad (38)$$

The integrals do not depend on γ, so they need to be computed only once for a given set of material parameters, and not for every value of γ, as (31) would require. Furthermore, the properties of the Fourier transform guarantee that

$$\int_{-\infty}^{\infty} \bar{\psi}_l \bar{\psi}_{l'}\, d\chi = \delta_{ll'}. \quad (39)$$

Agreement with exact computation of (31) is excellent with the first three terms in the expansion (38) and the computation time is reduced substantially, by nearly two orders of magnitude. This allows us to perform more extensive modeling using this method.

Fig. 7 shows plots of the modal loss $= \mathrm{Re}(\gamma)$ as a function of Δn, with g_0, the gain under the stripe, as a parameter. We notice that for each value of g_0, Δn can be decreased up to a certain value beyond which the fundamental mode becomes leaky, i.e., the antiguiding effect of the (negative) Δn offsets the guiding effect of the gain distribution.

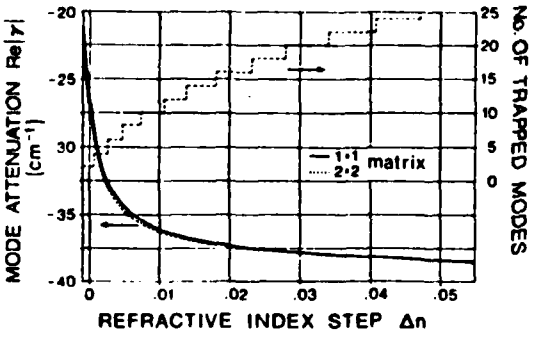

Fig. 6. Mode attenuation $\mathrm{Re}(\gamma)$ and number of discrete trapped modes versus Δn.

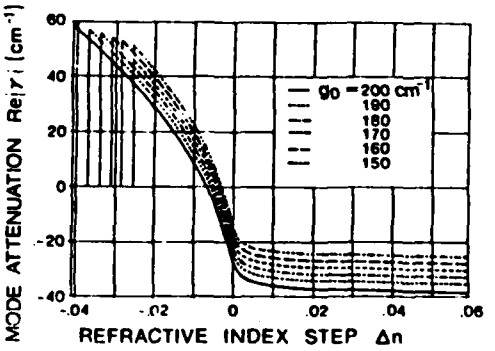

Fig. 7. Mode attenuation $\mathrm{Re}(\gamma)$ versus Δn for different values of g_0.

More negative values of Δn are required to offset higher values of g_0. For any given g_0, using (5), (18), and (20) with $l = 0$, it can be shown that the boundary value of Δn is

$$\Delta n = -\tfrac{1}{2} x_0^2 n_0 (g_0 + \alpha_S)^2. \quad (40)$$

These values are marked with vertical lines in Fig. 7. This relation shows that the guiding effect of the gain distribution does not depend on the individual values of g_0 (gain under the stripe) and $-\alpha_S$ (gain far away from the stripe), but only on their difference $g_0 - (-\alpha_S) = g_0 + \alpha_S$.

V. Effective-Index Calculation

The effective-index method consists basically in reducing a two-dimensional problem to an equivalent one-dimensional one. In our case, the two-dimensional character of the problem is given by the dependence of the dielectric constant on x and y. As a first approximation, the variation in one direction (in our case: x) is neglected; this is justified if this variation is much less than that in the y direction. This is equivalent to approximating the waveguide with a simple three-layer guide whose dielectric constants do not vary with x. The solution of this problem yields the transverse or vertical variation of the field. Next, the original equation describing the two-dimensional equation in x can be solved for the lateral variation of the field, and the overall solution is approximated by the product of this lateral field and the vertical field found from the

three-layer problem. We start with the wave equation in two dimensions, which is obtained merging (7) and (8)

$$\nabla_t^2\Psi + \left[\gamma^2 + k_0^2\kappa(x,y)\right]\Psi = 0 \tag{41}$$

where

$$\kappa(x,y) = \begin{cases} \kappa_A, & |y| \geq d/2 \\ \kappa_S + \dfrac{\Delta\kappa}{\cosh^2(x/x_0)}, & |y| < d/2 \end{cases} \tag{42}$$

For the simple three-layer guide we assume $\kappa(x) = \kappa_0$ inside the active layer. We then have

$$\frac{d^2\phi}{dy^2} = \begin{cases} -q^2\phi & |y| \leq d/2 \quad (43a) \\ p^2\phi & |y| > d/2 \quad (43b) \end{cases}$$

with

$$p^2 + q^2 = k_0^2[\kappa_0 - \kappa_A] \tag{44a}$$

$$p = q\tan(qd/2). \tag{44b}$$

Now, we transform (41) making $\Psi(x,y) = \psi(x)\phi(y)$, multiplying it by $\phi^*(y)$, and integrating it over y from $-\infty$ to ∞, taking into account (42) and (43) and defining the *confinement factor*

$$\Gamma \equiv \frac{\int_{-d/2}^{d/2} \phi^*(y)\phi(y)\,dy}{\int_{-\infty}^{\infty} \phi^*(y)\phi(y)\,dy}. \tag{45}$$

We obtain

$$\frac{d^2\psi}{dx^2} + \left[\gamma^2 - q_{eff}^2 + k_0^2\kappa_{Seff} + k_0^2\frac{\Delta\kappa_{eff}}{\cosh^2(x/x_0)}\right]\psi = 0 \tag{46}$$

with

$$q_{eff}^2 = \Gamma k_0^2 x_0 - p^2 - k_0^2\kappa_A \tag{47a}$$

$$\kappa_{Seff} = \Gamma\kappa_S \tag{47b}$$

$$\Delta\kappa_{eff} = \Gamma\Delta\kappa. \tag{47c}$$

Equation (46) has the same form as (10b). It will also have polynomial solutions similar to (17) that represent trapped modes

$$\psi_l(x) = \left[\cosh(x/x_0)\right]^{l - b_{0eff}} C_l^{b_{0eff} - l + \frac{1}{2}}\left(\tanh\frac{x}{x_0}\right) \qquad l = 0,1,2,\cdots \tag{48}$$

where b_{0eff}, $\Delta\kappa_{eff}$, and κ_{Seff} satisfy relations identical to (12b), (15b), and (18). For the fundamental mode, $l = 0$, $B = b_{0eff}$, and using (44b), we obtain

$$\gamma^2 = -k_0^2\kappa_A - \frac{b_{0eff}^2}{x_0^2} - \left(p^2 - k_0^2\Gamma\Delta\kappa\right) \tag{49}$$

for the propagation constant.

VI. Discussion

Values of γ obtained using (49) are compared with those obtained with the numerical method in Fig. 8. Solutions are very close for all values of Δn for which the mode exhibits a gain which is relatively high and with low sensitivity to Δn. The results differ most in the range of Δn for which the mode has a net loss or has a relatively low gain with higher sensitivity to Δn. This is the same region for which only one trapped mode exists, so the error in the numerical method is the greatest because the neglected continuum is more important.

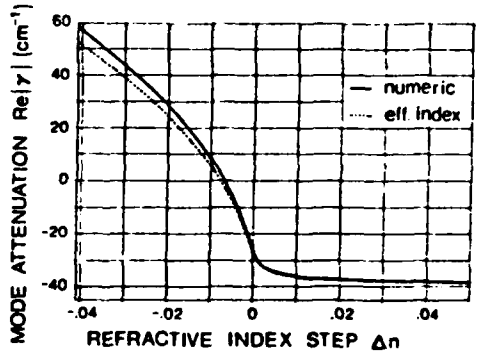

Fig. 8. Mode attenuation $\mathrm{Re}(\gamma)$ versus Δn for numeric and effective-index methods, for $g_0 = 200\ \mathrm{cm}^{-1}$.

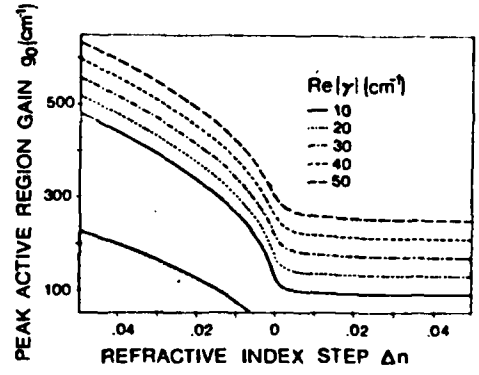

Fig. 9. Peak active region gain g_0 versus Δn for several values of $\mathrm{Re}(\gamma)$. Dotted area indicates region where fundamental mode becomes leaky.

Fig. 9 gives the required value of the peak power gain g_0 under the stripe to obtain a given modal gain G, as a function of Δn, using the effective-index method. Also included is the region for which the fundamental mode becomes leaky. Figs. 10–12 show the normalized lateral field distributions for different values of Δn. The increasing antiguiding effect of decreasing Δn is apparent. The distance x at which the gain is zero (loss/gain boundary) is shown in these figures with vertical dashed lines. It can be shown to be given by

$$\bar{x} = x_0\cosh^{-1}\left(1 + \frac{g_0}{\alpha_S}\cdot\frac{n_0}{n_S}\right)^{1/2}. \tag{50}$$

For the set of parameters considered, $\bar{x} = 1.45\ x_0$. This allows us to qualitatively understand why the modes have the loss (gain) indicated. The vertical confinement factor Γ did not vary appreciably with Δn; a typical value for the case considered was $\Gamma = 0.4963$. We see that lateral variations in the refractive index affect the gain much more by altering the lateral field distribution than by affecting the vertical variation.

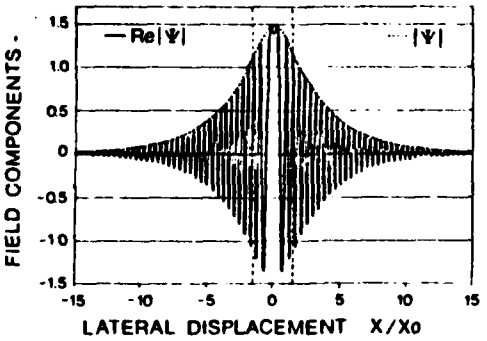

Fig. 10. Normalized lateral field distribution, for $\Delta n = -0.0156$. The resulting modal loss is 20 cm^{-1}. Vertical dashed lines indicate the distance at which the gain inside the active layer is zero.

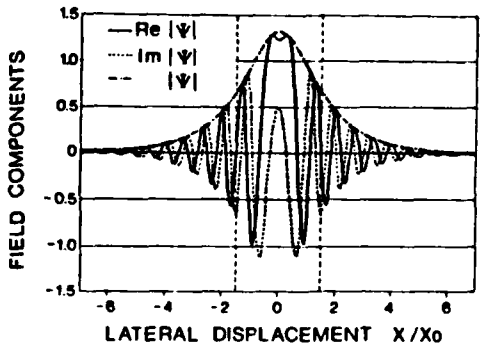

Fig. 11. Normalized lateral field distribution for $\Delta n = -0.006$. $Re\{\gamma\} = -4.46$ cm^{-1} (gain). Vertical dashed lines have the same meaning as in Fig. 10.

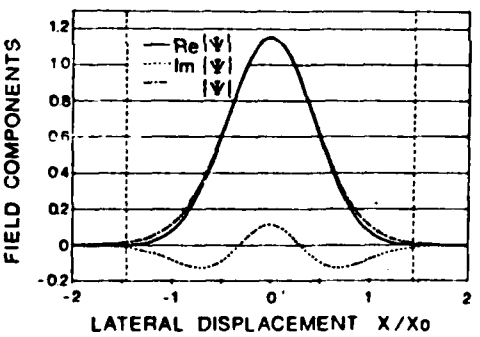

Fig. 12. Normalized lateral field distribution for $\Delta n = 0.002$. The modal gain, $-Re\{\gamma\}$, is now 32.3 cm^{-1}.

The effective-index method is seen to be a fast and relatively accurate way to obtain the field distributions for the class of waveguides considered, for which the numerical method we used is not practical for extensive modeling due to its long computation time in spite of all approximations. The remarkable agreement between the effective-index method and experimental results found by other workers ([10]) increases our confidence in this powerful approximate method.

References

[1] J. K. Butler and J. B. Delaney, "A rigorous boundary value solution for the lateral modes of stripe geometry injection lasers," *IEEE J. Quantum Electron.*, vol. QE-14, pp. 507–513, July 1978.

[2] T. L. Paoli, "Waveguiding in a stripe-geometry junction laser," *IEEE J. Quantum Electron.*, vol. QE-13, pp. 662–668, Aug. 1977.

[3] W. Streifer, D. Scifres, and R. Burnham, "Analysis of gain-induced waveguiding in stripe-geometry injection lasers," *IEEE J. Quantum Electron.*, vol. QE-14, pp. 418–427, June 1978.

[4] P. M. Asbeck, D. A. Cammack, and J. J. Daniele, "Non-gaussian fundamental mode patterns in narrow-stripe-geometry lasers," *Appl. Phys. Lett.*, vol. 33, pp. 504–506, Sept. 1978.

[5] R. M. Knox and P. P. Toulios, "Integrated circuits for the millimeter through optical frequency range," in *Proc. MRI Symp. Submillimeter Waves*, J. Fox, Ed. New York: Brooklyn Polytechnic, 1970.

[6] W. Streifer and E. Kapon, "Application of the equivalent-index method to DH diode lasers," *Appl. Opt.*, vol. 18, pp. 3724–3725, Nov. 1979.

[7] J. Buus, "A model for the static properties of DH lasers," *IEEE J. Quantum Electron.*, vol. QE-15, pp. 734–739, Aug. 1979.

[8] J. K. Butler and J. B. Delaney, "Field solutions for the lateral modes of stripe geometry injection lasers," *IEEE J. Quantum Electron.*, vol. QE-16, pp. 1326–1328, Dec. 1980.

[9] A. Erdelyi, W. Magnus, F. Oberhettinger, and F. Tricomi, "Higher transcendental functions," vol. I—Bateman Manuscript Project. New York: McGraw-Hill, 1953, Sect. 3.15, 3.16.

[10] J. K. Butler and D. Botez, "Mode characteristics of non-planar double-heterojunction and large-optical cavity laser structures," *IEEE J. Quantum Electron.*, vol. QE-18, pp. 952–961, June 1982.

Alfredo Linz was born in 1951 in Quito, Ecuador. He received the degree of Ingeniero en Electronica y Telecommunicaciones from Escuela Politecnica Nacional, Quito, in 1977, summa cum laude. From 1977 to 1979 he served as Instructor at EPN. Through the Fulbright Program he was awarded as assistantship at Southern Methodist University, Dallas, TX, where he obtained the M.S.E.E. degree in 1981, and is currently working toward a Ph.D. degree.

Mr. Linz's interests include optical communication, quantum electronics, and digital systems. He is a member of Tau Beta Pi.

Jerome K. Butler (S'59–M'65–SM'78) received the B.S. degree from Louisiana Polytechnic University, Ruston, in 1960, and the M.S. and Ph.D. degrees from the University of Kansas, Lawrence, in 1962, and 1965, respectively.

From 1960 to 1965 he was a Research Assistant at the Center for Research in Engineering Sciences, University of Kansas, Lawrence. His research was related to electromagnetic-wave propagation and to the optimization and synthesis techniques of antenna arrays. In 1965 he joined the staff of the School of Engineering and Applied Science, Southern Methodist University, Dallas, TX, where he is now Professor of Electrical Engineering. His primary research areas are solid-state injection lasers, radiation and detection studies of lasers, communication and imaging systems, integrated optics and the application of integrated optical circuits, and quantum electronics. In the summer from 1969 to 1982 he was a member of the Technical Staff, RCA Laboratories, Princeton, NJ, where he did research concerned with electromagnetic-wave propagation in solid-state injection lasers. Dr. Butler is coauthor of the book *Semiconductor Lasers and Heterojunction LED's* (New York: Academic). He has held consulting appointments with the Central Research Laboratory, Texas Instruments, Inc., the Geotechnical Corporation of Teledyne, Inc., Earl Cullum Associates, Dallas, TX, and the University of California Los Alamos Scientific Laboratory.

Dr. Butler is a member of Sigma Xi, Tau Beta Pi, Eta Kappa Nu, and is a Registered Professional Engineer in the State of Texas.

APPLICATION OF A GENERAL PURPOSE CIRCUIT SIMULATION PROGRAM TO SEMICONDUCTOR LASER MODELING - PART I : ELECTRICAL ANALYSIS*

A. Linz and J.K. Butler
Electrical Engineering Department
Southern Methodist University
Dallas, Texas 75275

Abstract

This article describes the application of SPICE to the electrical modeling of modern semiconductor laser structures which cannot be described analytically. Given the geometrical structure of the device and some material characteristics such as impurity concentration and type of semiconductor (p or n), we must obtain the distribution of potential and current density. We are mainly interested in knowing the current density at the edge of the active layer, since it determines the distribution of injected carriers inside it, together with the diffusion equation. The carrier concentration, in turn, determines the optical gain in the active layer. The gain profile will have a strong influence on the lateral dependence of the optical field. In this article we start analyzing a very simple structure which nevertheless contains many features found in real lasers. Then we present a discrete model which can be applied to virtually any geometry and we use it to explore some laser structures with nonlinear elements (p-n junctions). We confine ourselves to purely electrical effects; the interaction between carrier diffusion and electrical parameters is left for a subsequent article.

* Supported in part by the U. S. Army Research Office and RCA Laboratories.

APPLICATION OF A GENERAL PURPOSE CIRCUIT SIMULATION PROGRAM TO SEMICONDUCTOR LASER MODELING - PART II : DIFFUSION ANALYSIS*

A. Linz and J.K. Butler
Electrical Engineering Department
Southern Methodist University
Dallas, Texas 75275

Abstract

This article is the continuation of a previous one in which the modeling of electrical characteristics of semiconductor laser devices using SPICE was described. Here we consider the application of SPICE to the modeling of diffusion and the integration of the electrical and the diffusion models. The model is then applied to a particular structure and the results are discussed. The model shows that the junction current density distribution remains virtually unchanged for a wide range of diffusivities.

* Supported in part by the U. S. Army and RCA Laboratories.

AN INTEGRATED ELECTRICAL/DIFFUSION MODEL FOR THE P-N JUNCTION*

A.Linz, J.K. Butler, and K.H. Heizer
Electrical Engineering Department
Southern Methodist University
Dallas, Texas 75275

Abstract

A lumped parameter circuit model is presented, which solves for the coupled electrical/diffusion problem for a p-n junction. Externally, the model yields the electron and hole current components separately. Internally, an adjoint "diffusion network" which is an electrical equivalent of the one-dimensional diffusion equation, yields the values of excess carrier concentration in both the n and p regions. The model is then used to obtain the transient response of a diode. The effect of the material parameters (lifetime, diffusivity, resistivity) on the electrical response of the device can be readily modeled. When used with SPICE, the model can easily be used as a subcircuit to incorporate it into networks containing diodes.

* Supported in part by the U. S. Army Research Office and RCA Laboratories.

APPENDIX C

DISSERTATION ABSTRACTS

Delaney, Joseph Baxter

B.S.E.E., Southern Methodist University, 1973
M.S.E.E., Southern Methodist University, 1974

Mode Structure of $Al_xGa_{1-x}As$ Injection Lasers

Advisor, Professor Jerome K. Butler

Doctor of Philosophy degree conferred: August 8, 1980

Dissertation completed: June 18, 1980

The lateral dielectric constant in stripe geometry injection lasers is modeled with a step and a parabolic dependence. For the step profile a set of cutoff curves for the lateral modes is used to compare various laser designs. As the vertical geometry of a laser is varied a contour is described on the cutoff curves which is a measure of lateral mode stability. Two laser designs examined are the simple stripe geometry and channeled-substrate planar lasers. The parabolic model of the lateral dielectric constant is extended to include matched fields at the vertical heterojunctions. A result is a deformed fundamental mode shape in the case of small normalized frequencies and depression of the refractive index under the stripe. This presents an alternative explanation for the shoulders that have heretofore been attributed to leaky waves.

Lateral mode stability with drive current above threshold is complicated by an uncertain dielectric profile perturbed by free carrier effects and spatial hole burning. An experimental scheme is devised to measure the free carrier effect on the refractive

index in GaAs active regions of injection lasers. Transverse field and modal selection mechanisms of the active cavity are characterized for a broad area high power laser as a function of temperature and injection level. The amount of index depression as a result of carrier increase in the active region is measured to be (3 - 9) x $10^{-27} m^3$.

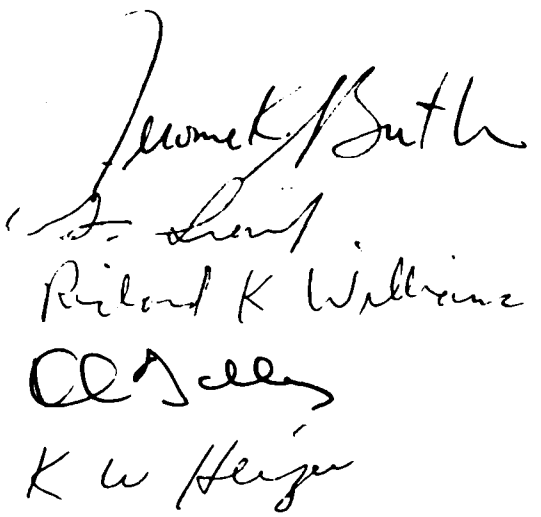

ABSTRACT

Linz , Alfredo R.

B.S.E.E. , Escuela Politecnica Nacional , Quito , Ecuador, August 1977

M.S.E.E. , Southern Methodist University , May 1981

MODELING OF SEMICONDUCTOR INJECTION LASERS

Advisor : Dr. Jerome K. Butler

Doctor of Philosophy Degree conferred :

Dissertation completed :

School of Engineering and Applied Science ,

Southern Methodist University

A set of programs to model the operation of semiconductor laser devices below and above threshold is presented, together with the design and construction of an automatic measurement system used to obtain far field radiation patterns. The programs incorporate electrical , diffusion and optical modeling.

The program SPICE is used to model electrical and diffusion phenomena, while direct numerical techniques are used to solve the optical and diffusion problems .

END

FILMED

5-85

DTIC